PLGA nanoparticles for delivery through the blood-brain barrier

Dissertation
zur Erlangung des Grades
des Doktors der Naturwissenschaften
der Naturwissenschaftlich-Technischen Fakultät
der Universität des Saarlandes

von

Sonia Lombardo

Saarbrücken

2022

Tag des Kolloquiums:	16. Mai 2022
Dekan:	Prof. Dr. Jörn Walter
Berichterstatter:	Prof. Dr. Marc Schneider
	Prof. Dr. Claus Jacob
Vorsitz:	Prof. Dr. Guido Kickelbick
Akad. Mitarbeiter:	Dr. Martin Frotscher

This work was carried on from October 2018 to September 2021 at MyBiotech GmbH (Überherrn, Germany) as well as Saarland University (Saarbrücken, Germany), under the supervision of Dr. Nazende Günday-Türeli and Prof. Dr. Marc Schneider.

This work is part of the NANOSTEM Innovative Training Network (ITN). This project has received funding from the European Union's Horizon 2020 research and innovation programme under grant agreement No 764958.

Table of contents

List of figures

Abstract

Treatments of central nervous system (CNS) diseases remains a real challenge for modern medicine due to the difficulty to cross the blood-brain barrier (BBB). Regenerative treatments based on increasing the differentiation of neural stem cells (NSCs) in new neuronal cells could prove interesting for improving the recovery of stroke patients, if these treatments were able to reach the deep brain structures where these cells are situated. All-trans retinoic acid (RA) is a promising molecule, able to increase the differentiation of NSCs. In this thesis, PLGA nanoparticles loaded with RA for delivery to the NSCs through the BBB were developed using the MicroJet reactor® (MJR) technology. These nanoparticles were coated with surfactants, polysorbate 80 and poloxamer 188. First, the nanoparticles were loaded with a fluorescent dye and their protein corona and their ability to cross the BBB were characterized using an *in vitro* coculture model. Both formulations were able to be internalized by the endothelial cells with different uptake profiles depending on their coating, and to be transcytosed to the abluminal compartment. Next, PLGA nanospheres and nanocapsules coated with surfactants were produced and loaded with retinoic acid. Nanoparticles with high encapsulation efficiency could be produced and their release profiles were measured. However, the nanoparticles showed a high burst release, which could be reduced by coating the nanocapsules with chitosan.

Kurzzusammenfassung

Die Behandlung von Erkrankungen des Zentralnervensystems (ZNS) bleibt eine echte Herausforderung für die moderne Medizin, da die Blut-Hirn-Schranke (BHS) nur schwer zu überwinden ist. Regenerative Behandlungen, die die Differenzierung von neuralen Stammzellen (NSZ) in neue neuronale Zellen steigern, könnten die Genesung von Schlaganfallpatienten verbessern, falls die Wirkstoffe diese Zellen erreichen. All-trans-Retinsäure (RS) ist ein vielversprechendes Molekül, welches die Differenzierung von NSZ erhöhen kann. In dieser Arbeit wurden RS beladene PLGA-Nanopartikel (NP) zum Transport des Wirkstoffs durch die BHS mittels MicroJet-Reaktor® (MJR)-Technologie entwickelt, um die NSZ zu erreichen. Diese NP wurden mit den Amphiphilen Polysorbat 80 und Poloxamer 188 stabilisiert. Zuerst wurden die NP mit einem fluoreszierenden Farbstoff beladen und ihre Proteinkorona, sowie ihre Fähigkeit, die BHS zu passieren, mit Hilfe eines In-vitro-Kokulturmodells charakterisiert. Beide Formulierungen konnten von den Endothelzellen, je nach Beschichtung, unterschiedlich gut aufgenommen und zum abluminalen Kompartiment per Transzytose weitergeleitet werden. Danach wurden Polysorbat- und Poloxamer-stabilisierte PLGA-Nanosphären und -Nanokapseln hergestellt und mit RS beladen. Es konnten NP mit hoher Verkapselungseffizienz hergestellt und deren Freisetzungsprofile gemessen werden. Allerdings zeigten die NP einen hohen Burst-Release, der durch Beschichtung mit Chitosan reduziert werden konnte.

Abbreviation list

acLDL	Acetylated low density lipoprotein
ACN	Acetonitrile
AMT	Adsorptive-mediated transcytosis
API	Active pharmaceutical ingredient
Apo A-I	Apolipoprotein A-I
ApoB	Apolipoprotein B
ApoE	Apolipoprotein E
BBB	Blood-brain barrier
BLEC	Brain-like endothelial cell
CNS	Central nervous system
DoE	Design of experiments
ECM (5%FCS)	Endothelial cell medium supplemented with 5% fetal calf serum
ECM (5%HS)	Endothelial cell medium supplemented with 5% human serum
ECS	Extracellular space
EE	Encapsulation efficiency
FCS	Fetal calf serum
FDA	Food and Drug Administration
HPLC	High performance liquid chromatography
HS	Human serum
LDL	Low density lipoprotein
LDLR	Low density lipoprotein receptor

MJR	MicroJet reactor
NaF	Sodium fluoroscein
NC	Not-coated
NGS	Normal goat serum
NP	Nanoparticle
NSCs	Neural stem cells
P188	Poloxamer 188
PBCA	Poly(butyl cyanoacrylate)
PBS	Phosphate buffered saline
PBS-CMF	Calcium and magnesium free phosphate buffered saline
PC	Pericyte
PDI	Polydispersity index
PLGA	Poly(lactic co-glycolic acid)
PS80	Polysorbate 80
RA	Retinoic acid
RH	Ringer HEPES
RMT	Receptor-mediated transcytosis
SR-B1	Scavenger receptor class B type 1
TFF	Tangential flow filtration
TW	Transwell®
USP	United States pharmacopeia

1. Introduction

Part of this chapter has been published in Lombardo, S.M.; Schneider, M.; Türeli, A.E.; Günday-Türeli, N. Key for Crossing the BBB with Nanoparticles: The Rational Design. Beilstein J. Nanotechnol. 2020, 11, 866–883, doi:10.3762/bjnano.11.72.

1.1 Scientific background

1.1.1 Stroke

According to the World Health Organization, cerebrovascular accidents, or stroke, were the third leading cause of disability and the second leading cause of death worldwide in 2019, with over 6 million deaths [1]. This tremendous number will go on growing in the future due to an aging population, with the rise of life expectancy worldwide. Ischemic strokes, caused by blockage of cerebral arteries by blood clots, represent up to 85% of all strokes [2]. Despite its huge impact on society, very few therapeutic solutions are available to treat this disease. Indeed, acute ischemic stroke treatment is limited to reperfusion therapy, whose time window is extremely narrow. Thrombolysis treatment, consisting in intravenous administration of recombinant tissue plasminogen activator (tPA), can only be administered within 4.5 hours of the symptom onset [3,4]. As 85% of patients are admitted beyond this time window, very few patients end up eligible for reperfusion treatment [5]. Treating patients outside this window could contribute to additional tissue damage and an increased risk of hemorrhagic transformation (a spectrum of ischemia-related brain hemorrhage), recognized as the most devastating complication after an ischemic stroke [6,7]. Furthermore, no regenerative treatments for stroke are currently on the market, to recover the brain areas damaged by the stroke. Most stroke patients suffer from neurologic damages and present motor or cognitive disabilities, that can only be improved nowadays by rehabilitation with limited success [8,9]. Thus, progress in stroke recovery treatment is needed, making stroke a disease with a huge medical need.

1.1.2 Neural stem cells

Neural stem cells (NSCs) are the stem cells of the nervous system. During development they give rise to the entire nervous system. In adults, a small number of NSCs remain and are mostly quiescent. In adult brains, NSCs are reduced and become restricted to specific brain regions. In adult rodents, NSCs persist in the subventricular zone (SVZ) and the subgranular zone (SGZ), which are specialized niches in which young neurons for the olfactory bulb and hippocampus, respectively, are generated [10–12]. These NSCs present radial morphology and glial features and are referred by several names in the literature including radial glial cells, radial cells or radial astrocytes [13,14].

Ample evidence supports the important roles of NSCs in plasticity, aging, disease, and regeneration of the nervous system. The self-renewing NSCs can differentiate in new neuronal cells: neurons, astrocytes and oligodendrocytes (Figure 1).

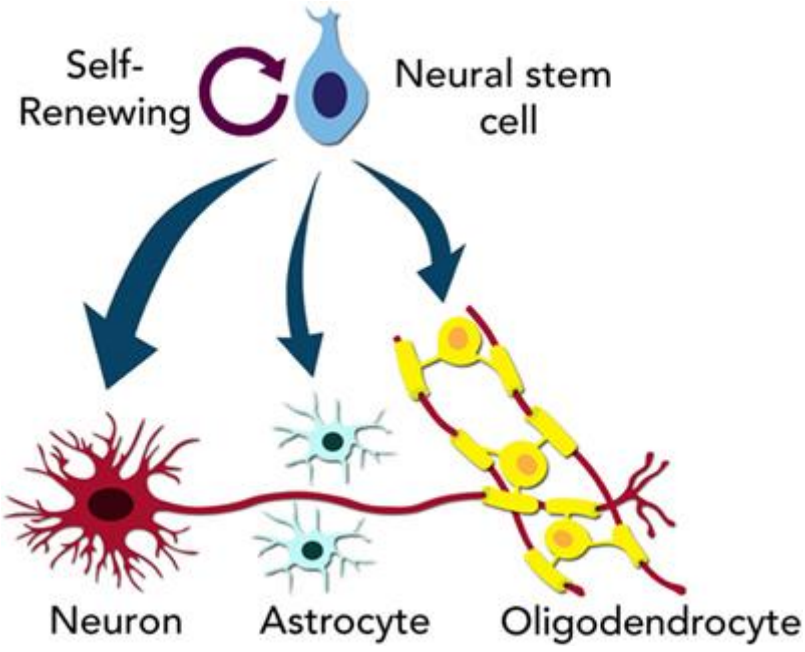

Figure 1: Neural stem cells differentiation pathway [15]

Because NSCs can differentiate into new neural cells including neurons, the regulation of their proliferation, differentiation and migration represents a promising regenerative/therapeutic strategy for Central Nervous System (CNS) diseases, including stroke. Indeed, the new neuronal cells might replace the necrotic tissue from stroke lesions and therefore improve stroke recovery. Thus, treating NSCs with pro-differentiation agent might be a promising treatment for stroke recovery therapy. To meet this goal, the agent needs to be able to reach the NSCs, and thus to cross the blood-brain barrier.

1.1.3 The blood-brain barrier

One of the main limitations for the treatment of neurological disorders is the difficulty to deliver drugs to the brain. Indeed, the brain is surrounded by the blood-brain barrier (BBB), a selective barrier formed by the endothelial cells of the cerebral microvessels [16,17]. The surface of the microvessels is the largest interface for blood-brain exchange with an average of 12 to 18 m^2 in adults [18]. The BBB is responsible for maintaining the brain homeostasis by regulating ion and nutrient transport as well as protecting the brain against neurotoxic molecules [19]. To fulfill its function, the BBB has a unique anatomy: the brain endothelial cells are joined to one another by tight junctions and do not present fenestrations [18–21]. The endothelial cells are surrounded firstly by a discontinuous layer of pericytes and secondly by the basal lamina, adjacent to the astrocyte feet (Figure 2). Unfortunately, most drugs cannot pass the BBB through physiological pathways due to the extreme selectivity of the barrier, which truly restrict systemic therapeutic treatments for most CNS diseases.

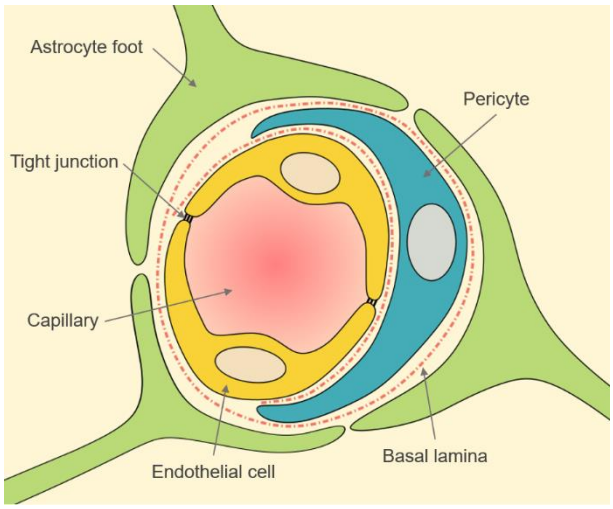

Figure 2: Blood Brain Barrier anatomy [22]

1.1.4 Crossing the BBB

As described in Figure 3, multiple pathways are available to cross the BBB. Their characteristics are described in the sections below.

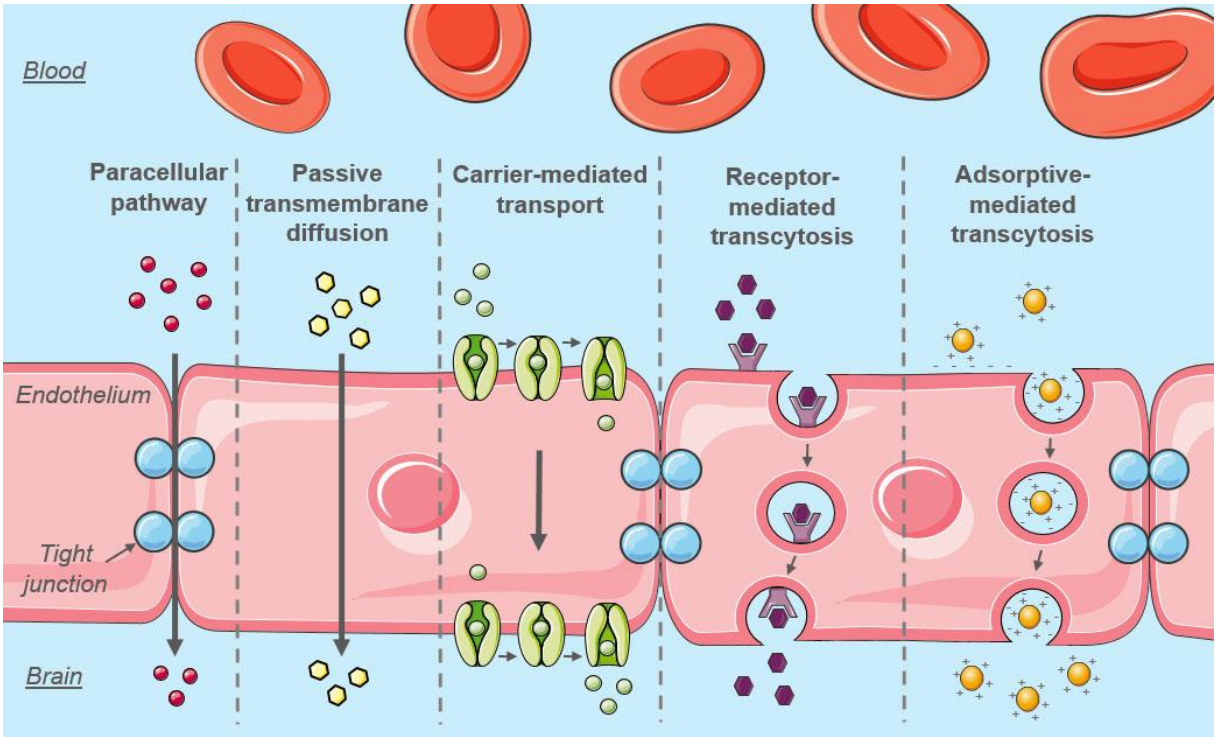

Figure 3: Physiological pathways through the BBB [22]

1.1.4.1 Paracellular pathway and passive transmembrane diffusion

The tight junctions between the endothelial cells severely limit paracellular pathway of hydrophilic molecules. Therefore, most molecules have to go through transcellular pathway to cross the BBB. However, only small lipophilic molecules with a molecular weight lower than 400 Da and less than 8 hydrogen bonds or small gas molecules (like CO_2 or O_2) can freely diffuse through the BBB by transmembrane diffusion [17]. Furthermore, the BBB endothelial cells have a low degree of pinocytic activity, which again restrains transport of molecules to the brain [16,21,23].

1.1.4.2 Transport proteins: carrier-mediated transport and efflux proteins

To assure the transport to the brain of specific molecules like nutrients or amino acids, transport proteins are present on the luminal and basolateral side of the endothelial cells. For instance, GLUT-1, large neutral amino acid transporters (LAT), nucleoside transporters and also organic cation and anion transporters have all been reported to play an important role for sustaining the brain's high metabolic needs [23–25]. Their substrates can therefore cross the BBB through carrier-mediated transport. These carriers are size and stereo selective [26].

Efflux proteins also contribute to maintaining the brain homeostasis by excreting possible neurotoxic substances. Active Pharmaceutical Ingredients (API) can also be substrates of these efflux proteins and therefore be excreted by them. Among the efflux proteins present on the BBB, the most active ones are the P-glycoproteins (P-gp) and the multidrug resistance proteins (MRP) [23,27,28]. With their ability to transport a large

variety of compounds, these efflux proteins cause a significant problem for drug delivery.

1.1.4.3 Receptor-mediated transcytosis

Endogenous molecules which do not have a specific transporter can also reach the brain through receptor-mediated transcytosis (RMT). The molecule binds to its receptor on the luminal side of the endothelial cells and endocytosis is initiated. The receptor-ligand complex is invaginated, which leads to formation of intracellular transport vesicles. The vesicles can then cross the cell to release the ligand to the basolateral side of the cell. The receptor is then recycled [29]. Some of the receptors found on the luminal side of the BBB are: transferrin receptor (TfR), insulin and insulin-like growth factor receptor, low density lipoprotein receptor (LDLR), low density lipoprotein receptor-related protein 1 and 2 (LRP1 and LRP2), scavenger receptor class B type I (SR-B1), leptin receptor, and lactoferrin receptor [26,29]. More recently, nicotinic acetylcholine receptors (nAChRS) and diphtheria toxin receptor have also been described [26,30].

1.1.4.4 Adsorptive-mediated transcytosis

Finally, one other potential physiological way to cross the BBB is through adsorptive-mediated transcytosis (AMT). Whereas RMT need an interaction between a ligand and a receptor, AMT is a non-specific pathway. Therefore, the binding affinity of AMT is low, but its binding ability is high, leading to similar transcytosis efficiency as RMT [31,32]. AMT occurs after an electrostatic interaction between a positively charged molecule, protein or peptide and the negatively charged luminal membrane of the brain

endothelial cells. It is an energy, time and concentration dependent process that last a few minutes, thus relatively slow when compared to carrier-mediated transport [33,34].

1.1.5 Enhancing nanoparticles BBB permeation with surfactant coating

To increase their BBB permeation ability, most nanoparticles are designed to be able to cross the BBB through transcytosis. To reach this goal, their surfaces have to be modified: either non-covalently with coating or covalently by functionalization.

Coating nanoparticles with surfactant was the first used method to enhance their BBB permeation ability. Indeed, the first reported nanoparticle system able to cross the BBB *in vivo* was developed by Kreuter *et al*. [35]. In their study, PBCA nanoparticles coated with polysorbate 80 (PS80) were able to successfully deliver dalargin, an anti-nociceptive peptide unable to cross the BBB by itself, *in vivo*. A significant increase of the analgesia was measured, showing that PS80-coated PBCA nanoparticles were able to deliver dalargin through the BBB to the brain. Following this discovery, different surfactants were tested to coat PBCA nanoparticles [36]. Dalargin-loaded PBCA nanoparticles were coated with polysorbate 20, 40, 60 and 80, poloxamer 184, 188, 388, 407 and 908, Brij® 35 and Cremophors® EZ and RH. Only PBCA nanoparticles coated with polysorbates showed a significant analgesic effect, where the highest effect was obtained for PS80-coated nanoparticles. Further studies showed that PS80 did not cause any toxic effects and did not disrupt the BBB at the dose used [37]. At the same time, Lück published in his thesis that apolipoprotein E (ApoE) was adsorbed on the surface of nanoparticles coated with polysorbate 20, 40, 60 or 80 after their incubation in human plasma [38]. However, ApoE was not adsorbed on uncoated nanoparticles or nanoparticles coated with poloxamer 338 and 407, Cremophor® EL

or Cremophor RH40®. Building on this work and to study the mechanism behind the PBCA nanoparticles transcytosis, dalargin-loaded PBCA nanoparticles were coated with apolipoproteins A-II, B, C-II, E and J with or without precoating with PS80 [39] and the anti-nociceptive effect of dalargin on mice was measured. A significant increase of the anti-nociceptive effect was noticed for nanoparticles coated with apolipoproteins B (ApoB) and E without precoating with PS80, showing that these apolipoproteins increased BBB crossing of PBCA nanoparticles. Interestingly, the anti-nociceptive effect of dalargin was even more pronounced for PBCA nanoparticles precoated with PS80 and overcoated with ApoB and ApoE. In the same study, loperamide-loaded PBCA nanoparticles coated with PS80 were injected to ApoE-deficient and control mice. Loperamide anti-nociceptive effect could only be observed on control mice, showing that apolipoproteins were involved in the BBB crossing mechanism of PS80-coated PBCA nanoparticles. Thus, it was concluded that PS80-coated nanoparticles could adsorb apolipoproteins selectively in the blood and cross the BBB through RMT by interacting with LDL receptors present on the luminal side of brain endothelial cells.

In another study by Kreuter's team, PBCA nanoparticles loaded with doxorubicin and coated with either PS80 or poloxamer 188 (P188) could increase survival of rats implanted with intracranial glioblastoma [40]. Interestingly, P188 coating was also able to increase the BBB permeation ability of PBCA nanoparticles. However, in their first study, P188-coated dalargin-loaded PBCA nanoparticles were not able to increase significantly dalargin anti-nociceptive effect [36]. Thus, it was proposed that the binding of doxorubicin led to an alteration of the nanoparticle surface properties that allowed ApoE and B to be bound. It was then concluded that the BBB permeation ability of nanoparticles was not only dependent of the surfactant coating but also of the nature of the nanoparticle core composition, not only of the polymer, but also of the API [41].

The ability of the surfactants to interact with apolipoproteins was confirmed in another study by Petri et al., where the efficacy of PBCA nanoparticles loaded with doxorubicin and coated with either PS80 or P188 for the treatment of rat intracranial glioblastoma was investigated [42]. The results showed that, when coated with either PS80 or P188, the anti-tumor effect of doxorubicin-loaded PBCA nanoparticles was significantly enhanced. The plasma proteins adsorbed on coated PBCA nanoparticles were investigated by 2-D PAGE and the results showed that a considerable amount of apolipoproteins A-I (Apo A-I) were adsorbed on PS80 and P188-coated nanoparticles. No significant differences of the amount of adsorbed apolipoproteins between PS80 and P188-coated nanoparticles could be observed.

Similar results were observed for PLGA nanoparticles stabilized with PS80 or P188. PLGA nanoparticles loaded with either loperamide or doxorubicin were coated with PS80 or P188 and tested *in vivo* in rodents [43]. In both cases, P188-coated PLGA nanoparticles showed the best efficacy over PS80-coated nanoparticles but both formulations were able to cross the BBB and deliver their cargo. On the other hand, in another study, 6-Coumarin loaded PLGA nanoparticles coated with either chitosan or PS80 showed better crossing ability than P188-coated nanoparticles [44]. This result seems to be in accordance with Kreuter *et al*. suggestion that nanoparticles core could influence the nanoparticles surface properties and therefore their ability to bind with apolipoproteins in the blood.

PS80 coating was also successful for PLA-b-PEG nanoparticles [45] but failed for PLA nanoparticles [46]. PLGA-PEG-PLGA nanoparticles loaded with loperamide and coated with either PS80 or P188 were compared [47]. Both formulations could cross the BBB but P188 seemed to permeate more than PS80.

In conclusion, PS80 is nowadays the gold standard for increasing BBB crossing of polymeric particles as it was shown to be able to increase apolipoprotein-nanoparticle interaction on a wide range of polymers without any toxicity to the BBB. However, alternatives, like P188, exist. Furthermore, the efficacy of the coating is also influenced by the composition of the nanoparticle core, meaning the polymer and API used.

1.1.6 Influence of size and zeta-potential

It has been shown that surface functionalization or surface coating is the most important determinant for BBB crossing. For functionalized nanoparticles, size seems to have little impact and a large variety of nanoparticle sizes has been found able to cross the BBB, from 12 to 340 nm [22]. Gao and Jiang studied in their publication the influence of the size of methotrexate-loaded PS80-coated PBCA nanoparticles on their ability to cross the BBB *in vivo* [48]. Nanoparticles from size of 70 to 345 nm were studied. Between 170 and 345 nm, no impact of nanoparticle size on brain delivery of methotrexate could be observed. Only 70 nm nanoparticles showed a slight increase in brain delivery. Indeed, it has been proven that endocytosis is a size-dependent process and that smaller nanoparticles under 100 nm can be endocytosed more easily by cells [49–51]. Moreover, it has been shown that gold nanoparticles under 15 nm were able to cross the BBB without any functionalization, probably through transmembrane or paracellular pathway, whereas gold particles bigger than 50 nm were not found in the brain [52–54]. Thus, very small particles may cross the BBB more easily.

Furthermore, after successfully crossing the BBB, size can have an impact on the diffusion of the nanoparticles through the brain extracellular space (ECS). The ECS is a well-connected foam-like structure formed from the interstitial space between neural cells [55,56]. It has been shown to have a wide variety of dimensions from 40 nm to

700 nm in local expansions, also known as “dead spaces” [55,57]. Thus, small nanoparticles can diffuse further in the ECS and therefore deliver their cargo to the brain more efficiently, whereas bigger particles might get stuck in the narrowest parts of the ECS.

As already described above, zeta-potential can also have an impact on the BBB crossing ability of nanoparticles. Nanoparticles expressing positive charges on their surface can cross the BBB through AMT. However, positively charged nanoparticles have a faster plasma clearance rate which lower their residence time in brain microvessels and therefore their brain delivery is reduced [51]. Furthermore, attention should be given to the toxicity of cationic nanoparticles, as they may alter cell membranes during adsorption. For instance, cationic gold nanoparticles have been shown to be 27 times more cytotoxic than their negative counterparts, due to the disruption of the cell membranes [58–60].

1.1.7 Pegylation

Pegylation of nanoparticles increases their circulation time by granting them “stealth” properties, thus increasing their residence time in brain microvessels and their brain delivery [61]. Pegylation alone does not allow nanoparticles to cross the BBB, as it has been shown in multiple studies [62–65]. However, coating nanoparticles with PEG allows them to better diffuse through the ECS [66]. Indeed, an important constituent of the ECS is the extracellular matrix, constituted of proteoglycans, hyaluronan and small proteins that can interact with nanoparticles and drastically hinder their diffusion [55]. By densely coating 40 and 100 nm fluorescent polystyrene nanoparticles with PEG, the nanoparticles were able to diffuse through the brain ECS of live mice, thanks to

PEG limiting the ECS-nanoparticles adhesive interactions, whereas the uncoated nanoparticles were stuck in the tissue [66]. Interestingly, neither the pristine nor the pegylated 200 nm nanoparticles could penetrate the brain tissue due to steric hindrance, confirming the importance of nanoparticle size for ECS diffusion described above. Thus, nanoparticles larger than 200 nm are able to cross the BBB but unable to move on forward and diffuse through the ECS.

1.1.8 Polymeric nanoparticles for brain delivery through the BBB

Polymeric nanoparticles are the most studied nanoparticle system for brain delivery. They can be produced from synthetic or natural polymers. Polymeric particles can cross the BBB when coated with surfactants, as described above, or after surface functionalization. To be used for brain delivery, the polymeric nanoparticles need to be biodegradable and biocompatible, thus limiting the choice of polymers. As already discussed above, PBCA nanoparticles were the first nanoparticles shown able to cross the BBB [35]. Soon after, PLA and PLGA nanoparticles demonstrated the same abilities [43]. For example, PLGA nanoparticles loaded with loperamide and functionalized with glycopeptide g7 or with a mutated form of diphtheria toxin (CRM197) have been shown to significantly increase the analgesic effect of loperamide in mice [67]. Furthermore, it was shown that CRM197 allowed the carrier system to cross the BBB by RMT as well as by up-regulation of caveolin-1 mediated transport. Investigation on g7-Nanoparticles and CRM197-Nanoparticles tropisms revealed that both formulations could reach all brain areas without impacting BBB integrity and accumulated in interneurons. Both PBCA and PLA/PLGA polymers are biodegradable and biocompatible polymers. However, PLA and PLGA present some advantages when compared to PBCA: they are FDA-approved and have a slower

degradation rate than PBCA, allowing for more sustained delivery [68,69]. Some other polymers have also been used to develop nanoparticles for brain delivery like polycaprolactone (PCL) [70] or chitosan [71,72] but in less extent than PBCA and PLA/PLGA nanoparticles. For instance, enhanced accumulation in *in vivo* intracranial glioma mice model of PEG-PCL nanoparticles functionalized with Angiopep-2 could be observed by real time fluorescence imaging [70]. Nanoparticles could be observed in the glioma bed and infiltrating margin, showing that nanoparticles functionalized with Angiopep-2 could exhibit dual-targeting abilities: first, Angiopep-2 allowed the nanoparticles to cross the BBB through RMT by recognition of LRPs on the BBB and, secondly, Angiopep-2 increased the nanoparticles accumulation in glioma cells thanks to recognition of the LRPs on the glioma cells surface.

1.2 Techniques of interest

1.2.1 Nanoprecipitation

The nanoprecipitation technique is an interesting production method for polymeric nanoparticles, which does not need any preliminary emulsification steps. This top-down technique, also called solvent-displacement method, is based on the solubility properties of the polymer. The polymer must be insoluble in water and soluble in an organic solvent miscible in water, like acetone, ethanol, tetrahydrofuran (THF) or dimethyl sulfoxide (DMSO).

First, the polymer is dissolved in the organic solvent, forming the organic phase often referred to as the “solvent solution”. The polymer solution is then added in a huge volume of water, which can also contain dissolved surfactant, referred to as the “non-solvent solution”. The organic solvent, due to its water miscibility, diffuses toward the

aqueous phase to form an organic solvent/water mixture in which the polymer is no longer soluble. As the polymer concentration is now over its thermodynamic solubility, the polymer chains precipitate to form nuclei, which then grow through addition of polymer chains on top of them, until forming nanoparticles. Finally, the organic solvent must be eliminated, for instance by evaporation or by dialysis, so that the nanoparticles can be employed safely for a therapeutic use (Figure 4) [73,74].

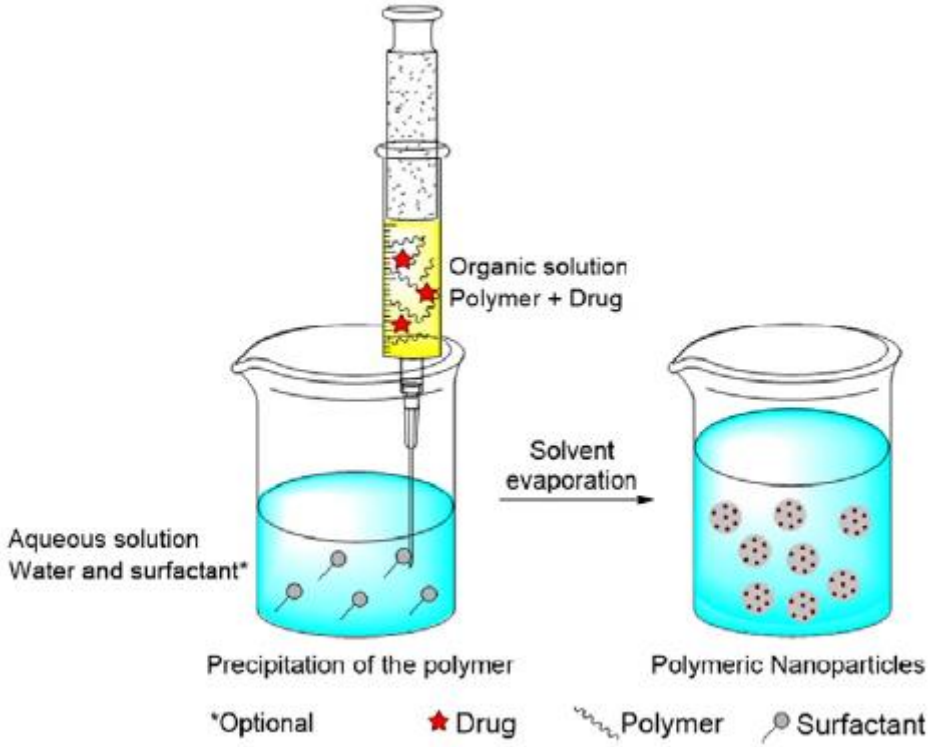

Figure 4: Nanoprecipitation method [74]

For nanoparticles to be prepared by nanoprecipitation, the organic solvent, the aqueous solution and the polymer must be mixed in precise proportions to obtain the so called “Ouzo effect”, as described on the phase diagram below (Figure 5). The Ouzo effect is a spontaneous microemulsion phenomenon, based on the phenomenon observed in Ouzo, a Greek alcoholic drink.

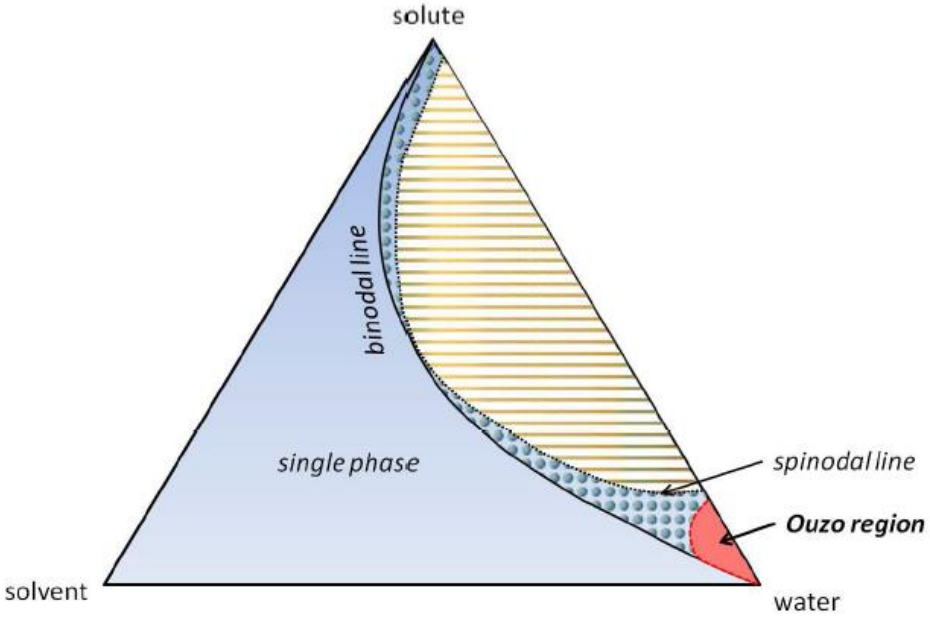

Figure 5: Ternary phase diagram showing the proportions of water, organic solvent and solute (polymer in this case) necessary to obtain nanoparticles through the Ouzo effect (red region). The continuous line is the equilibrium binodal line that separates the single-phase region (in solid blue) from the two-phase regions (dotted, striked and red regions). The dotted line is the spinodal line which separates the domain where the system evolves by nucleation (blue dots), and the domain where spontaneous phase separation occurs (yellow stripes) [75].

To be in the Ouzo region, the polymer concentration as well as the organic solvent/water ratio must be low [75]. In these proportions, independent nanoparticles can be obtained. Their size can be controlled through different factors [76]. Indeed, the diffusion speed of the organic solvent in the aqueous phase directly impacts the nanoparticle size. The better the organic solvent is miscible with water, the faster it will diffuse and the smaller the produced nanoparticles will be [77]. The viscosity of the phases can also impact the diffusion speed of the organic solvent. An excess of surfactant in the aqueous phase might increase its viscosity and thus hinder the

organic solvent diffusion and increase the nanoparticle size [78]. The polymer concentration can impact nanoparticle size in different ways. Increasing the polymer concentration increases the organic phase viscosity, as well as the number of polymer chains able to precipitate. Thus, increasing the polymer concentration leads to larger nanoparticles. Finally, the surfactant concentration; when not in excess, can decrease nanoparticles size by decreasing the surface tension and by stabilizing the polymer nuclei, avoiding their agglomeration during the process.

API are mostly added in the organic phase to encapsulate them. The more hydrophobic and ultrasaturated the API is in the aqueous phase, the more it will distribute in the polymeric nuclei during nanoprecipitation and the higher the encapsulation efficiency will be.

The internal structure of the formed nanoparticles depends on the formulation composition. Adding oil in the organic phase allows the formation of nanocapsules with an oily core [79].

1.2.2 MicroJet reactor technology

Due to its simple process, nanoprecipitation method is one of the most popular nanoparticles production method at laboratory scale. The formed nanoparticles can be tuned to obtain small size and low polydispersity index. However, the same results are harder to obtain at large scale, in batch production. To produce small nanoparticles, the mixture of the organic and aqueous phase should be fast. Furthermore, to obtain a narrow size distribution, the mixing efficacy should remain constant during the whole production process, from the first to the last drop of added organic phase. Mixing homogeneity is easy and quick to obtain with the small volumes at laboratory scale but

harder to master at industrial volumes, leading to difficulties in scale-up of the technique [80]. Nanoparticles produced at high scale might then be larger with a larger size distribution than the nanoparticles developed at laboratory scale. As the nanoparticle size is a critical quality attribute of the product, such discrepancies can hinder the development of nanoparticles for commercial use.

To solve this issue, continuous production techniques have been developed, like the MicroJet reactor® (MJR) technology from MyBiotech GmbH (Figure 6). Instead of mixing the two phases in a tank, like the batch technique, the phases are added on opposite sides of a reactor, using pumps. The two jets meet in the middle of the reactor and mixing occurs in milliseconds, leading to nanoprecipitation. The produced nanoparticles are immediately ejected by a third opening of the reactor. When using this system, mixing can be controlled from the beginning to the end of the production by managing the addition flow rate of the phases [81,82]. The nanoparticle size can be tuned by playing with the flow rates, the reactor size, or the temperature. Using a fourth opening, nitrogen gas can be added in the reactor to help the ejection of the nanoparticles out of the reactor and maintain the mixing efficiency constant. This continuous system allows the large scale production of nanoparticles by simply running the process for longer times and batch size can be easily increased via “number up”, namely running the microreactors in parallel, facilitating the translation from laboratory to industrial scale.

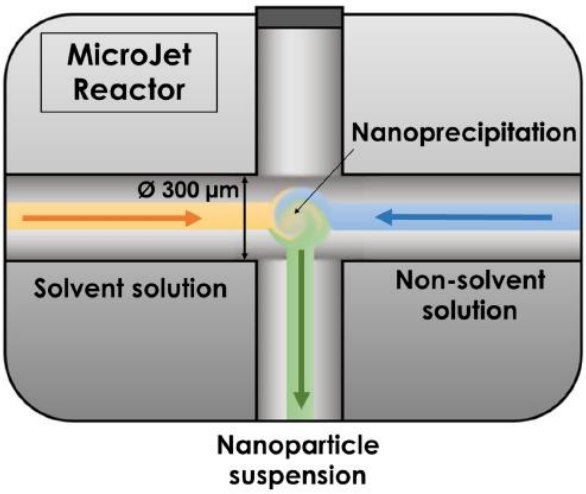

Figure 6: the MicroJet reactor® technology

1.2.3 Nanoparticle release and NanoDis System

One critical quality attribute of nanoparticles is the release kinetics of their loaded API, which must be characterized. To obtain bio-relevant data, the release must be done in medium and at a temperature representative of biologic conditions. For parenteral formulations, phosphate buffered saline (PBS) pH 7.4 is classically accepted as relevant, due to its osmolarity and pH matching human blood. Furthermore, when administered in the body, most formulations will be extremely diluted in biological fluid. To reproduce such conditions, the nanoparticle release must be performed under sink conditions, where the release is not limited by concentration gradient or by saturation, and is thus not dependent of the test conditions [83]. To be in sink conditions, the release should be performed at concentrations at least 3 times below the saturation concentration of the API in the release medium. Reaching sink conditions for poorly water-soluble substances can be a struggle, as the concentration needed is often lower than the quantification limit of the drug. Solubilizing agents like polysorbate 80 or

sodium dodecyl sulfate (SDS) might then be added in the medium to increase the solubility of the drug.

API release from polymeric nanoparticles is mostly driven by five mechanisms: detachment of API adhered to the outer layer, diffusion through the polymer matrix, membrane controlled diffusion, erosion of nanoparticles matrix or combination of diffusion and erosion process [84]. Polymeric nanoparticles are mostly formulated as sustained released systems, due to the slow degradation of the polymer in aqueous medium, leading to slow erosion of the polymer matrix. However, one phenomenon often observed with polymeric nanoparticles is an initial phase of burst release. Once diluted under sink conditions, a rapid release of the drug can occur during the first hours, due to leakage of the API located near the particle surface [85–87]. The burst release is then followed by a slower release kinetic of the API, most of the time over days [86].

Different techniques can be applied to measure the release kinetic of the drug [87,88]. Dialysis is one of the methods used in drug release testing of extended release nanoparticle formulations, ensuring the physical separation of the nanoparticles from the sampling compartment [89–92]. The nanoparticles are dispersed in release medium and filled into a dialysis bag or tube, which acts as the donor compartment. The bag is stirred in a large volume of release medium —referred to as the acceptor compartment— which allows the diffusion of the released drug from the donor to the acceptor compartment due to the concentration difference (Figure 7). The released drug can then be measured by sampling from the acceptor compartment. Despite being widely used, dialysis techniques suffer from severe drawbacks such as the permeation kinetic of the free drug through the dialysis membrane, which often limits the measured release of the API [93,94]. If the permeation kinetic of the free drug is

slower than the release rate of the drug, the amount of API found in the acceptor compartment will not reflect the real release profile of the drug at this time point [95,96]. The limited permeation of the drug through the membrane can also lead to non-sink conditions inside of the dialysis bag, thus impacting the release profile. The so-called sink conditions refer to experimental *in vitro* conditions where the maximum drug concentration in the bulk fluid should not exceed about 20-30% of the drug's saturation concentration in the respective medium [97]. In these conditions, the release from the particles is not limited by the concentration gradient or by saturation. If free drug accumulates inside the dialysis bag due to low permeation kinetics, saturation can be reached, leading to recrystallization and precipitation of the drug, thereby forming a new drug depot inside the bag instead of free API diffusing towards the acceptor compartment. Furthermore, due to the lack of agitation inside the bag, adsorption of excipients or precipitates of drug can easily occur on the membrane, further reducing the effective surface area for medium exchange and thus impacting the permeation kinetic and the measured release even more [96]. Based on the aforementioned reasons, the measured release profile, and especially the profile of the burst release, are often underestimated when using dialysis techniques.

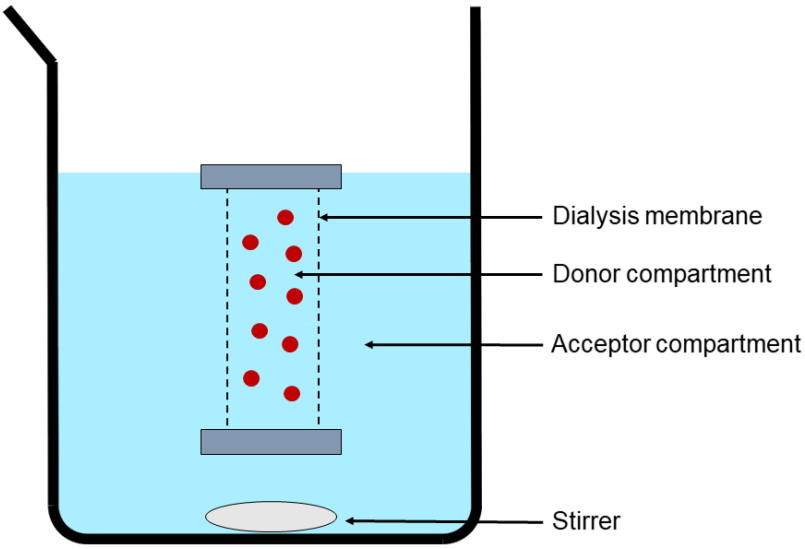

Figure 7: Dialysis set-up for nanoparticles release testing

To solve this issue, “sample and separate” methods have been developed. In these methods, the nanoparticles are directly diluted in the release medium under sink conditions and stirred. Samples are taken at various time points, nanoparticles and dissolved API are separated and the dissolved API is quantified [88,96,98]. As no dialysis membrane is necessary, the release kinetic might be measured more accurately. To achieve separation, centrifugation, filtration techniques, or centrifugal ultrafiltration devices can be employed [86,99,100]. Centrifugation techniques are only applicable for nanoparticles of sufficient density, which can be easily pelleted. As release can continue during centrifugation time, this technique might not be applicable for analysis of burst release at short time points. Use of high centrifugation speed might also lead to disruption of the carriers, and thus force release of the drug [96]. Filtration techniques can also be employed but selection of the filter must be done keeping in mind the nanoparticle size distribution, to avoid leakage of the nanoparticles through the filter [98]. Syringe filters 0.2, 0.1 or 0.02 µm can be used to filter the sample but

clogging or filter breakage may occur. Furthermore, the high mechanical strength employed to filter the nanoparticle dispersions may also lead to breakage or forced release of sheer-sensitive nanoparticles. Using centrifugal ultrafiltration devices can be an alternative to syringe filters (Figure 8). Lower molecular cut off can be used and lower mechanical stress can be employed by controlling the centrifugal speed. At high centrifugal speed, clogging and filter rupture can still occur.

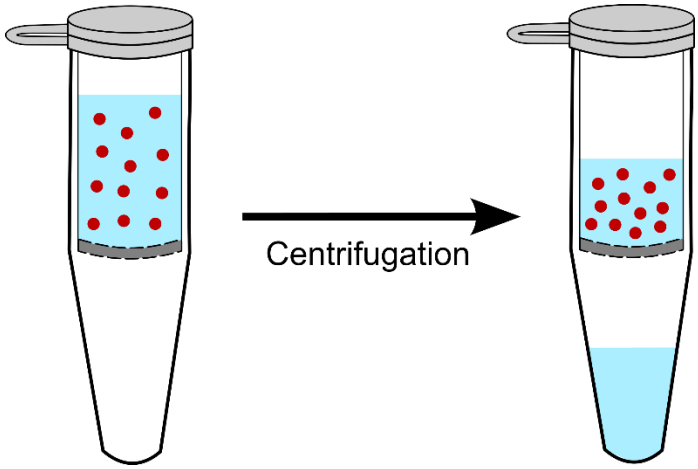

Figure 8: Centrifugal ultrafiltration set-up for nanoparticle release testing

The use of tangential flow filtration (TFF), also referred to as cross-flow filtration, can reduce clogging of the membranes. The nanoparticle dispersion feed is streamed parallel to the membrane face with one portion passing through the membrane (filtrate or permeate), whereas the remainder (retentate or concentrate) is circulated back to the feed reservoir [101]. The cross-flow prevents particle from clogging the membrane and reduces the sheer force on the nanoparticles. TFF is an efficient technique for the purification of nanoparticles and can also be employed for the separation of released drug from nanoparticles.

During the last year, a new device was developed by MyBiotech GmbH in collaboration with Agilent Technologies, Inc., the NanoDis System. The NanoDis System can be coupled with a USP II dissolution apparatus (paddle) to perform automatized nanoparticle release test by “sample and separate” technique. The nanoparticles are diluted in sink conditions in the release vessels. With the help of an autosampler, samples are taken at different time points and filtered through hollow fiber membranes by TFF. The filtrate containing the release drug can then be analyzed, while the retentate is circulated back in the vessels (Figure 9). This technique allows for a fast separation of the nanoparticles and released API, while limiting the risk of clogging or rupture of the filter membrane. Indeed, the cross flow prevents the formation of filter cakes on top of the membrane and thus its fouling [102]. As a large selection of membrane cut off are available, the NanoDis System can be used for the release test of a variety of nanoparticles. Release kinetics with the NanoDis System are thus more predictive and reproducible than those obtained using classical dialysis or filtration techniques.

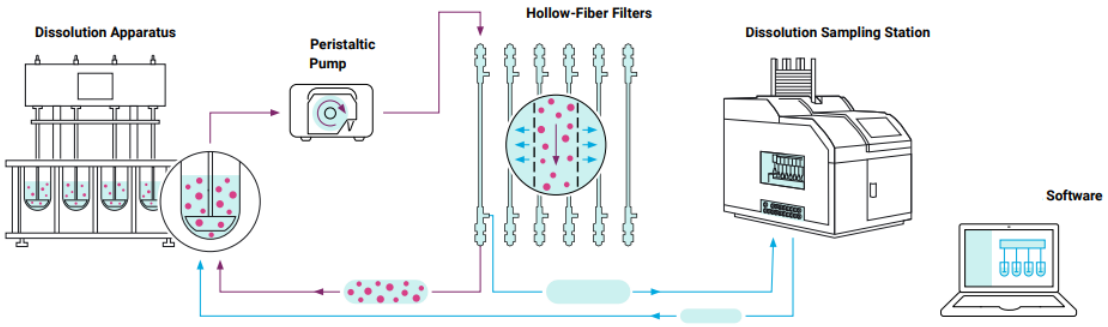

Figure 9: the NanoDis System. © Agilent Technologies, Inc. 2020. Reproduced with permission, courtesy of Agilent Technologies, Inc.

2. Aim and scope of the thesis

The goal of this PhD project is to develop poly(ester) nanoparticles able to cross the blood-brain barrier to deliver drugs to NSCs. The formulation should be able to increase the NSCs differentiation in new neuronal cells to improve stroke recovery. All-trans retinoic acid (RA) (Figure 10) has been proven to be an interesting molecule for stimulating the differentiation of NSCs in neuronal cells, both *in vitro* and *in vivo* [103,104]. RA is a molecule physiologically found in the adult CNS and heavily implicated in the CNS formation during fetal development [105]. Due to poor solubility in water (around 0.2 µM [106]), it is impossible to reach therapeutic concentration in the brain for NSC differentiation when administrating the molecule in solution through the systemic route, as therapeutic concentration for NSCs differentiation *in vitro* has been reported between 100 and 500 nM [107–109]. Loading RA in nanocarriers could solve this solubility problem and allow for the therapeutic concentration in the brain to be met. In a study by Santos *et al*., by delivering RA with the help of nanocarriers, NSCs differentiation could be obtained at a RA concentration of 4 nM, which was not possible for the molecule in solution at the same concentration [104]. Thus, loading nanoparticles with RA could also increase RA cell uptake by NSCs and thus decrease the necessary therapeutic concentration when compared to the molecule in solution. In conclusion, loading RA in nanoparticles seems to be a promising method to increase neuronal differentiation of NSCs. This PhD project will aim to develop a novel approach to target NSCs by using RA-loaded nanoparticle formulations, which will be able to diffuse across the BBB to transport drugs, reach NSCs and deliver their payload.

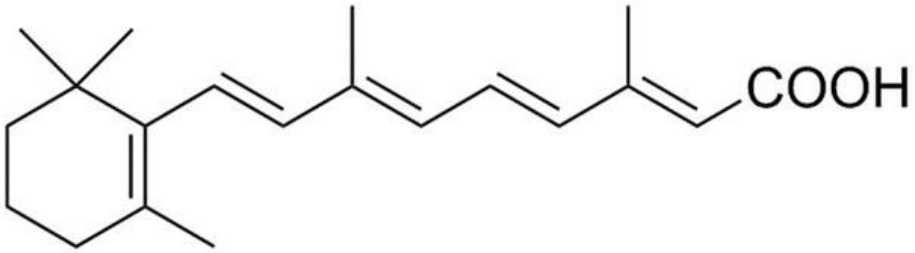

Figure 10: All-trans retinoic acid

To reduce the time for the nanoparticles to reach the market, only material approved by health agencies should be used for the production of these new delivery systems. Thus, targeting the BBB by surface functionalization is not evaluated as an option to enhance the barrier crossing properties, as it would involve covalent modifications of the material. Such modifications lead to additional safety and toxicity investigations to fulfil the regulatory requirements of novel excipients that are time and cost intensive. Instead, non-covalent BBB targeting was chosen as a strategy to improve the crossing ability of the nanoparticles: coating of polymeric nanoparticles with surfactant. PLGA, a poly(ester) polymer approved by the FDA for the parenteral route, was chosen to produce the nanoparticles. PS80 and P188, also FDA approved surfactants, were chosen to coat the nanoparticles, based on a literature review. Furthermore, the nanoparticles were produced using the MJR technology. By controlling the process parameters, the mixing properties of the solvent and non-solvent solutions can be optimized to yield reproducible nanoparticles of small size and low polydispersity index (PDI), at high scale.

First, nanoparticles loaded with a fluorescent probe were produced and tested on an *in vitro* BBB model, to assess their crossing ability through the BBB. Next, PLGA nanoparticles loaded with RA and coated with surfactants were developed and characterized.

3. Nanoparticles for in vitro BBB permeation

Cell culture and nanoparticle cell tests were performed by Elisa Jimenez Moya at Université d'Artois, as part of the partnership from the NANOSTEM project.

3.1 Introduction

PLGA nanoparticles coated with specific surfactants, polysorbate 80 (PS80) and poloxamer 188 (P188), have been reported being able to cross the BBB *in vivo* [43,44]. Studies on PBCA nanoparticles coated with the same surfactants showed that P188 and PS80 allowed the adsorption of apolipoproteins on the surface of the nanoparticles, and hypothesized that the nanoparticles could then be recognized by the LDL receptors present on the luminal face of brain endothelial cells [39,40,42]. Furthermore, discrepancies have been noticed where some formulations showed superior crossing ability when coated with P188 and others with PS80 [22], which might suggest that both surfactants do not exactly share the same uptake mechanism.

Indeed, once in biological media, nanoparticles interact with proteins, which will adsorb on their surface to form the so-called protein corona. The kind of protein corona that forms around nanoparticles surface depends on the nanoparticles surface properties (size, shape, composition, surface functional groups and charges), biophysical properties of the biological medium and the time of interaction [110]. The protein corona formation is a dynamic process. First, a layer of proteins with high affinity for the nanoparticles forms quickly by strongly bonding on the nanoparticle surface: this layer is called the hard corona. Next, proteins with lower affinity adsorb slowly by protein-protein interaction around the hard corona, forming the soft corona [111]. The soft corona can be rapidly exchanged or lost following some changes in the biological media, while the hard corona remains adsorbed, even during biological events like endocytosis [111,112]. Thus, it is believed that the hard corona gives a new biological identity to the particles in the biological environment and will determine their physicochemical behavior and biodistribution [113,114].

Contrary to surfactant-coated PBCA nanoparticles, the protein corona forming around surfactant-coated PLGA nanoparticles and the mechanism they use to cross the BBB have never been investigated, to the best of our knowledge. Thus, in this chapter, we tried to characterize the protein corona forming around PS80-coated, P188-coated and not-coated nanoparticles. PS80 and P188-coated nanoparticles were then used for *in vitro* BBB permeation studies, where their mechanisms of uptake were investigated.

3.2 Material and Methods

3.2.1 Nanoparticle production and characterization

The nanoparticles were prepared with a solvent solution containing 1% (w/v) of PLGA Resomer® RG 502 H 50:50 (Evonik, Essen, Germany) with 28 µg/ml of Lumogen F Red 305® (BASF, Ludwigshafen, Germany) in acetone. The non-solvent solution was prepared by dissolving either PS80 (Tween® 80 from Merck, Darmstadt, Germany) or P188 (Kolliphor® P188 from Sigma-Aldrich, Darmstadt, Germany) in water to obtain a 1% (w/v) surfactant solution, or with only water for not-coated (NC) nanoparticles. The nanoparticles were produced using a 300 µm reactor in a 25°C water bath. The solvent:non-solvent ratio was 1:2 with a solvent flow rate at 25 ml/min and a non-solvent flow rate at 50 ml/min (Figure 11). The nanoparticles coated with PS80, P188 and not-coated were labelled PS80 NP, P188 NP and NC NP respectively.

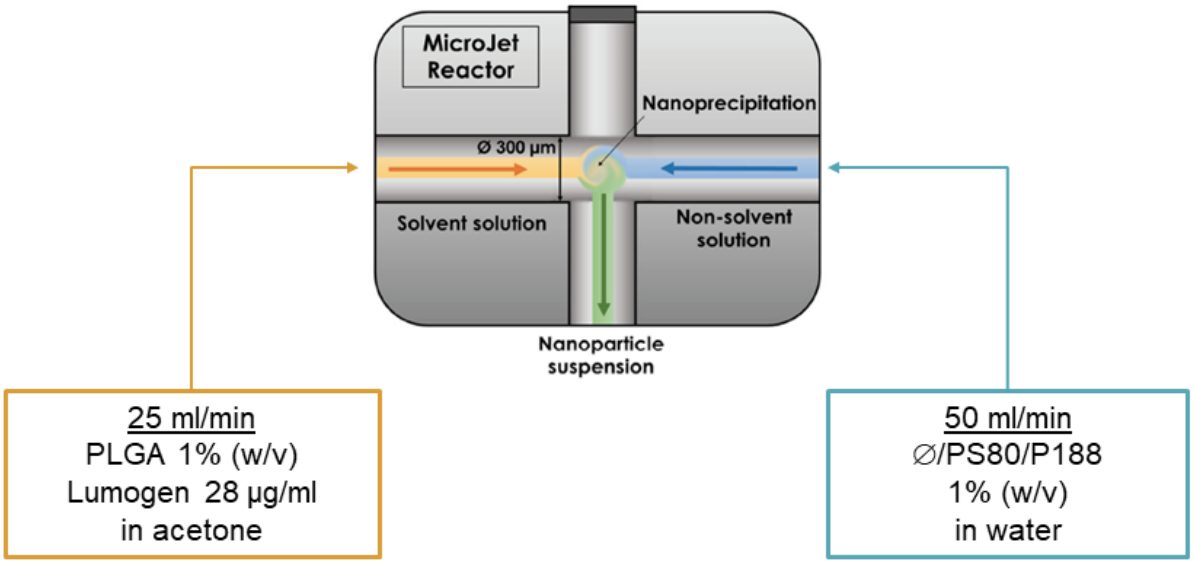

Figure 11: MicroJet reactor production of PLGA nanoparticles loaded with Lumogen F Red 305. Polysorbate 80 (PS80); poloxamer 188 (P188); no surfactants (Ø).

After this step, the nanoparticles were stirred under the hood covered in aluminum foil with small holes to evaporate acetone. To wash the excess surfactant and the free dye, the nanoparticles were washed using TFF (Figure 12). A MicroKros® hollow fiber membrane 100 kD, 20 cm² from Repligen (Waltham, USA) was used at a membrane pressure of 15 psi (1 bar). Clean water was added in the nanoparticle solution at the same rate as the filtrate was discarded to try to keep the nanoparticle solution volume, and thus concentration, constant. The dead volume of the system was taken into account when measuring the volume of the solution and recovered at the end of the process. The NC and P188 NP were washed with a volume of water 6 times the volume of the nanoparticle suspensions, while the PS80 NP were washed with 12 volumes of water, to completely remove all non-encapsulated Lumogen.

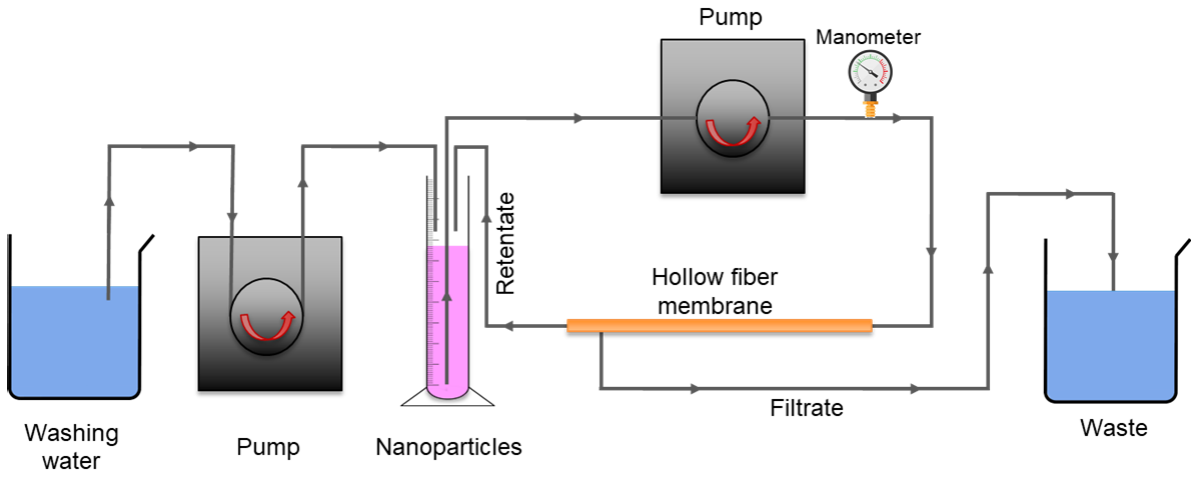

Figure 12: Tangential flow filtration set-up. With a peristaltic pump, the nanoparticles dispersion is filtered through a hollow fiber membrane, adjusting the flow rate to reach a membrane pressure of 1 bar. The nanoparticles cannot cross the membrane and are recovered in the retentate, which is circulated back in the nanoparticles' reservoir. The free dye, excess of surfactant or free polymer chains cross through the membrane in the filtrate and are discarded. Clean water is added with the help of a second pump at the same flow rate as the filtrate flow rate, to keep the concentration in the nanoparticle reservoir constant. The process is stopped after recovering either 6 or 12 times the starting volume of the nanoparticle dispersion in the filtrate.

After purification by TFF, the nanoparticle size was measured by dynamic light scattering (DLS), using a Zetasizer ZS90 from Malvern Instruments (Malvern, United-Kingdom).

3.2.2 Protein corona analysis

3.2.2.1 Size measurement of protein layer

PS80, P188 and NC NP were incubated for 1h30 at 37°C by diluting them 10-fold in different media: endothelial cell medium (ECM, Sciencell, Carlsbad, USA) supplemented with 5% (v/v) fetal calf serum (FCS, Sciencell, Carlsbad, USA), 1% (v/v) endothelial cell growth supplement (Sciencell, Carlsbad, USA) and 0.5% (v/v) gentamicin (Biochrom AG, Berlin, Germany), this medium was labelled ECM (5%FCS);

ECM supplemented with 5% (v/v) human serum (obtained from "l'Etablissement Français du Sang" (EFS), following an agreement with Artois University), 1% (v/v) endothelial cell growth supplement and 0.5% (v/v) gentamicin, labelled ECM (5%HS); or pure human serum. The size of the nanoparticles and media as control were measured by DLS after incubation, after dilution in water. Nanoparticles incubated in water were used as control.

For the nanoparticles incubated in ECM (5%FCS), to wash away the soft corona, the nanoparticles were centrifuged at 2,400 g for 5 min. The supernatant was removed, and the nanoparticle pellets were resuspended in distilled water and measured again by DLS. PS80-NP were also washed one, two or three times by centrifugation at 2,400 g for 3 min. The nanoparticles incubated in ECM (5%HS) and human serum were also measured after washing by centrifugation: the nanoparticles were centrifuged at 13,000 g for 45 min, their supernatants were discarded, and the pellets were redispersed with distilled water.

3.2.2.2 BCA assay

BCA assay was performed on PS80 and P188 NP incubated for 1h30 at 37°C after dilution 10-fold in pure human serum. After incubation, the nanoparticles were washed either one, two or three times by centrifugation to remove the soft corona and the free proteins from the serum. The nanoparticles were centrifuged at 14,000 g for 45 minutes. The supernatants were discarded and the pellets were redispersed in water by sonication and vortexing. The washed nanoparticles-protein corona complexes were analyzed with a QuantiPro™ BCA protein assay kit (Sigma-Aldrich, Darmstadt, Germany) to quantify the amount of proteins in each sample, using a linearity curve

made with human serum albumin (Sigma-Aldrich) as reference. In a 96-well plate, 150 µl of sample and 150 µl of reagent were added and the plate was incubated at 60°C for 1 hour. The plate absorbance was then read at 562 nm with a Tecan™ plate reader (Männedorf, Switzerland). Nanoparticles incubated in water and centrifuged the same way were used as negative control.

3.2.2.3 SDS-PAGE

SDS-PAGE was also performed to characterize nanoparticle protein corona, following a protocol described by Docter *et al*. [115]. After incubation for 1h30, 37°C, in human serum or ECM (5%HS), the nanoparticles were washed 3 times with PBS pH 7.4 by centrifugation at 13,000 g for 30 min, to isolate the nanoparticle-protein complexes. Next, the nanoparticle pellets were redispersed in SDS-PAGE sample buffer (prepared at 3X and diluted by 3 in water before use, 3X buffer contains 62.5 mM Tris base, 10% (v/v) glycerol, 2% (w/v) SDS, 50 mM dithiothreitol and 0.01 % (w/v) bromophenol blue salt) and boiled for 5 min at 95°C, to denaturate the proteins. The samples were centrifuged again at 13,000 g for 30 min and the supernatants, containing the desorbed proteins from the protein corona, were recovered for analysis. Controls were prepared by diluting pure human serum by 100 and ECM (5%HS) by 5 in SDS sample buffer, to reach approximately 600-800 µg/ml of proteins (human serum has a mean protein concentration of 60-80 mg/ml), and boiling them 5 min at 95°C. The samples were prepared in triplicates. 20 µl of each sample were deposed on a 12% (w/v) Tris-Glycine SDS gel and separated at 13 mA per gel, in SDS running buffer (3 g Tris, 14.4 g glycine, 10 ml 10% (w/v) SDS in 1 l of distilled water). The gels were stained overnight with Coomasie blue (BioRad, Feldkirchen, Germany) and then destained for 4 hours in 10% (v/v) MeOH, 10% (v/v) glacial acetic acid in distilled water. On each gel, a protein

ladder PageRuler™ Plus Prestained (10-250 kDa) from Thermo Scientific (Waltham, USA) was run.

3.2.3 Human *in vitro* BBB coculture models

Human in vitro BBB coculture models experiments were performed at NanoSTEM project partner Université d'Artois by Elisa Jimenez Moya.

Human BBB *in vitro* models were produced using human brain-like endothelial cells (BLECs), derived from $CD34^{+}$hematopoietic stem cells isolated from human umbilical cord blood according to the method described by Pedroso *et al*. [116]. The protocol was approved by the French Ministry of Higher Education and Research (reference: CODECOH DC2011-1321) and the sample collection was obtained under the written and informed consent from the donor's parent of umbilical cord blood, in accordance with the French Legislation. Once isolated from umbilical cord blood, CD34+-cells were differentiated *in vitro* into endothelial cells (ECs) using endothelial cell growth medium (EGM; Lonza Walkersville, MD, USA) containing 50 ng/mL vascular endothelial growth factor (PeproTech, Rocky Hill, USA) and 20% fetal calf serum (FCS; Sigma Aldrich, St Louis, USA). BLECs were obtained after non-contact coculture with brain pericytes (PCs) [117,118], using Transwell® (TW) systems.

Different TW system formats were used to develop the human BBB *in vitro* models in this study. A miniaturized and automated model in 96 multiwell system was used for nanoparticle screening at different concentrations and time-points [119]. This model was developed as a replicate from a well-established and patented model from Cecchelli *et al*. [120]. Moreover, the original model in 12 TW format in a syngeneic form was used for the nanoparticles' uptake and transport experiments. The miniaturized

model was developed in 96 multiwell insert systems (Falcon, Corning Life science, Massachusetts, USA. Plates 1 µm Polyethylene Terephthalate (PET); 0.0804 cm^2 cell growth surface area) as a coculture with bovine pericytes [117] by automated seeding of 15,000 PCs per well, and 18,000 ECs per filter, using a Multiflo robot (BioTek Instruments, Winooski, USA), while the syngeneic original model was developed in 12 TW plates (Corning, New York, USA. Plates 0.4 and 3 µm Polycarbonate (PC) filters; 1.12 cm^2 cell growth surface area) as a coculture with human pericytes provided by Professor Takashi Kanda's group (Department of Neurology and Clinical Neuroscience, Yamaguchi University Graduate School of Medicine, Ube, Japan) [118]. The cells were seeded by hand 50,000 PCs per well, and 80,000 ECs per filter.

To produce the human coculture BBB models, brain PCs were seeded on bottom well plates coated with pig gelatin (2 mg/L; Sciencell, Carlsbad, USA) for bovine PCs, and with rat tail type I collagen for human PCs (10 µg/cm^2; Corning, New York, USA) in ECM (5%FCS) medium. The cells were incubated during 3h at 37 °C. Next, $CD34^+$-derived ECs were seeded on TW inserts coated with Matrigel™ diluted by 1/48 (v/v) (BD Biosciences, San Jose, USA) and immediately cocultured with brain PCs seeded on the bottom wells of the plates. However, to generate the coculture model in 3 µm porosity filter, the 80,000 $CD34^+$-derived ECs were seeded on TW inserts one week before their coculture with the PCs [121]. The medium was renewed every 2 days. On day 5 of coculture, 24 hours before incubation with the nanoparticles, ECM (5%FCS) was substituted by ECM (5%HS). After 6 days of coculture with brain pericytes, the BBB endothelial cells acquired the BBB phenotype (named brain-like endothelial cells (BLECs) at that stage) and were used for the following experiments.

3.2.4 BBB integrity evaluation after nanoparticles treatment

BBB integrity evaluation after nanoparticles treatment experiments were performed at Université d'Artois by Elisa Jimenez Moya.

The BLECs physical integrity was evaluated by measuring the diffusion of the integrity marker sodium fluorescein (NaF; Sigma Aldrich, Darmstadt, Germany), a small hydrophilic molecule which poorly crosses the intact BBB. Human BBB miniaturized models were used for the evaluation of the impact of the nanoparticles on the BBB integrity, at different concentrations and time-points. The nanoparticles were diluted in ECM (5%HS) to reach a concentration of 5, 10, 25, 50, and 100 µg/ml of nanoparticles. The nanoparticles were added in the luminal compartment of the BLECs inserts and incubated during 3, 6, and 24 hours at 37°C. BLECs incubated in ECM (5%HS) without nanoparticles for 24h were used as negative control. As positive control of BBB disruption, a neurotoxic compound, Rotenone (Sigma Aldrich, Darmstadt, Germany), was also incubated during 24h [119,122]. At the end of the incubation time, the BLECs physical integrity was evaluated by measuring NaF diffusion. To do so, the BLECs inserts were transferred into new 96 TW systems (Falcon HTS 96 square well; Corning Life science, Massachusetts, USA) containing 300 µl of Ringer-HEPES (RH) buffer (150 mM NaCl, 5.2 mM KCl, 2.2 mM CaCl2, 0.2 mM MgCl2·6H2O, 6 mM NaHCO3, 5 mM HEPES, 2.8 mM glucose; pH 7.4) per well which constituted the abluminal compartment. The cell culture medium from the BLECs inserts containing nanoparticles dilution was removed, and 70 µl of RH solution containing 1 µM NaF (the integrity marker) were added in the upper (luminal) compartment. RH was used to avoid any interference of the cell phenol red media with NaF. The cells were incubated at 37°C for 1 hour. Next, aliquots from the lower and upper compartments were collected, as well as from the stock solution at time zero. Their fluorescence at

excitation/emission wavelength 490/525 nm was measured using a fluorimeter (Synergy H1; BioTek, Winooski, VT, USA) in a 96-well plate. The endothelial permeability coefficient (Pe) of NaF was calculated in cm/min. The clearance principle was used to obtain a concentration-independent index of transport. Briefly, the mean volume cleared was plotted against time, and the slope was estimated by linear regression. The permeability values of the inserts (PSf, for inserts with a Matrigel coating only) and the inserts plus BLECs (PSt, for inserts with Matrigel coating and cells) were taken into consideration by applying Equation 1:

$$1/PSe = 1/PSt - 1/PSf \quad \textbf{(1)}$$

To obtain the endothelial permeability coefficient (Pe, in cm/min), the permeability value (PSe) corresponding to the endothelium alone was then divided by the insert porous membrane surface area (S) (S= 0.0804 cm^2 cell growth surface area for 96 TW system, or S= 1.12 cm^2, for 12 TW plates) (Equation 2).

$$Pe = PSe/S \quad \textbf{(2)}$$

3.2.5 Cell visualization by confocal microscopy

This part was performed partly at Université d'Artois by Elisa Jimenez Moya. Only the CLSM imaging from 3.2.5.4 was performed at Saarland University by Sonia Lombardo.

3.2.5.1 Cell fixation

BLECs were fixed on their inserts and PCs were fixed on the bottom wells using paraformaldehyde 10% (PFA; Sigma-Aldrich, Darmstadt, Germany) for 10 minutes. Then, the cells were washed 3 times during 5 minutes with calcium and magnesium-free phosphate buffered saline (PBS-CMF).

3.2.5.2 Immunocytochemistry

After cell fixation, permeabilization was done with Triton 0.1% (w/v) (Sigma-Aldrich, Darmstadt, Germany) and the cells were again washed 3 times during 5 minutes with PBS-CMF. Cells were incubated with SEA BLOCK blocking buffer (Thermo Fisher Scientific; Massachusetts, USA) for 30 minutes. BLECs were incubated away from light for 1h at room temperature with primary antibodies against zonula occludens-1 (ZO-1) (Invitrogen; Thermo Fisher Scientific; Massachusetts, USA), diluted by a factor of 200 in PBS-CMF supplemented with 2% (v/v) normal goat serum (NGS). After three washing steps with 2%NGS-PBS-CMF, BLECs were incubated with secondary antibodies for 30 min at room temperature using goat anti-rabbit Alexa Fluor 488 (Invitrogen, Massachusetts, USA; dilution: 1/500 in 2%NGS-PBS-CMF). Nuclei were stained using Hoechst reagent (Sigma-Aldrich, Darmstadt, Germany) diluted 1,000 times in the same secondary antibody solution. Finally, the cells were washed 3 times during 5 minutes with PBS-CMF. Filters with BLECs for miniaturized model were directly placed in the microscope, while 12 TW inserts were cut and mounted on a glass slide under a coverslip. Stained preparations were observed with an ImageXpress Micro Confocal High-Content Imaging System (Molecular devices, San Jose, CA, USA), using blue DAPI filter (excitation/emission wavelength 358/461 nm) for nuclei, green fluorescein isothiocyanate (FITC) filter (excitation/emission wavelength 480/530 nm) for ZO-1. Images were processed in MetaXpress software version 6.5.2 (2018, Molecular Devices, LLC, San Jose, CA, USA).

3.2.5.3 Visualization of nanoparticles

Human BBB miniaturized model was used for the visualization of the nanoparticles of different concentrations at incubation time-points. Thus, the nanoparticles were diluted in ECM (5%HS) at concentrations of 5, 10, 25, 50 and 100 µg/ml of nanoparticles. The nanoparticles were added in the luminal compartment of the BLECs inserts and incubated during 3, 6, and 24 hours at 37°C. At the end of the nanoparticles incubation time, BLECs inserts were rinsed 5 times with cold RH, and fixed as described above. Nuclei were stained using Hoechst reagent diluted by 1,000 in 2%NGS-PBS-CMF for 15 min at room temperature, away from light. Inserts with BLECs from the miniaturized 96 TW systems were placed directly on the microscope, visualizing the BLECs from the abluminal face. Nanoparticles were observed using a red Texas Red filter (excitation/emission wavelength 580/620 nm); and nuclei using a blue DAPI filter (excitation/emission wavelength 358/461 nm) using ImageXpress Micro Confocal High-Content Imaging System (Molecular devices, San Jose, CA, USA). Images were processed in MetaXpress software version 6.5.2 (2018, Molecular Devices, LLC, San Jose, CA, USA).

3.2.5.4 Early endosomes staining for nanoparticles colocalization study

For nanoparticles colocalization study, 12 TW models (0.4 µm filters) were used. After the end of the 30 min incubation period, BLECs inserts were rinsed 5 times with cold RH, and cells were fixed as described above. Primary antibodies against early endosome vesicles (EEA-1) (Invitrogen, Massachusetts, USA) diluted by 100 in 2%NGS-PBS-CMF were incubated for 2h at room temperature, away from light. After

three washing steps in 2%NGS-PBS-CMF, the samples were incubated with secondary antibodies for 30 min at room temperature (goat anti-rabbit Alexa Fluor 488, Invitrogen, Massachusetts, USA; dilution: 1/500 in 2%NGS-PBS-CMF). Finally, the cells were washed again three times for 5 minutes with PBS-CMF. Filters were cut and mounted on a glass slide with a drop of DAPI mounting medium (Thermo Fisher Scientific; Massachusetts, USA) under a coverslip. BLECs were observed from the luminal face. Stained preparations were observed by confocal microscopy using a Zeiss Axio Observer LSM 710 Scanning Module coupled with ZEN 2 (blue edition) software (Zeiss, Jena, Germany). The nanoparticles were visualized with an excitation/emission wavelength 561/629 nm, detection range 603-656 nm. The EEA-1 stained with Alexa Fluor 488 was visualized with an excitation/emission wavelength 488/525 nm, detection range 496-554 nm. The nuclei stained with DAPI were visualized with an excitation/emission wavelength 405/459 nm, detection range 410-507 nm.

3.2.6 Nanoparticles uptake and internalization mechanisms

3.2.6.1 Nanoparticles uptake studies

For nanoparticles uptake studies, both miniaturized and 12 TW models (0.4 µm filters) were used. After incubation time was reached BLECs inserts were rinsed 5 times with cold RH in order to remove the nanoparticles not internalized stucking on the cell surfaces. Then, cells were lysed using RIPA buffer (Pierce^{TM}, Thermo Scientific, Massachusetts, USA). Aliquots of 25 µl (for 96 TW systems) and 200 µl (for 12 TW model) were collected from each insert. Fluorescence analysis was done in a black color 96-well plates (Thermo Scientific, Massachusetts, USA) at sensitivity 110,

excitation/emission wavelength 578/613 nm, using a Synergy™ H1 fluorimeter (BioTek Instruments, Winooski, VT, USA).

3.2.6.2 Nanoparticles co-incubation with other molecules

Human BBB model in 12 TW plates (0.4 µm filters) were used in this experiment. To evaluate a possible receptor competition, nanoparticles were diluted at 10 µg/ml in ECM (5%HS) and were mixed with either Alexa Fluor 488 acetylated low density lipoproteins (acLDL) (Fisher Scientific, New Hampshire, USA) or Bodipy^{FLTM} low density lipoproteins (LDL) (Fisher Scientific, New Hampshire, USA), both molecules internalized by receptor-mediated endocytosis [123]. Instead of acLDL and LDL, the nanoparticles were also incubated with Inulin-FITC (Sigma Aldrich, Merck KGaA Darmstadt, Germany), a molecule with non-specific vesicular transport, [124,125], at 15 µg/ml. Molecule-nanoparticle mixtures were added on BLECs and incubated for 1 hour at 37°C. Cells incubated with nanoparticles only were used as uptake control. Nanoparticles cell uptake was measured as described above.

3.2.6.3 Cell metabolism experiments

This experiment was performed using human BBB model in 12 TW plates (0.4 µm filters). BLECs were pre-incubated at 4°C for 90 minutes to stop their metabolism. Then, the nanoparticles were diluted to 10 µg/ml in ECM (5%HS), added to the luminal compartment, and incubated for 1 hour at 4°C. Nanoparticles cell uptake was measured as described above. Inulin-FITC, used as negative control, was incubated at a concentration of 15 µg/ml, and Alexa Fluor 488 acLDL at 15 µg/ml as positive control.

3.2.6.4 Inhibitors of transport

Both formats, the miniaturized BBB model and the 12 TW model, were used for these experiments. A set of transport inhibitors were tested to assess their effects on endocytic transport [126–128]. Preliminary tests of a wide concentration range of inhibitors (from Sigma Aldrich, Merck KGaA Darmstadt, Germany, except for FCCP (Carbonyl cyanide 4-(trifluoromethoxy)phenylhydrazone) purchased from Abcam, Cambridge MA, USA) were done, to assess their toxic impact on the BLECs. After optimization, BLECs were pre-incubated for 45 min at 37°C with the following inhibitors: FCCP at 20 µM, inhibitor of ATP dependent active transport; filipin III at 5 µg/ml and genistein at 30 µg/ml, both inhibitors of caveolae endocytic routes; dynasore hydrate at 400 µM and chlorpromazine hydrochloride at 20 µg/ml, both inhibitors of clathrin-mediated endocytosis; 5-(N,N-dimethyl)amiloride hydrochloride (dimethylamiloride) at 60 µM and cytochalasin D at 1 µM, both inhibitors of macropinocytosis. All inhibitors were diluted in ECM (5%HS). Next, nanoparticles were added in the luminal compartment at 10 µg/ml and incubated for 1 hour. Nanoparticles cell uptake was measured as described above.

3.2.7 Nanoparticles crossing through BLECs

Crossing studies were performed using the 12 TW format (3 µm filters) as previously described [121]. One day before the experiment, ECM (5%FCS) was substituted for ECM (5%HS) phenol red-free (PRF) (ref. 1001-prf; Sciencell, Carlsbad, USA) (ECM (5%HS)-PRF), in order to facilitate nanoparticles detection within the cell medium. Then, nanoparticles were diluted to 10 µg/ml in ECM (5%HS)-PRF and added to the luminal compartment and incubated for 3, 6 and 24 hours. At the end of the

incubation times, aliquots from the luminal (L) and abluminal (A) compartments were taken, as well as samples from the initial dilution (t0). Fluorescence was measured in a black color 96-well plate (Thermo Scientific, Massachusetts, USA) at sensitivity 110, excitation/emission wavelength 578/613 nm, using a Synergy™ H1 fluorimeter (BioTek Instruments, Winooski, USA). The background emitted by the medium was subtracted and the percentage of crossing (Equation 3) and nanoparticles recovery (Equation 4) were calculated using the following equations:

$$\%\text{Crossing} = 100 \times (\text{Quantity A (tx)} \div \text{Initial Quantity (t0)}) \quad \textbf{(3)}$$

$$\%\text{Recovery} = 100 \times (\text{Quantity A (tx)} + \text{Quantity L (tx)}) \div \text{Initial Quantity (t0)} \quad \textbf{(4)}$$

3.3 Results and discussion

3.3.1 Nanoparticle production and characterization

PLGA nanoparticles, coated with PS80 (PS80 NP) or P188 (P188 NP) or not-coated (NC NP), labelled with a fluorescent probe Lumogen F Red 305®, were prepared using the MJR technology. All nanoparticle formulations, with and without surfactant coating, had sizes close to 65 nm and negative zeta potential due to the carboxylic acid end groups of PLGA (Table 1). Using the MJR technology allowed the formation of small nanoparticles with low PDI, easy to upscale for industrial production. The formulations were tailored to obtain nanoparticles lower than 100 nm, as it has been reported that small nanoparticles could be endocytosed more easily by the brain endothelial cells and then further diffuse through the brain extracellular space [48,66]. These formulations could therefore be promising delivery systems for the brain, able to be produced at large scale and to efficiently deliver cargo through the BBB without need of functionalization.

Table 1: Nanoparticles size and zeta potential (n=3)

Nanoparticles	Size (nm)		PDI		Zeta Potential (mV)	
	Mean	SD	Mean	SD	Mean	SD
PS80 NP	65.9	1.7	0.14	0.01	-29.1	1.7
P188 NP	63.0	0.3	0.14	0.04	-32.4	3.9
NC NP	64.1	1.8	0.15	0.01	-38.5	1.1

During purification by TFF, no Lumogen was seen in the filtrate of P188 NP and NC NP, while the filtrate of PS80 NP was pink, revealing that Lumogen was not completely loaded inside of the nanoparticles. PS80 probably formed micelles loaded with Lumogen, which decreased the loading of the dye inside of the particles. Purifying the PS80 nanoparticles with 12 times their starting volume allowed the complete removal of the micelles from the formulation, while only 6 volumes were necessary for P188 and NC nanoparticles, to simply remove excess of surfactant or free polymer.

3.3.2 Protein corona analysis

3.3.2.1 Size measurement

First, the protein corona forming around the nanoparticles was studied by DLS after incubation in ECM supplemented with either FCS or human serum, or in pure human serum.

Incubation in ECM (5%FCS): ECM (5%FCS) alone did not show any particles when measured by DLS and therefore did not interfere with nanoparticle size measurements.

All nanoparticle sizes increased significantly after incubation in ECM (5%FCS), probably due to the formation of a protein corona around the nanoparticles (Figure 13). PS80 NP size increased by 258 nm, from 66 nm to 324 nm after incubation in cell medium, P188 NP by around 70 nm and NC NP by 44 nm. Both surfactant-coated nanoparticles had a significant higher size increase than NC NP. Furthermore, PS80 NP size increased significantly more than P188 NP. Thus, the nanoparticles seemed to have different protein corona profile forming around them in ECM (5%FCS), where PS80 NP might have the thickest protein layer. The PDI of the all the nanoparticles incubated in ECM (5%FCS) increased slightly from 0.1-0.2 in water to 0.2-0.3 in cell medium, but did not show differences between formulations.

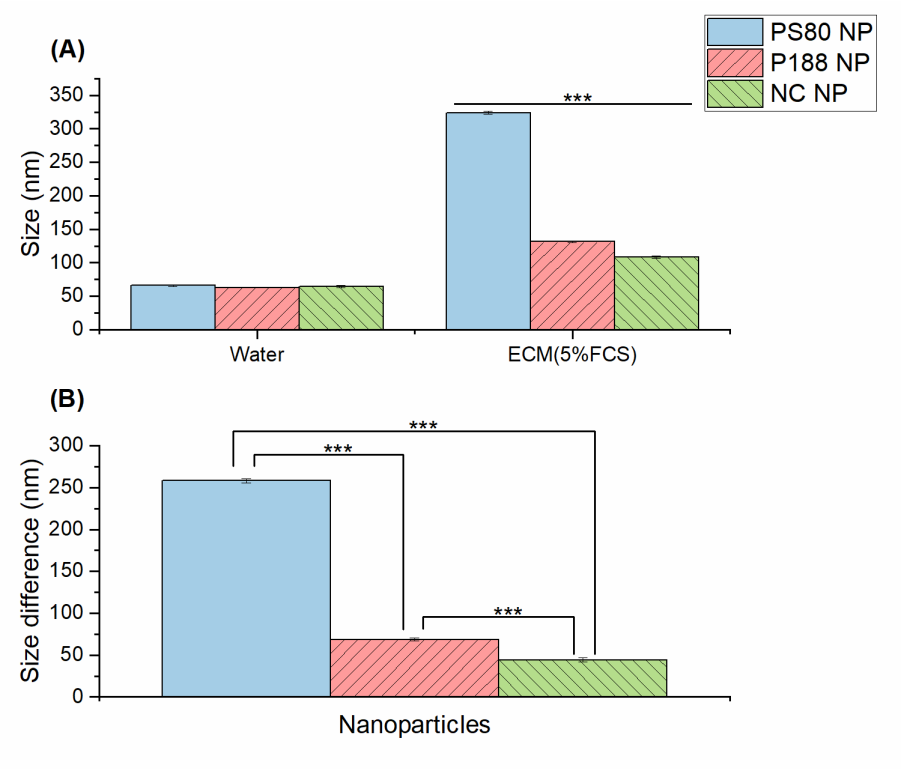

Figure 13: Protein corona size analysis after incubation in ECM (5%FCS). **A.** Nanoparticles size after incubation in water or in ECM (5%FCS). Independent two-samples t-test, ****p-value*< 0.0005, n=3; **B.** Nanoparticles size difference between incubation in ECM (5%FCS) and water. One-way ANOVA followed by Tukey test, ****p-value*< 0.0005, n=3.

The next step was to try to observe the hard corona. For this purpose, the soft corona composed of unspecific proteins interacting lightly with the nanoparticles had to be remove. To wash away the soft corona, the nanoparticles were centrifuged and redispersed in water. If the soft corona was removed, nanoparticle size was expected to decrease. The nanoparticles incubated in water did not sediment at the mild centrifugation speed used whereas the nanoparticles incubated in ECM (5%FCS) could be pelleted. The supernatants were removed, and the nanoparticle pellets were resuspended in distilled water. P188 and NC NP size increased greatly after this washing step, probably due to agglomeration during centrifugation. Even at the mildest centrifugation conditions possible (1,900 g, 5 min), agglomeration still occurred. It was therefore impossible to observe the hard corona of these formulations (Figure 14). Only PS80 NP did not agglomerate during centrifugation. However, no size decrease that would indicate the removal of the soft corona could be observed, suggesting that this washing process might not be strong enough to remove the soft corona.

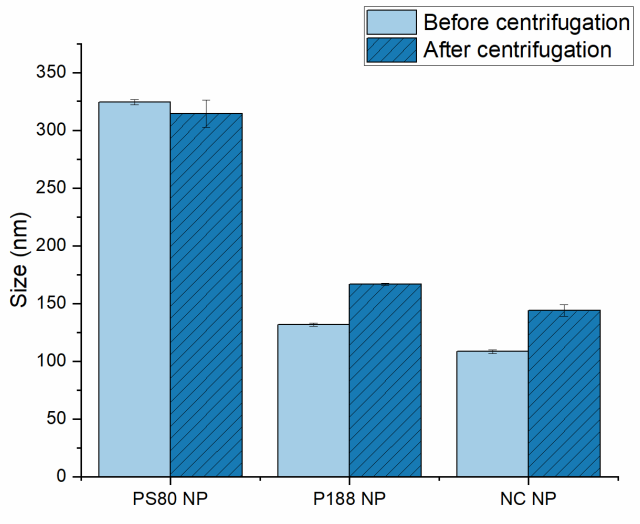

Figure 14: Nanoparticles size after incubation in ECM (5%FCS), before and after centrifugation (n=3).

In another experiment, to see if the soft corona could be removed with more washing steps, PS80 NP were incubated and then centrifuged and washed once, twice or thrice at 2,400 g for 3 minutes. The nanoparticle size was measured and compared (Figure 15).

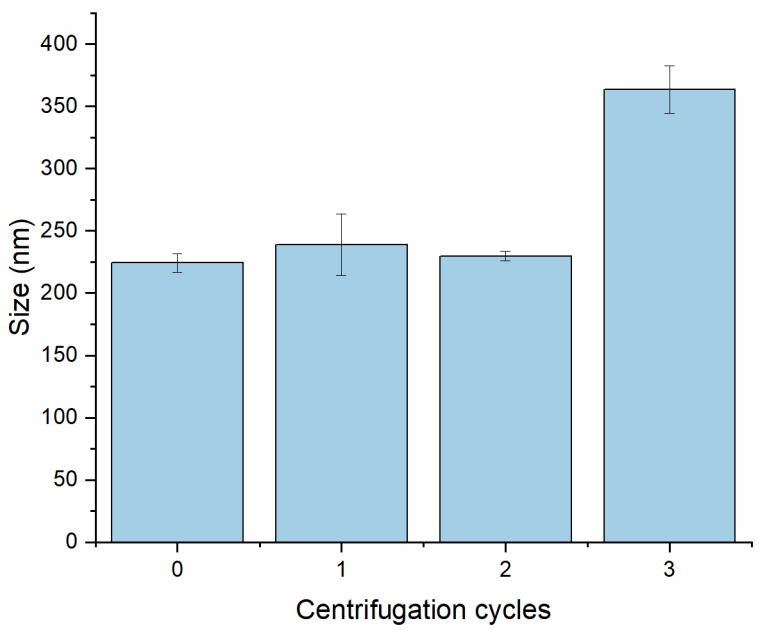

Figure 15: PS80 NP size after incubation in ECM (5%FCS), depending on number of centrifugation cycles (n=3).

Up to two centrifugation/washing steps, the nanoparticle size remained unchanged, whereas after three washing steps, agglomeration occurred. Thus, a maximum of two washing cycles could be applied on PS80 NP, which did not lead to a size decrease of the nanoparticles. The mild washing conditions used were possibly not strong enough to remove the soft corona from the particles. However, stronger centrifugation force could not be applied, to avoid agglomeration of the nanoparticles. Another explanation for the lack of size decrease could be that the size difference between the soft and hard corona was too small and could not be detected by DLS. Moreover, the dilution in water of the samples before their measurement by DLS might have also led to the

disruption of the soft corona. Then, only the hard corona could be measured, thus explaining the lack of size difference after washing.

Incubation in ECM (5%HS) and pure human serum: human serum and ECM (5%HS) were diluted the same way as the nanoparticles and measured by DLS, as controls. Both media had particle sizes of their own with high PDI, which gave too much background for accurate measurement of the nanoparticle size. Indeed, after incubation, the nanoparticles had high particle size, close to the one of the medium alone, with high PDI over 0.4 in ECM (5%HS) and over 0.7 in human serum (Figure 16). Probably, the high content in proteins in human serum led to proteins agglomerates which could be measured by DLS and thus interfere with the measurements of the nanoparticles.

It was therefore attempted to wash the nanoparticles by centrifugation, to isolate the nanoparticles from the media. The nanoparticles incubated in ECM (5%HS) could not be redispersed without agglomeration after centrifugation, even at the mildest settings. Thus, the nanoparticles could not be isolated from the medium and their nanoparticle size could not be accurately measured. The nanoparticles incubated in pure human serum could be pelleted by centrifugation and resuspended in water twice before starting agglomerating. The nanoparticles after one washing step showed still presence of the serum background, whereas after the second washing step, a monomodal distribution could be obtained. The nanoparticles size increased compared to nanoparticles incubated in water, but no significant difference in nanoparticle size could be observed between the three formulations (Figure 17). The nanoparticle size in human serum after washing was significantly smaller than in ECM (5%FCS) for P188

and PS80 NP, especially for PS80 NP. This difference could be explained by the difference in composition of both media, in the type of proteins and their quantity.

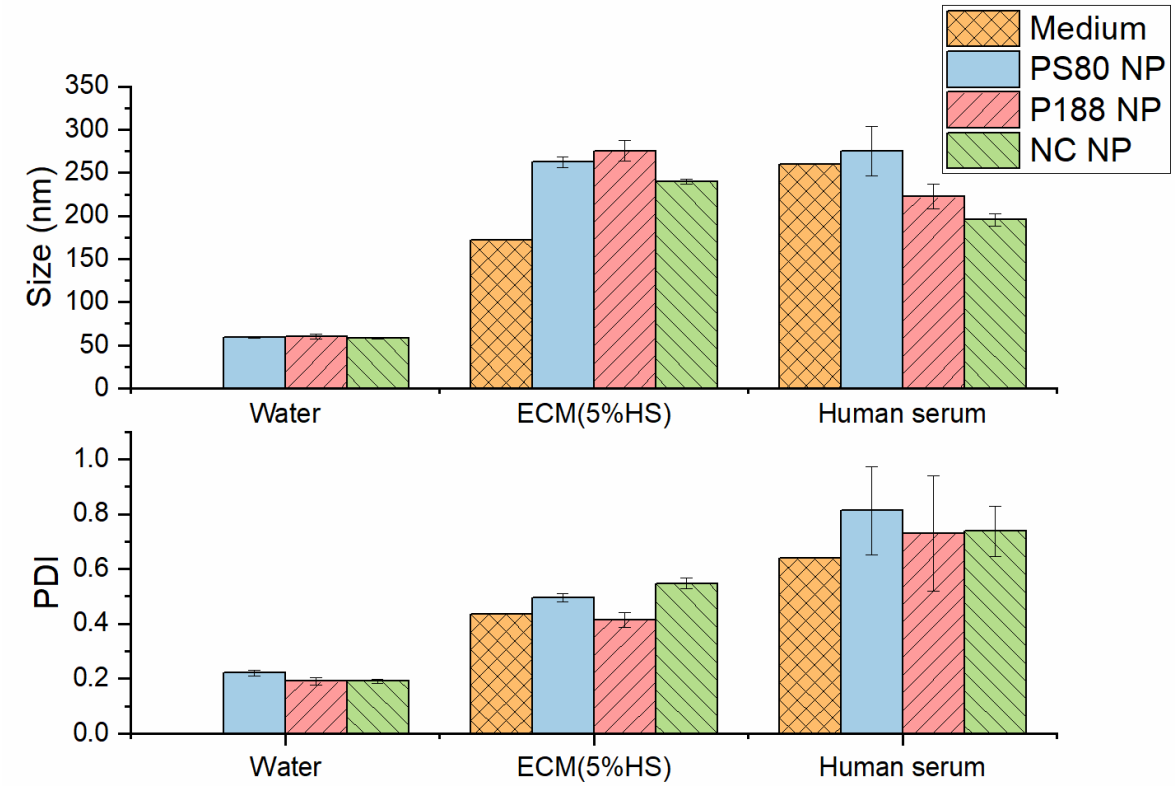

Figure 16: Nanoparticles size and PDI after incubation in ECM (5%HS) or pure human serum. As control, ECM (5%HS) and pure human serum without nanoparticles (labelled medium) were also measured (n=3 for nanoparticles, n=1 for medium).

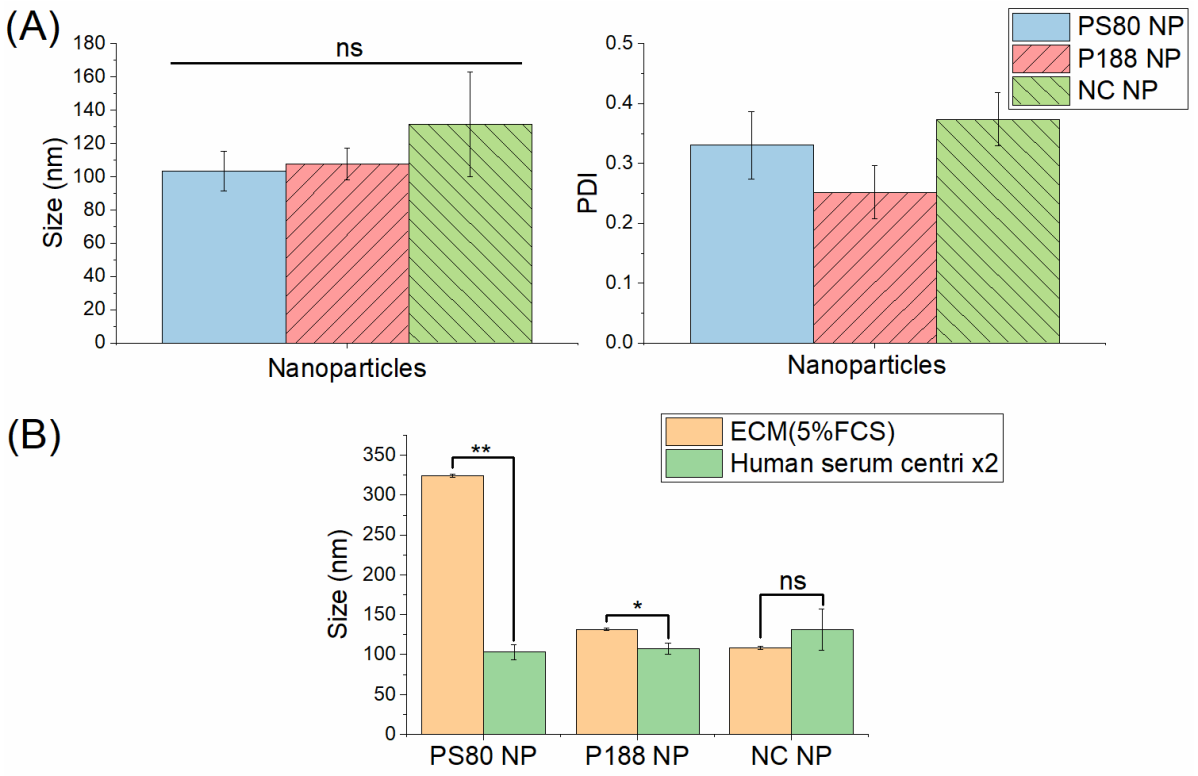

Figure 17: A. Nanoparticles size and PDI after incubation in human serum, washed by two centrifugation cycles in water. ns= not significant, one-way ANOVA *p-value*>0.05, n=3. **B.** Size comparison of nanoparticles after incubation in ECM (5%FCS) and human serum, washed by two centrifugation cycles. Two samples t-tests, ***p-value*<0.005, **p-value*<0.05, n=3.

3.3.2.2 BCA assay

The nanoparticles incubated in human serum were washed by centrifugation, isolated and the amount of protein adsorbed on their surface were quantified by BCA assay (Figure 18). Nanoparticles incubated in water and centrifuged the same way were used as negative control and did not show any absorbance. PS80 and P188 NP pellets could be redispersed by vortexing and sonication in water.

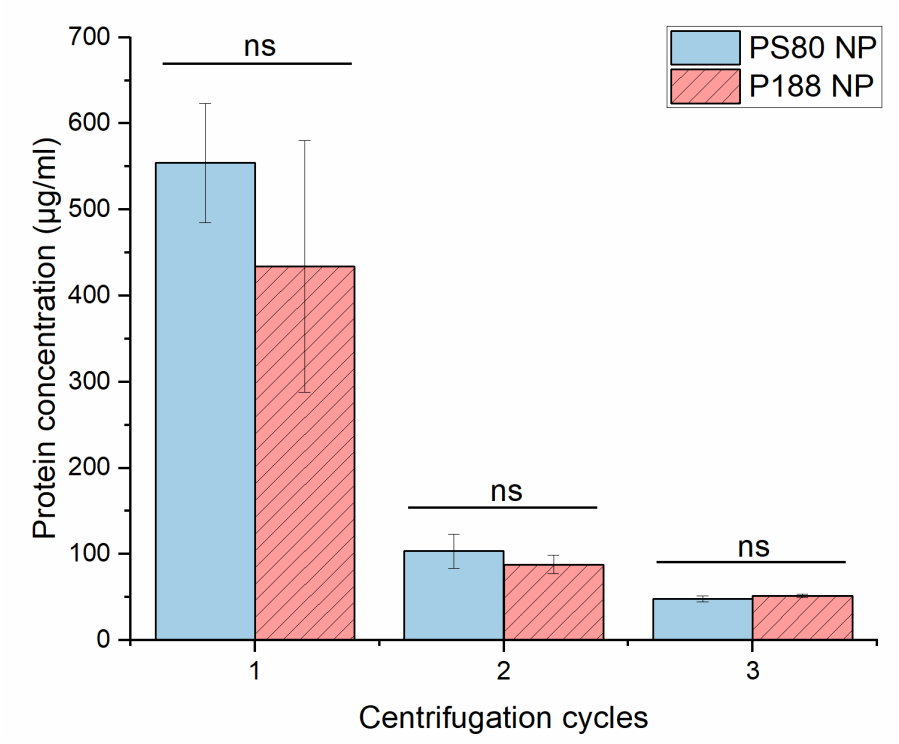

Figure 18: Protein concentration of protein-nanoparticle complexes after incubation in human serum for 1h30, depending on nanoparticle formulation and centrifugation steps. ns= not significant, independent two samples t-tests, *p-value*>0.05, n=3.

Centrifugation removed part of the free proteins from the medium and the proteins adsorbed on the surface of the particles, until reaching a concentration of around 50 µg/ml for PS80 and P188 NP after three centrifugation cycles. No significant difference could be observed between the amount of protein adsorbed on PS80 and P188 NP, at all washing steps. Hence, PS80-NP and P188-NP seems to have similar amount of proteins adsorbed on their surface after incubation 1h30 in human serum, confirming what was observed with DLS, where no size difference could be seen.

3.3.2.3 SDS-PAGE analysis

After incubation in pure human serum or in ECM (5%HS), the nanoparticles were washed and their protein corona were desorbed and denaturated, isolated and

analyzed by SDS-PAGE (Figure 19). No differences could be observed in the protein corona profiles of the three formulations after incubation in both media. Compared to the diluted media, the protein corona of the nanoparticles contained less albumin (70 kD). Furthermore, their protein corona seemed to be enriched in low molecular weight proteins, between 35 and 25 kD, which could correspond to the molecular weight of apolipoproteins A-1 and E (28 and 34 kD respectively). Nanoparticles incubated in pure human serum had a protein corona composition close to the one observed in ECM (5%HS) but enriched in high molecular weight proteins around 70-100 kD. The lack of differences observed between the formulations and between the media could come from the poor resolution of SDS-PAGE, which might not be precise enough to reveal slight differences in composition between the protein corona profiles.

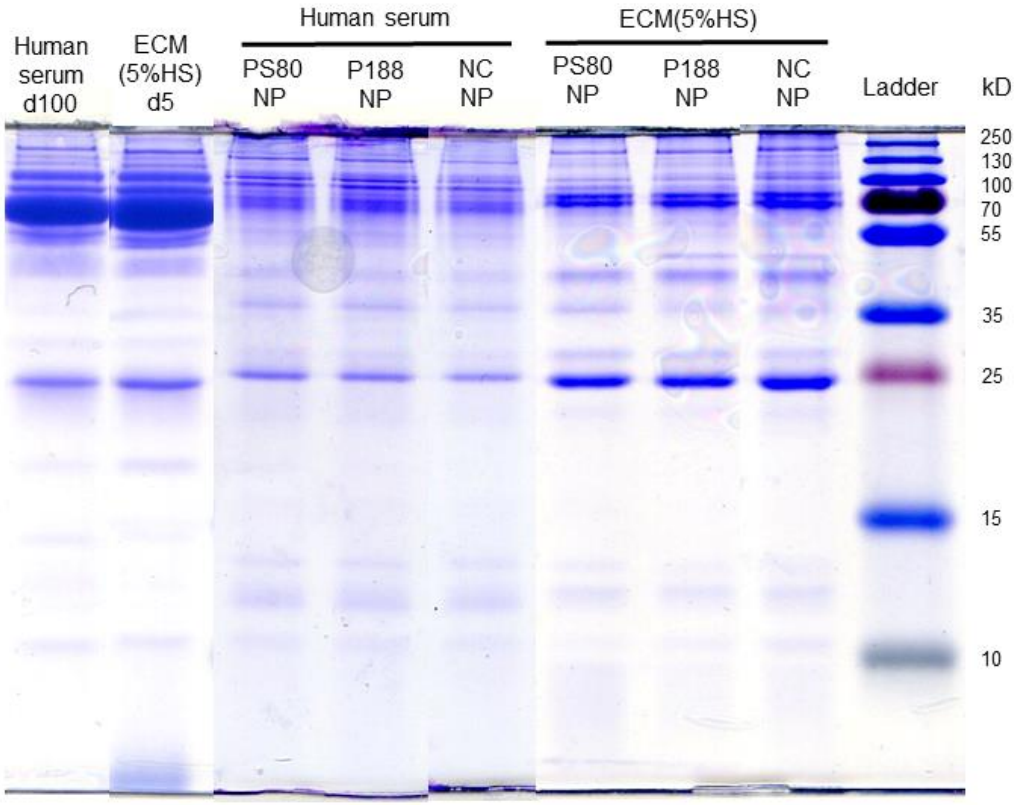

Figure 19: SDS-PAGE gels of proteins desorbed from the nanoparticle surfaces after incubation in either pure human serum or ECM (5%HS).

To summarize the protein corona studies performed in this chapter, except during DLS analysis of nanoparticles incubated in ECM (5%FCS), no differences could be seen between the protein corona profile of NC, PS80 and P188 nanoparticles. Maybe the techniques employed here were not precise enough to detect small changes in the protein corona in complex medium containing human serum. Otherwise, in ECM (5%FCS), it seemed that PS80 nanoparticles had the largest protein corona, compared to NC and P188 nanoparticles.

3.3.3 Human BBB *in vitro* models development

To study the nanoparticles crossing through the brain endothelial cells and uptake mechanism, a patented and well established human BBB *in vitro* model [119,120], based on $CD34^+$ stem cells-derived endothelial cells ($CD34^+$-ECs) co-cultivated with brain pericytes [117,118] was used. In addition, for this nanoparticle interaction study with the BLECs, the fetal calf serum used as a supplement in the cell medium was replaced by human serum 24 hours before performing nanoparticles assays (Figure 20.A), since it has been shown that nanoparticles interact not only with the cells but also with components present in the media, like the serum proteins to form their protein corona [129]. This corona is believed to have a huge effect on the biodistribution of nanoparticles by impacting the cell recognition of the formulation [110,130]. Hence, to obtain results that could be more easily translated to human blood *in vivo*, the fetal calf serum classically used in the cell medium was substituted 24 hours before experiments with human serum, to work with a nanoparticle protein corona profile closer to the one expected to form in human blood. Hence, after a coculture of 6 days, the BBB phenotype of the $CD34^+$-ECs was validated by the presence of zonula occludens-1 (ZO-1) expression, a protein involved in the tight junctions and located continuously at

the edge of these cells (Figure 20.B). Moreover, the impact of the change in serum composition on the BLECs layer integrity was controlled using NaF, an integrity marker. No significant differences were found between the models supplemented with FCS or HS. Hence, FCS could be replaced by HS without inducing disruption of BBB properties during the experimental conditions.

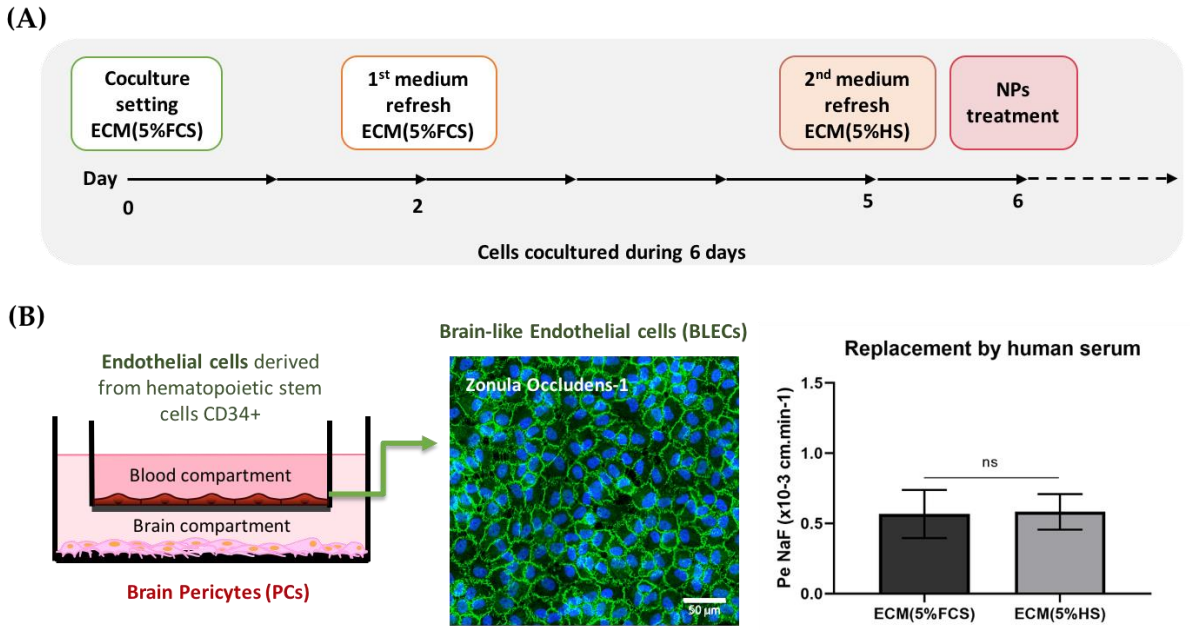

Figure 20: Human BBB *in vitro* model characteristics and conformation. **A.** Human *in vitro* BBB model cell culture protocol. Two days after cell thawing in ECM (5%FCS), brain-like endothelial cells (BLECs) were cultured on the luminal side of the insert in a non-contact coculture with brain pericytes (PCs), seeded on the plates, the abluminal side of the setup. First medium refresh was done 2 days after the coculture setting. Then, 24h before nanoparticles studies, a second medium refresh was done using ECM supplemented with 5% human serum. **B.** After 6 days of coculture, BLECs were visualized by immunostaining of zonula occludens-1 (ZO-1), a protein involved in the tight junctions (scale bar = 50 µm). Endothelial permeability coefficient (Pe) to sodium fluorescein (PeNaF) of the coculture model supplemented with ECM (5%FCS) as control, or with ECM (5%HS). ns = not significant. unpaired t-test, *p-value*>0.05, n=6; N=2.

3.3.4 BBB integrity evaluation after nanoparticles treatment

By using the BBB miniaturized system, the evaluation of nanoparticles interaction within BLECs depending on concentrations and time was performed. The BBB integrity was evaluated by calculating the permeability coefficient of the integrity marker NaF after incubation with nanoparticles from 5 to 100 µg/ml, for 3, 6 and 24 hours. Filters without nanoparticles treatment incubated during 24h acted as negative control. Rotenone, a neurotoxic compound, was incubated for 24h and used as a BBB breakdown control. No significant differences in the BLECs permeability to the integrity marker (Pe^{NaF}) between the control (no nanoparticles) and both nanoparticles formulation, PS80 and P188 NP over the different concentrations and time-points studied could be observed (Figure 21). The BBB tightness integrity was not impacted, hence nanoparticles treatment did not show toxicity in the range of concentrations and time points tested up to 100 µg/ml and 24h incubation. Therefore, PLGA nanoparticles demonstrated good biocompatibility with the BBB model, as no BBB integrity disruption could be observed at a maximum concentration of 100 µg/ml up to 24h of incubation time.

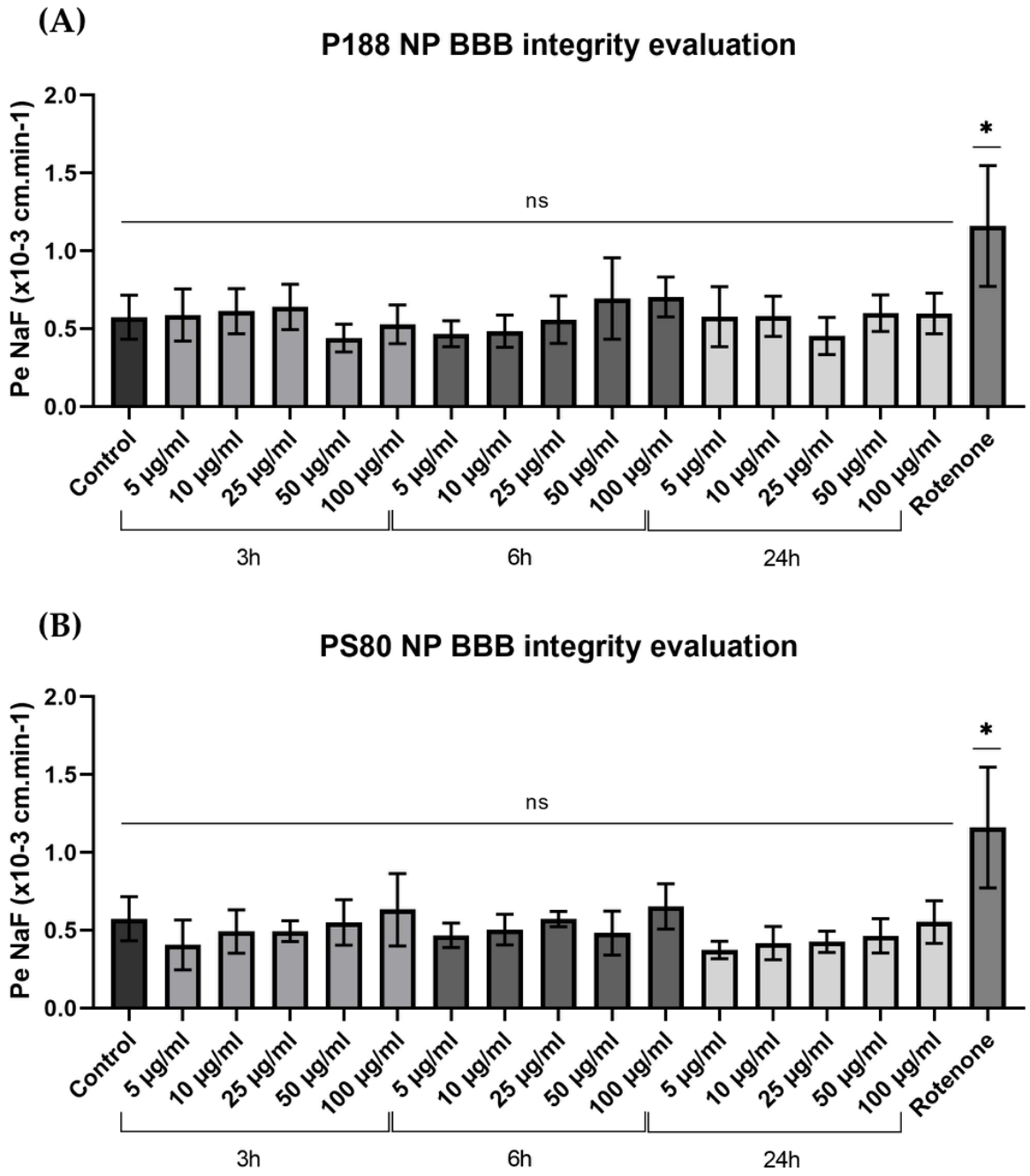

Figure 21: Endothelial cell permeability coefficient (Pe) values of NaF after incubation with nanoparticles. **A.** Evaluation of BBB integrity after P188 NP incubation. **B.** Evaluation of BBB integrity after PS80 NP incubation. Unpaired t-tests versus negative control were performed, **p-value*<0.05, ns = not significant. Control and samples n=5, N=2 independent experiments; Rotenone (n=2, N=2).

3.3.5 Evaluation of PS80 and P188 coated PLGA nanoparticles transport pathway

3.3.5.1 Nanoparticles internalization and visualization within BLECs

By using the automated ImageXpress Micro Confocal High-Content Imaging System, both formulations could be seen in the cell cytoplasm of BLECs at different concentrations (5 to 100 µg/ml) and incubation times (3, 6 and 24h) (Figure 22), meaning that both surfactant-coated PLGA nanoparticles could be internalized by the BLECs. From visual inspection, NPs seemed to present two different profiles. Due to fluorescence saturation in concentration above 50 µg/ml and after 24h of incubation, quantitative information cannot be extracted. However, P188 NP uptake seemed to be faster than PS80 NP, whose uptake seemed less dependent on time and concentration.

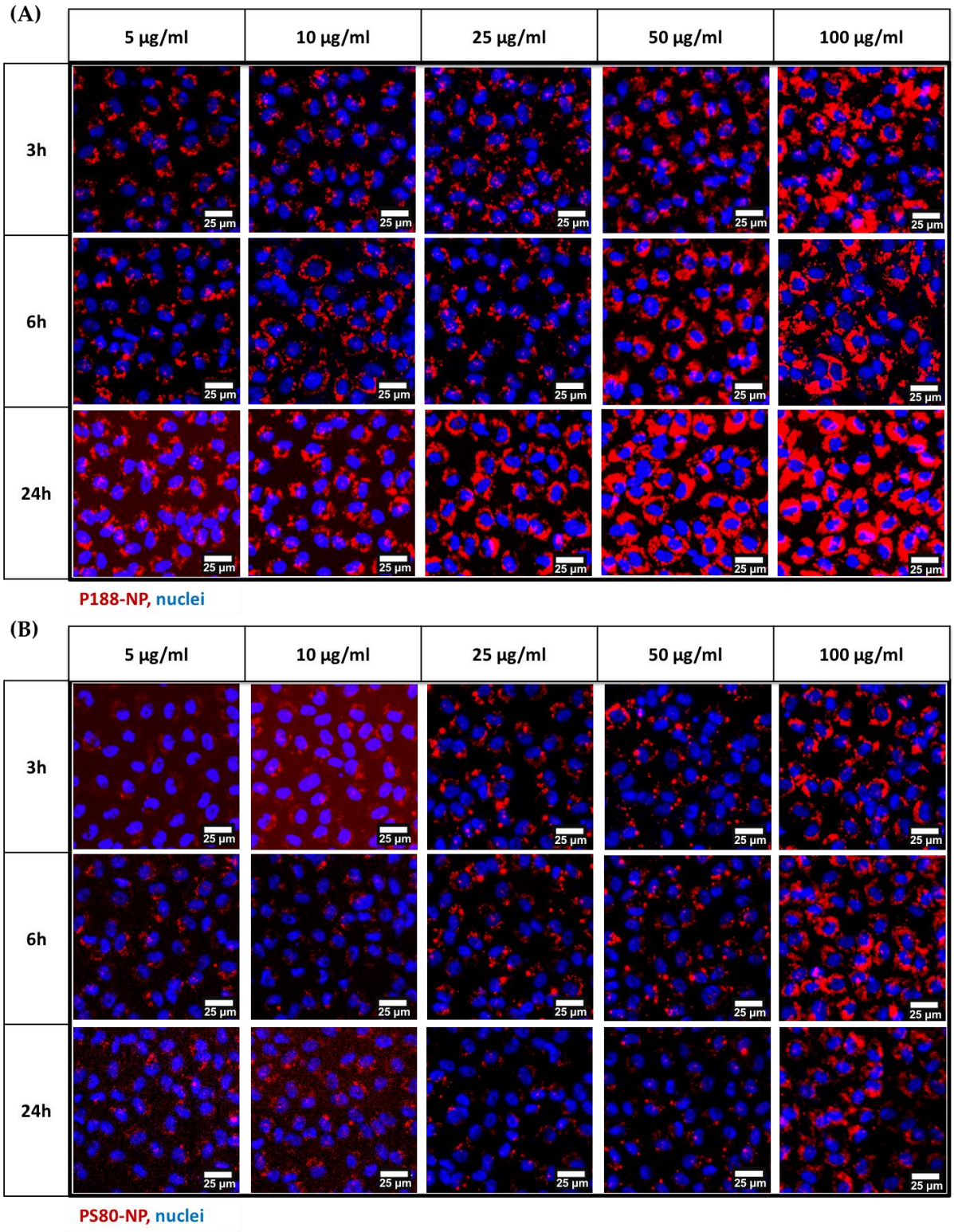

Figure 22: Confocal images of nanoparticles within the BLECs at different concentrations and incubation times. **A**. BLECs incubated with P188 NP. **B**. BLECs incubated with PS80 NP. Both nanoparticles visualized as red dots, cell nuclei staining in blue. Scale bar = 25 µm.

3.3.5.2 Nanoparticles uptake profile

The uptake profiles of the formulations were also evaluated at low concentrations and short time, by cell lyses. BLECs were incubated with the nanoparticles, lysed, and the fluorescence intensity of the loaded dye was quantified (Figure 23). First, the nanoparticles uptake was studied depending on their concentration, from 5 to 25 µg/ml to avoid fluorescence saturation within the BLECs, for 90 minutes. The formulations showed again two different profiles. After 90 min of incubation, P188 NP was uptaken in significantly higher quantities than PS80 NP by the BLECs, at 10 and 25 µg/ml (Figure 23.A). Moreover, P188 NP uptake increased with nanoparticles concentrations and incubation time after 60 minutes (Figure 23.B). Meanwhile, PS80 NP uptake was not impacted by incubation time or by concentration, the uptake seemed to be already maximal at the lowest concentration and time tested, around 3%. However, P188 NP could be uptaken more readily by the BLECs up to 30% at 25 µg/ml, after 90 min.

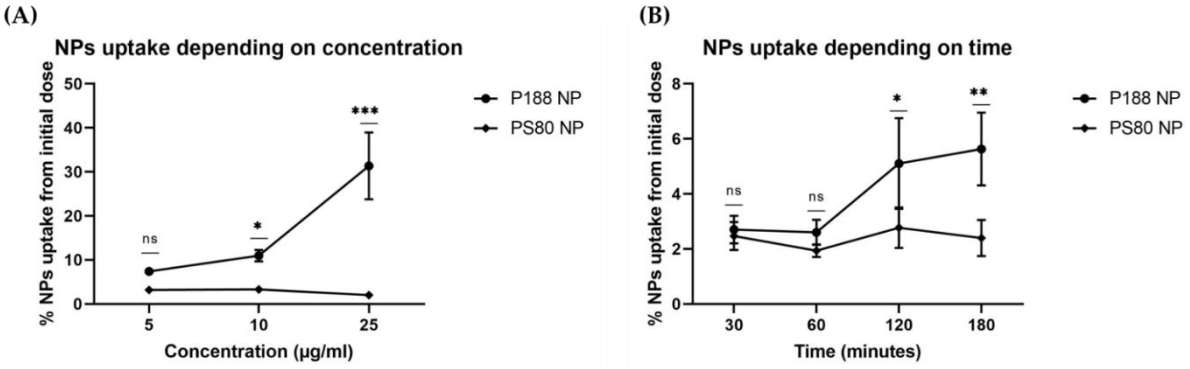

Figure 23: A. Nanoparticles uptake within the BLECs depending on nanoparticles concentration after 90 min of incubation. **B.** Nanoparticles uptake depending on incubation time, at 10 µg/ml. Samples n=3 per condition. Statistical analyses performed by two-way ANOVA, multiple comparisons test. Data expressed in mean percentage ± SD. ns = not significant, *p-value*> 0.05; **p-value*< 0.05, ***p-value*< 0.005.

3.3.5.3 Uptake process: metabolic activity

In a temperature dependent experiment, a significant decrease of 70-80% in nanoparticles uptake could be observed when cell metabolism was decreased by incubating the cells at 4°C (Figure 24.A). Thus, both formulations internalization pathways were significantly reduced. Acetylated low density lipoproteins (acLDL) a protein uptaken by receptor-mediated endocytosis through scavenger receptor B type 1 (SR-B1) was used as a positive control. AcLDL uptake was also significantly decreased, whereas inulin uptake, a molecule with non-specific transport used as negative control, did not show any significant differences between 4°C and 37°C. Moreover, when an ATP synthesis inhibitor, FCCP, was added in the cell medium for both nanoparticle formulations, a significant decrease of 50% in nanoparticles uptake could also be observed (Figure 24.B). Thus, both formulation uptake mechanisms were active transport-dependent.

3.3.5.4 Nanoparticles co-incubation with LDL, acLDL and inulin

To check whether LDL or acLDL could compete with the surfactant coated PLGA nanoparticles or promote their uptake, both formulations were co-incubated with LDL, acLDL, and inulin used as negative control. Nanoparticles uptake was measured (Figure 24.C). A significant decrease in nanoparticles uptake by more than 50% for both PS80 and P188 NP was observed when co-incubated with acLDL, in addition to a slight but not significant decrease when co-incubated with LDL. No significant decrease in uptake was observed when the nanoparticles were co-incubated with inulin. Thus, a clear specific receptor competition between acLDL and the nanoparticles seemed to occur, in addition to a slight interference with LDL receptors.

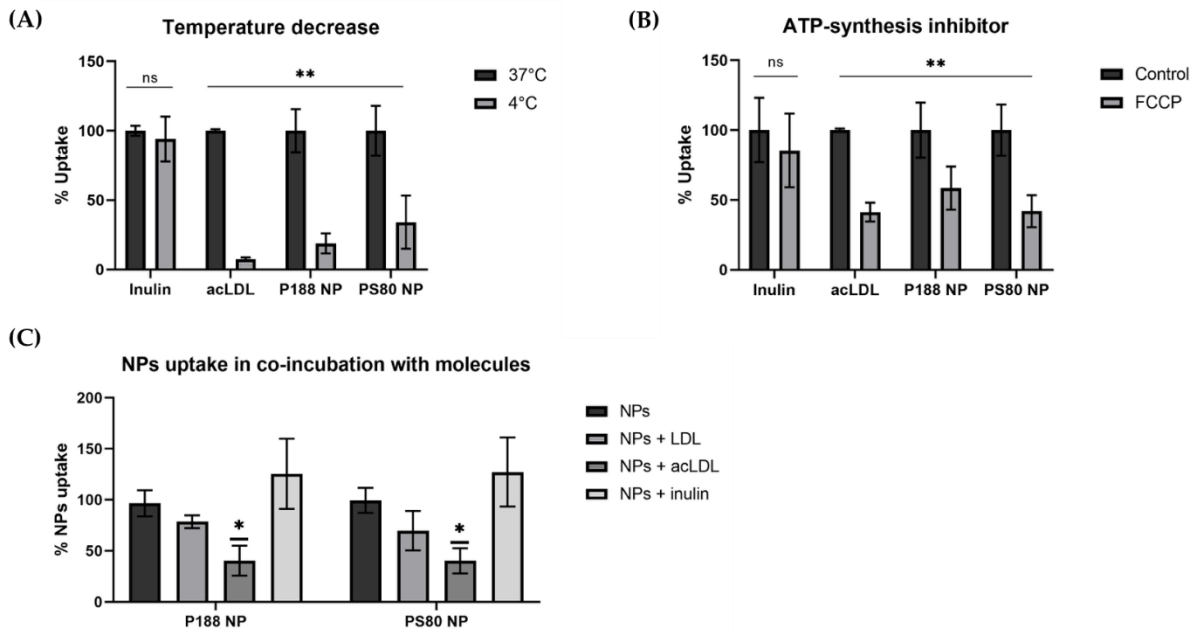

Figure 24: Nanoparticles receptor-mediated active transport. **A.** Nanoparticles uptake under temperature decreased conditions. Percentage of inulin, acLDL and nanoparticles uptake after 1 hour of incubation at 37°C and 4°C. Multiple t-tests, ***p-value*< 0.005 and ns = not significant. Inulin and acLDL replicates in n=3; Nanoparticles n=6, N=2 independent experiments. **B.** Nanoparticles uptake under active transport inhibition. Percentage of nanoparticles uptake after 1 hour incubation, with FCCP (ATP inhibitor) pre-incubated 45 min, plus 1h inulin, acLDL and nanoparticles incubation. Control = molecules/nanoparticles uptake without FCCP. Multiple t-test, ***p-value*<0.005 and ns = not significant. Inulin and acLDL n=3; Nanoparticles n=11, N=4 independent experiments. **C.** Nanoparticles co-incubation with LDL, acLDL, and inulin. Relative percentage of nanoparticles uptake in co-incubation with the molecules, compared to control (nanoparticles only), after incubation 1 hour in ECM (5%HS). Multiple *t*-test, **p-value*< 0.05, n=4; N=2 independent experiments.

3.3.5.5 Response to metabolic inhibitors of distinct vesicular endocytotic pathways

The nanoparticles internalization pathways were studied by testing a range of selected inhibitors involved in different metabolic internalization routes in the BLECs. Inhibitors for caveolae (filipin III and genistein), clathrin (dynasore and chlorpromazine) and

macropinocytosis (cytochalasin D, and dimethylamiloride) pathways were tested (Figure 25.A). Their non-toxic impact over the BLECs of the inhibitors was previously studied (data not shown). While a decrease of P188 NP uptake could be observed with genistein and chlorpromazine, no significant differences were found for any of the inhibitors. However, a significant decrease of the uptake could be observed for PS80 NP, with filipin III and chlorpromazine, at 67% from control. Thus, the nanoparticles seemed to internalize using both caveolae and clathrin-mediated endocytosis pathways.

3.3.5.6 Colocalization with early endosomes

To study whether nanoparticles were internalized through a vesicular endocytosis pathway and localized within the BLECs cytoplasm, immunostaining against early endosomes vesicles (EEA-1) was performed after incubating the BLECs with P188 NP and PS80 NP independently for 30 min and 1h. P188 and PS80 NP could be seen mostly colocalized with EEA-1 or close to each other, visible by the superposition of green and red color, sometimes yielding yellow pixels (Figure 25.B). The presence of nanoparticles colocated with EEA-1 indicates that the nanoparticles followed the endocytosis metabolic process of the BLECs.

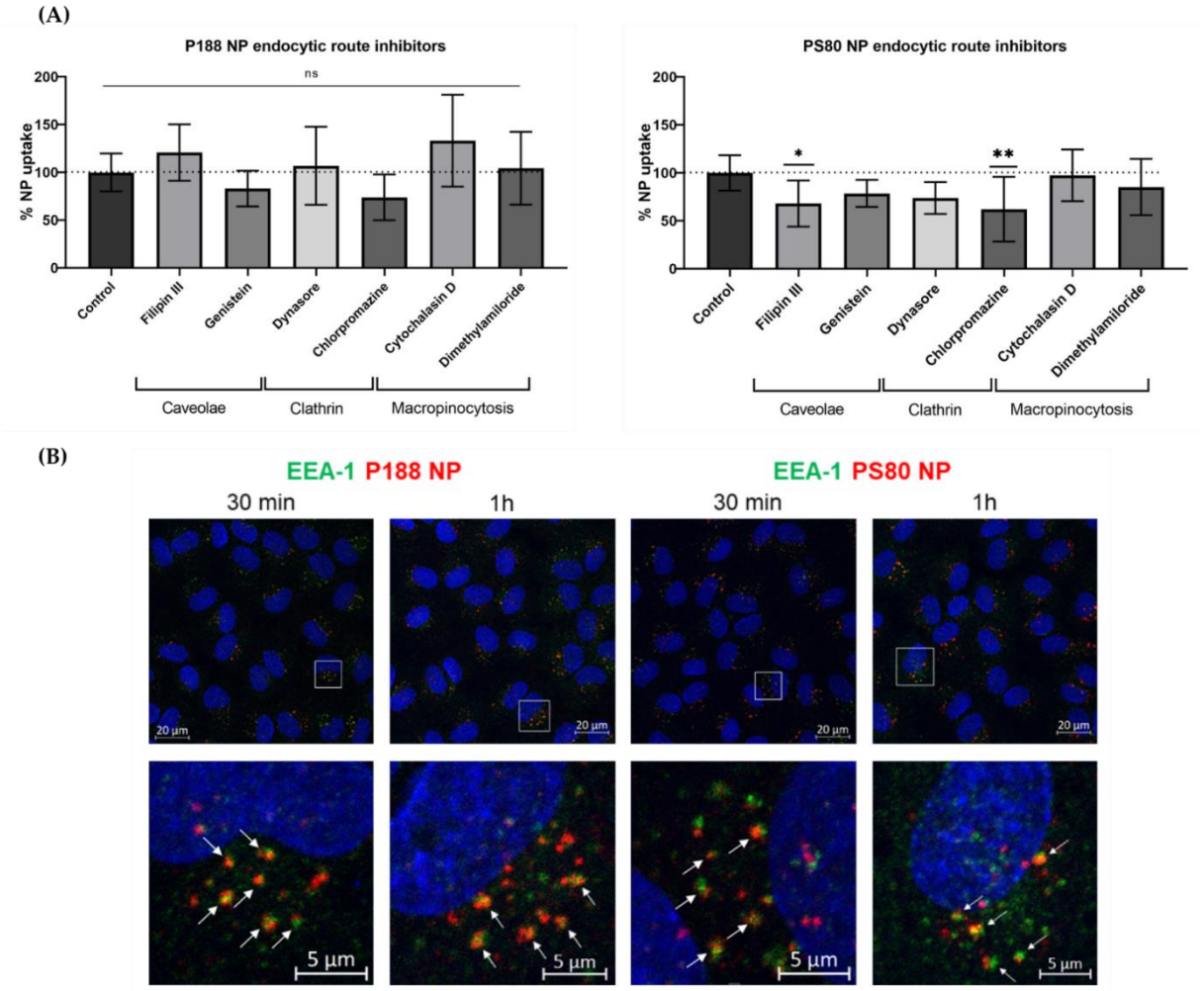

Figure 25: Endocytosis routes**. A.** Endocytosis routes inhibitors. Percentage of P188 NP and PS80 NP uptake, when a set of caveolae, clathrin and macropinocytosis pathway inhibitors were present in the cell media, after 1 hour incubation. One-way ANOVA (multiple comparisons), **p-value*< 0.05; ns = not significant. n=11 replicates; N=4 independent experiments. **B.** Nanoparticles colocalization with early endosome vesicles. Nuclei stained in blue with DAPI, P188 and PS80 NP red fluorescent dots, with EEA-1 vesicles stained green. Initial images scale bar = 20 µm, zoom images scale bar = 5 µm.

In summary, nanoparticles uptakes were temperature and ATP-dependent and showed significant competition with acLDL. The uptake was also sensitive to the presence of LDL. Thus, results suggested that nanoparticles might be uptaken by endocytosis, through similar receptors as acLDL, which have been reported to be

uptaken by SR-BI, following the clathrin receptor-mediated endocytosis pathway, and possibly by LDLR too, following the caveolae receptor-mediated endocytosis route [123,131–133]. Moreover, the results obtained with the inhibitor studies showed a significant decrease of PS80 NP uptake when using clathrin and caveolae-dependent pathways inhibitors, as well as a slight but not significant decrease of P188 NP uptake. The low effect of the inhibitors on P188 NP could however be explained by the high uptake of this formulation. As the inhibitors are tested independently, the inhibition of one route did not inhibit the others, which might then hide the significant decrease in nanoparticles uptake through a single inhibited route. Thus, the nanoparticles might be uptaken by the cells through multiple pathways, as also observed with the BBB uptake of silica nanoparticles and glycopeptide PLGA nanoparticles [127,134]. In addition, the presence of serum in the cell medium has been reported to hinder the effect of inhibitors [114]. However, performing these experiments without serum was not possible as it would have modified the protein corona forming around the nanoparticles. The modification of the protein corona might then have an impact on their internalization pathways and thus lead to results impossible to translate *in vivo*.

3.3.6 Evaluation of P188 and PS80 NP crossing through BLECs

Nanoparticles were incubated in the luminal compartment of BLECs at 10 µg/ml for 3, 6 and 24h. The amount of nanoparticles in the abluminal compartment after the end of the incubation time was quantified by fluorometry and the percentage of crossing through the BBB was calculated. Both nanoformulations could be found in the abluminal compartment, showing the ability of the nanoparticles to cross through the BBB endothelium (Figure 26.A). Both formulations showed a similar transport profile at 3 and 6h of incubation, of 1.5-2% of crossing. However, at 24h, PS80 NP showed a

significantly higher transport percentage of 3% (0.3 µg/ml), compared to P188 NP transport percentage which stayed stable around 1.5-2%.

The percentage of nanoparticles recovery was assessed. Nanoparticles recovery decreased with increasing incubation time (Figure 26.B). For both formulations, less than 100% recovery was obtained, with a significant decrease for both formulations after 24h incubation. This loss could be due to a higher uptake of nanoparticles than the amount of particles able to undergo transcytosis to the brain (abluminal) compartment. Thus, some nanoparticles were still sequestered inside the BLECs, or degraded inside the cells, and thus could not be recovered.

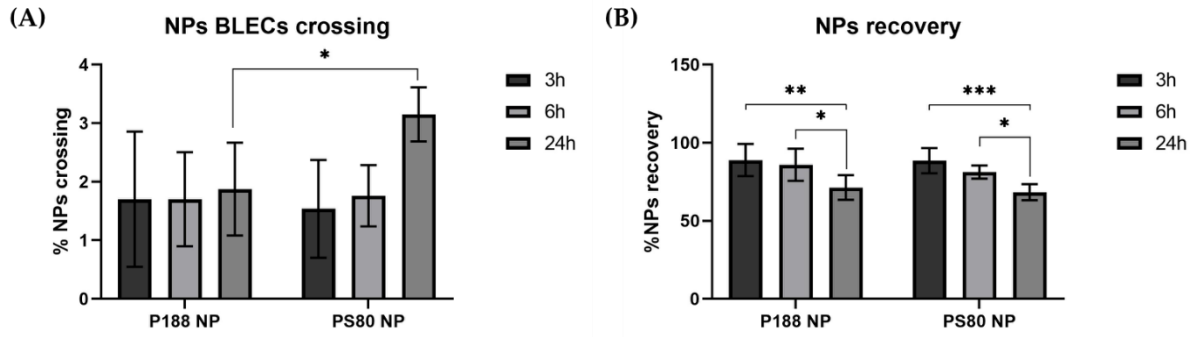

Figure 26: A. Percentage of nanoparticles crossing across the human BLECs. P188 NP and PS80 NP were incubated during 3, 6 and 24 hours at concentrations 10 µg/ml. **B**. Percentage of nanoparticles recovery at different incubation time. Statistical analyses performed by two-way ANOVA, following Sidak´s multiple comparisons test, **p-value*< 0.05, ***p-value*< 0.005, ****p-value*< 0.0005. Samples n=6, in N=2 independent experiments.

Thus, the two formulations were able to be released by the BLECs towards the brain compartment. Even though P188 NP were uptaken in higher quantities than PS80 NP, most of them were not able to cross the cell layer. Indeed, it is likely that only a fraction of the uptaken nanoparticles was able to be transcytosed through the BLECs to reach the abluminal compartment, while the remaining nanoparticles might be meant to be

degraded. In addition, the low percentage of crossing observed could suggest that the concentration studied of 10 µg/ml was already too high, saturating the crossing mechanism pathway. However, lower concentrations could not be studied as they would have required working under the detection limit of the nanoparticles fluorescence.

3.4 Conclusions

Hence, in this chapter, the interaction of the PLGA nanoparticles coated with PS80 or P188, produced using the MicroJet reactor® technology, with BLECs have been analyzed using a well-established *in vitro* coculture human BBB models. Despite not finding differences in their protein corona when incubated in human serum with the technique used in this study, the nanoparticles showed different uptake and crossing profiles. Both surfactant-coated PLGA nanoparticles presented a good biocompatibility with the BLECs at a maximum concentration tested of 100 µg/ml. Both formulations were internalized in the BLECs, showing different uptake profiles: P188 NP presented a higher and faster uptake than PS80 NP. Moreover, the nanoparticles seemed to be uptaken by the cells through receptor-mediated endocytosis, by presenting a significant competition with acLDL, and a slight competition with LDL, suggesting a possible interaction with the same receptors. The nanoparticles might then be internalized using clathrin and caveolae endocytic routes, being localized afterwards in the early endosomes vesicles. Both nanoformulations were released afterwards by the BLECs in the brain compartment in the same range, despite the significantly higher and faster uptake found for P188 NP compared to PS80 NP. However, PS80 NP presented the highest release percentage after 24h incubation.

4. Nanoparticles loaded with retinoic acid

Part of this chapter has been published in Lombardo, S.M.; Günday Türeli, N.; Koch, M.; Schneider, M.; Türeli, A.E. Reliable Release Testing for Nanoparticles with the NanoDis System, an Innovative Sample and Separate Technique. *International Journal of Pharmaceutics* **2021**, *609*, 121215, doi:10.1016/j.ijpharm.2021.121215

4.1 Introduction

All-trans retinoic acid (RA) is a derivative of vitamin A and has proven to be an interesting molecule for stimulating the differentiation of neural stem cells (NSCs) into new neuronal cells, both *in vitro* and *in vivo* [103,104]. Because NSCs can differentiate into new neural cells, including neurons, the regulation of their proliferation, differentiation and migration represents a promising regenerative and therapeutic strategy for central nervous system (CNS) diseases, like strokes or neurodegenerative diseases, such as Alzheimer's disease. Loading nanoparticles with RA could increase RA cell uptake by NSCs and thus prove valuable in therapeutic applications.

For RA to reach NSCs in therapeutic concentration, RA needs to be loaded inside nanoparticles able to cross the BBB. Thus, in this project surfactant-coated PLGA nanoparticles loaded with RA were developed. Two different nanoparticle types were developed: nanospheres and nanocapsules. Nanospheres are composed of a full matrix of polymer, while nanocapsules have an oily core surrounded by a polymer membrane. The formulations were optimized using design of experiments (DoE), either to optimize the formulation composition or the production parameters with the MJR technology. The size, PDI and encapsulation efficiency (EE) of the produced particles were studied.

Next, the release kinetics of the nanoparticle formulations were investigated. Indeed, PLGA nanoparticles have been reported to have controlled and extended release properties thanks to their slow degradation kinetic. However, these formulations often suffer from burst release, wherein a large amount of the encapsulated drug is released within the first hours due to leakage of the API (Active Pharmaceutical Ingredient) located close to the particle surface [85,135]. A high burst release can lead to a toxic effect if the drug concentration exceeds the therapeutic window and must therefore be

well characterized. Also, for the nanoparticles to be an efficient delivery system for RA, their cargo should not be released before the particles have crossed the BBB and reached the NSCs.

Until now there has been no standardized technique for release testing of extended release nanoparticle systems. Current dissolution methodologies suffer from the inefficient separation of nanoparticles from the dissolution medium, independent of the equipment used for the dissolution studies. In this chapter, two different techniques were used and compared. Indeed, release testing of the nanoparticles was performed using an innovative sample and separate method coupling a USP II dissolution apparatus with TFF, the NanoDis System, as well as a classical dialysis method.

In summary, PLGA nanospheres and nanocapsules loaded with RA were developed and their release kinetics were studied.

4.2 Material and Methods

4.2.1 Nanospheres loaded with retinoic acid

4.2.1.1 Design of experiments

A design of experiments (DoE) was performed to optimize the MJR production of a chosen nanoparticle formulation of PLGA nanospheres, with a solvent solution composed of 1% (w/v) PLGA Resomer® RG 502 H 50:50 (Evonik, Essen, Germany), 0.5% (w/v) all-trans retinoic acid Acros Organics (Geel, Belgium) in acetone, and a non-solvent solution composed of 1% (w/v) PS80 (Tween® 80, Merck, Darmstadt, Germany), at a solvent:non-solvent ratio of 1:5. The reactor used was 300 µm. The factors studied were the pump flow rates (10 to 40 ml/min for the non-solvent solution pump, and 2 to 8 ml/min for the solvent solution pump, keeping the ratio at 1:5), N_2

pressure (0 to 1 bar), and the temperature (25 to 40°C). The responses were nanoparticles hydrodynamic size and PDI, encapsulation efficiency and drug loading. A Box-Behnken design was performed, with 17 runs including 5 center points, and the results were analyzed using Design-Expert® 11 (Stat-Ease) software. The nanoparticles size and PDI were measured by DLS, using a Zetasizer ZS90 from Malvern Instruments (Malvern, United-Kingdom). To calculate the encapsulation efficiency, an indirect method was performed. The nanoparticles were centrifuged at 13,000 g for 45 min and the supernatants were diluted in acetonitrile (ACN) and measured by HPLC-UV at 350 nm (Hitachi Elite LaChrom® equipped with Chromaster 5410 UV Detector, VWR, Darmstadt Germany). A Waters® (Eschborn, Germany) X Bridge Shield 3.5 µm RP18 150x4.6 mm column was used, with a gradient method (Table 2), at 1.5 ml/min.

Table 1: Retinoic acid HPLC assay method gradient

Time (min)	Mobile Phase A (%) 0.2 ml glacial acetic acid in 900 ml HPLC water	Mobile Phase B (%) 100% ACN
0	40	60
2.5	40	60
13.5	20	80
13.6	40	60
15	40	60

The encapsulation efficiency of RA was calculated following Equation 5.

$$\boldsymbol{EE}\ (\%) = \mathbf{100} - \left(\frac{\boldsymbol{RA\ concentration\ in\ supernatant}}{\boldsymbol{initial\ RA\ concentration}} \times \mathbf{100}\right) \qquad \textbf{(5)}$$

To measure RA loading, 1 ml of nanoparticles were centrifuged in weighted Eppendorfs at 13,000 g for 45 min. The supernatants were discarded and the pellets were dried at 50°C for 2 hours, in a drying oven. The Eppendorfs were then weighed and the dried pellets weight calculated. The pellets were redispersed and dissolved in 1 ml ACN and their RA content was measured by HPLC-UV, using the method described above. RA loading was calculated using Equation 6.

$$\boldsymbol{Loading}\ (\%\ \boldsymbol{w/w}) = \frac{\boldsymbol{RA\ weight\ in\ pellet}}{\boldsymbol{Total\ pellet\ weight}} \times \mathbf{100} \qquad \textbf{(6)}$$

4.2.1.2 Nanospheres release

Nanospheres were prepared benchtop by nanoprecipitation with different amounts of PLGA and RA dissolved in acetone (the solvent solution) (Table 2). The non-solvent solution was composed of 1% (w/v) PS80 in water. While stirring the non-solvent solution at 500 rpm, the solvent solution was added slowly and continuously, to reach a solvent:non-solvent ratio of 1:5. Acetone was evaporated by stirring the nanoparticles under the hood. The nanoparticles were then washed by TFF with 12 volumes of water at 15 psi (~1 bar) through a Spectrum® 300 kD MicroKros hollow fiber membrane from Repligen. Their size and PDI were measured by DLS. The nanospheres release was tested using the NanoDis System. The nanospheres were diluted in PBS pH 7.4 supplemented with PS80 1% (w/v) to 10 µg/ml of RA to be in sink conditions. The nanospheres were stirred at 50 rpm at 37°C and automatically sampled and filtered through Spectrum® 500 kD MicroKros hollow fiber membranes from Repligen. The filtrates were measured by UV spectrophotometry at 345 nm (spectrophotometer UV-1600PC, VWR, Darmstadt, Germany) and the RA concentration was calculated using a calibration curve in PBS pH 7.4 supplemented with PS80 1% (w/v).

Table 2: Composition of solvent solution of RA-loaded nanospheres

Nanospheres PLGA to drug ratio	PLGA concentration (mg/ml)	RA concentration (mg/ml)
10/5	10	5
20/5	20	5
20/2.5	20	2.5

4.2.2 Nanocapsules loaded with retinoic acid

4.2.2.1 Retinoic acid solubility in oils

Different oils were tested. 1 mg of retinoic acid was stirred in 2 ml of either oleic acid (PanReac AppliChem, Darmstadt, Germany), castor oil (Alfa Aesar, Kandel, Germany), soybean oil (Société Industrielle des Oléagineux, Saint-Laurent-Blangy, France) or Miglyol® 812 (medium-chain triglycerides, Caelo, Hilden, Germany). After 3 hours stirring, the oily dispersions were centrifuged at 13,000 g for 15 min. The supernatants were recovered, diluted in ACN and their RA concentration was determined by UV spectrophotometry at 355 nm, using an already established calibration curve in ACN.

4.2.2.2 Design of experiment of benchtop oleic acid nanocapsules

PLGA nanocapsules were first prepared benchtop. Their composition was optimized using a Box-Behnken DoE, with 17 runs including 5 center points. PLGA concentration (3 to 10 mg/ml), oleic acid concentration (3 to 15 mg/ml) and RA concentration (20 to 300 µg/ml) were chosen as factors, and nanoparticles hydrodynamic size, PDI and encapsulation efficiency as responses. The results were analyzed using Design-Expert® 11 software. Briefly, the solvent solution was prepared by dissolving PLGA, oleic acid and RA in acetone. A 1% (w/v) PS80 solution was used as non-solvent solution. While stirring 10 ml of non-solvent solution, 5 ml of solvent solution was added

slowly and continuously. Acetone was evaporated under the hood and the nanoparticles size was measured by DLS. Nanocapsules were centrifuged for 5 min at 1,000 g through Nanosep® Centrifugal devices with Omega™ membrane (mPES) 300 kD from Pall Laboratory purchased from VWR (Darmstadt, Germany). The filtrates were measured with a spectrophotometer UV-1600PC from VWR (Darmstadt, Germany) at 355 nm. The EE was calculated using Equation 5. If no RA could be measured in the filtrate, the encapsulation efficiency (EE) was estimated based on the detection limit of RA in water with 1% (w/v) PS80 (0.1 µg/ml) using Equation 7.

$$EE > 100 - \frac{0.1\ [\mu g/ml]}{total\ RA\ concentration\ [\mu g/ml]} \times 100 \qquad (7)$$

4.2.2.3 MJR production of nanocapsules

Nanocapsules were produced using the MJR technology at different flow rates while keeping the formulation constant. The solvent solution was composed of 1% (w/v) PLGA Resomer RG 502H, 1.5% (w/v) oleic acid and 0.03% (w/v) RA in acetone. The non-solvent solution was composed of 1% (w/v) PS80 in water and the solvent:non-solvent ratio was kept constant at 1:2. A 300 µm reactor was used, in a 25°C water bath. The nanoparticle size and PDI were measured by DLS immediately after production.

4.2.2.4 Nanocapsules with P188 and Span

The nanocapsules were prepared benchtop with different amount of Span 80 (sorbitan monooleate, Guangdong Runhua Chemistry Co, Guangdong, China). Their solvent solutions were composed of 0.3% (w/v) PLGA Resomer RG 502H, 0.9% (w/v) oleic acid, 0.03% (w/v) RA and various concentration of Span 80 in acetone. The non-solvent solution was composed of 1% (w/v) PS80 or P188 in water. While stirring 5 ml

of the non-solvent solution, 2.5 ml of solvent solution were added. The nanocapsules size and PDI were measured immediately by DLS.

4.2.2.5 Chitosan coated nanocapsules

The nanocapsules were prepared benchtop with different amount of chitosan (50-190 kDa, Sigma-Aldrich). Their solvent solutions were composed of 0.3% (w/v) PLGA Resomer RG 502H, 0.9% (w/v) oleic acid, 0.03% (w/v) RA. The non-solvent solution was composed of 1% (w/v) PS80, various concentrations of chitosan and acetic acid 2% (v/v) in water. While stirring 5 ml of the non-solvent solution, 2.5 ml of solvent solution were added. The nanocapsules size and PDI were measured immediately by DLS.

4.2.3 Release testing of nanocapsules loaded with retinoic acid

4.2.3.1 Nanocapsules production

The nanocapsules were produced with a continuous nanoprecipitation method in a confined chamber. Two formulations, P188 benchtop and PS80 benchtop, were produced benchtop by simply adding the solvent solutions in the non-solvent solutions under stirring. PLGA, oleic acid, retinoic acid and Span 80 dissolved in acetone were used as solvent solution (Table 3). Polysorbate 80 (PS80) or poloxamer 188 (P188) were dissolved in water to form the non-solvent solution. A solvent:non-solvent ratio of 1:2 was used for the production of the nanocapsules. To produce nanocapsules coated with chitosan, the same technique was used but chitosan was added in the non-solvent solution, dissolved in water with 1% v/v of acetic acid. The particles produced with this extra-layer of chitosan were labelled P188-C and PS80-C for nanocapsules coated with P188 and PS80 respectively. One formulation coated with chitosan and PS80 was prepared with higher amount of PLGA and oil and was labelled PS80-C high. The

particles were purified by TFF using a 300 kD mPES Spectrum® MicroKros hollow fiber filter from Repligen (Waltham, USA) at 15 psi (~1 bar), with 6 volumes of water, or acetic acid 1% v/v in water for chitosan-coated nanocapsules. Their size and zeta potential were measured by dynamic light scattering (DLS) with a Zetasizer NanoZS 90 from Malvern Instruments (Malvern, UK).

Table 3: Solvent and non-solvent solutions composition for nanocapsules preparation

NC	Solvent solution				Non-solvent solution		
	PLGA (% w/v)	**Oleic acid (% w/v)**	**Span 80 (% w/v)**	**Retinoic acid (% w/v)**	**Surfactant type**	**Surfactant (% w/v)**	**Chitosan (% w/v)**
P188	1.0	1.5	0.5	0.03	Poloxamer 188	1.0	0
P188 benchtop	1.0	1.5	0.5	0.03	Poloxamer 188	1.0	0
PS80	1.0	1.5	0.5	0.03	Polysorbate 80	1.0	0
PS80 benchtop	1.0	1.5	0.5	0.03	Polysorbate 80	1.0	0
P188-C	0.3	0.9	0	0.03	Poloxamer 188	1.0	0.05
PS80-C	0.3	0.9	0	0.03	Polysorbate 80	1.0	0.05
PS80-C high	1.0	1.5	0	0.03	Polysorbate 80	1.0	0.05

4.2.3.2 Cryo-TEM imaging

Cryo-TEM imaging of the P188 nanocapsules was conducted by placing a 3 µL droplet of the aqueous solution on a S147-4 holey carbon film (Plano, Germany) before blotting the liquid droplet to a thin film for 2s and plunging into undercooled liquid ethane at T

= 108 K using a Gatan (Pleasonton, USA) CP3 cryo plunger. The vitrified samples were transferred under liquid nitrogen to a Gatan model 914 cryo-TEM holder and imaged at T=100 K using a JEOL (Akishima, Japan) JEM-2100 LaB6 TEM operating at an accelerating voltage of 200 kV under low-dose conditions. TEM micrographs were obtained using a Gatan Orius SC1000 CCD camera and an acquisition time of 4 seconds.

4.2.3.3 Encapsulation efficiency

The nanocapsules were centrifuged for 5 min at 1,000 g through Nanosep® Centrifugal devices with Omega™ membrane (mPES) 300 kD from Pall Laboratory purchased from VWR (Darmstadt, Germany). The filtrates were measured with a spectrophotometer UV-1600PC from VWR (Darmstadt, Germany) at 345 nm. No RA could be measured in the filtrate, so the encapsulation efficiency (EE) was estimated based on the detection limit of RA in water with 1% (w/v) PS80 using Equation 7.

4.2.3.4 RA solubility in release media

To measure RA solubility, 1 mg of RA was stirred in 2 ml of release medium for 24h at 20°C. Samples were taken at 3 and 24h. The sample suspensions were centrifuged for 15 min at 16,000 g and the supernatants were measured with a UV spectrophotometer at 345 nm for PBS-PS80 media and 355 nm for PBS-SDS media. RA concentration was calculated from calibration curves in either PBS-PS80 or PBS-SDS.

4.2.3.5 Release testing

4.2.3.5.1 NanoDis method

To measure the nanocapsules release profile, a USP II dissolution apparatus 708-DS coupled with a NanoDis System and an 850-DS Sampling Station from Agilent (Santa

Clara, USA) was used. The nanoparticles were diluted to reach 5 µg/ml of retinoic acid in the vessel and reach sink conditions in 750 ml of PBS-PS80 or PBS-SDS. The NanoDis System was fitted with 500 kD mPES Spectrum® MicroKros hollow fiber filters from Repligen. The dispersions were stirred at 50 rpm at 37°C. At chosen time points, the suspension was automatically filtered through the filters by TFF. The filtrates were collected and the retentates were circulated back into the vessels (Figure 1). Control of the lag time of filtration and permeation of the dissolved API were done with RA dissolved in release medium to check the permeation of free RA through the filters. The filtrates were measured with a UV spectrophotometer at 345 nm for PBS-PS80 and 355 nm for PBS-SDS. RA concentration was calculated from calibration curves in either PBS-PS80 or PBS-SDS. The release percentage was calculated using Equation 8.

$$\boldsymbol{NanoDis\ release\ percentage} = \frac{\boldsymbol{RA\ concentration\ in\ the\ filtrate}}{\boldsymbol{Total\ RA\ concentration\ in\ the\ medium}} \times \mathbf{100} \qquad \textbf{(8)}$$

4.2.3.5.2 Dialysis method

The P188-span nanocapsules were diluted to reach 20 µg/ml of RA in release medium, either PBS-PS80 or PBS-SDS, to ensure sink conditions. 10 ml of the suspension was placed inside a 10 ml 300 kD cellulose ester Float-A-Lyzer® from Repligen. The tubes were stirred at 150 rpm in 150 ml of release medium at 37°C in a drying oven. At chosen time points, 300 µl of medium from the acceptor compartment was sampled and replaced with 300 µl of fresh medium. At 6, 24 and 30h, the complete medium from the acceptor compartment was replaced with fresh medium. The samples were measured with a UV spectrophotometer at 345 nm for PBS-PS80 and 355 nm for PBS-SDS. RA concentration was calculated from calibration curves in either PBS-PS80 or PBS-SDS. The release percentage was calculated using Equation 9.

$$\boldsymbol{Dialysis\ release\ percentage} = \frac{\boldsymbol{RA\ amount\ in\ the\ acceptor\ compartment}}{\boldsymbol{RA\ amount\ in\ the\ donor\ compartment\ at\ t0}} \times \mathbf{100} \qquad \textbf{(9)}$$

4.3 Results and discussion

4.3.1 Nanospheres loaded with retinoic acid

4.3.1.1 Design of experiment of MJR production

To study the impact of the MJR set up on a chosen nanosphere formulation loaded with retinoic acid, a design of experiments was performed, using a Box-Behnken design (Figure 27 and Table 4). All responses were fitted on various models. Their fits were confirmed with an ANOVA: all of the responses had significant fit and not significant lack of fit. The size values were analyzed using a 2FI model, whose R^2 was 0.9474. PDI values fitted on a linear model, with a R^2 of 0.8149. EE values fitted on a linear model with a R^2 of 0.8116. Finally, the loading values fitted on a 2FI model with a R^2 of 0.9886.

Flow rate and gas had a significant impact on the nanoparticles characteristics, acting in opposite way on the nanoparticle size, PDI and loading. Increasing flow rate increased nanoparticle size, decreased PDI and increased loading, while the opposite was true for the gas flow. Temperature only had an impact on RA loading: increasing temperature decreased loading. All the obtained encapsulation efficiency values were very close to one another (between 94 and 96%). Thus, EE did not seem to strongly depend on any of the factors, as can be seen by the small coefficients calculated. As the desired nanoparticles had to have small particle sizes, PDI under 0.2 and a high RA loading, a solution with a maximum desirability of 0.722 was found for a formulation produced with a non-solvent flow rate at 10 ml/min (with a corresponding solvent flow rate of 2 ml/min), at 25°C and no gas pressure. The predicted values for this

formulation were a size of 304 nm, PDI of 0.138, EE of 95% and loading of 38% (w/w). The predicted best formulation was produced and characterized: the nanospheres produced had a smaller hydrodynamic size than expected, of 287 nm with a PDI of 0.27. The encapsulation efficiency and loading were as predicted 97% and 37% (w/w).

However, with this configuration, it was not possible to obtain nanoparticles smaller than 300 nm, which is not optimal for BBB crossing, as particles smaller than 100 nm have been shown to cross more easily.

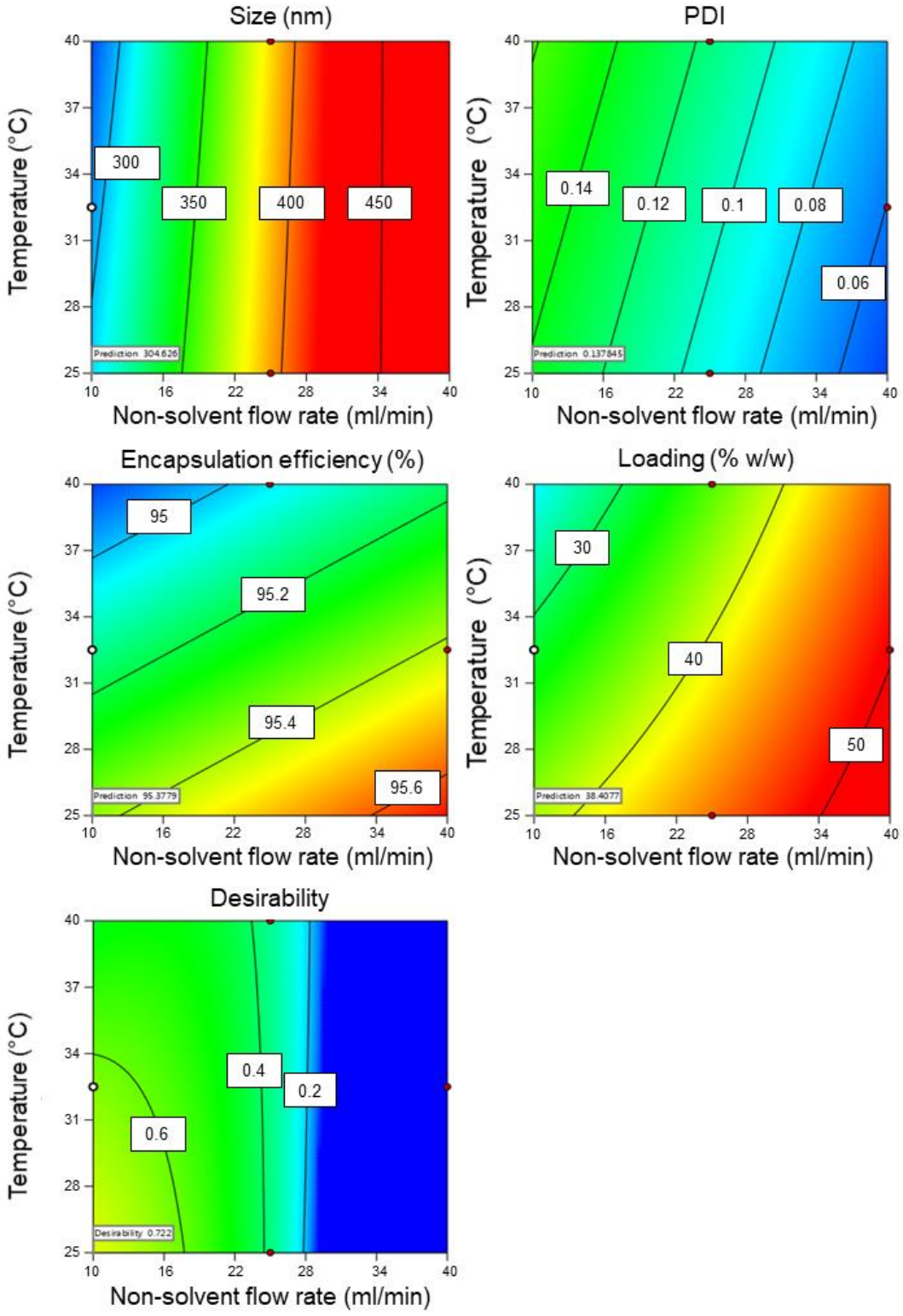

Figure 27: Summary of Box-Behnken design of MJR production of nanospheres loaded with retinoic acid. Rainbow graphs show the impact of temperature and flow rates on desirability, size, PDI, encapsulation efficiency and loading, with gas pressure at 0 bar. The color scale varies from blue (smallest values) to red (highest values).

Table 4: Box-Behnken design coefficient table of MJR production of nanospheres loaded with retinoic acid. ***p-value* < 0.05**

	Intercept	Flow rate (A)	T° (B)	Gas pressure (C)	AB	AC	BC
Size (nm)	350.68	**63.00**	3.88	**-39.60**	6.13	**-33.03**	8.13
p-values		**< 0.0001**	0.4388	**< 0.0001**	0.3889	**0.0036**	0.2604
PDI	0.1768	**-0.0450**	0.0118	**0.0712**			
p-values		**0.0166**	0.418	**0.0003**			
EE (%)	95.35	**0.14**	**-0.24**	0.07			
p-values		**0.0232**	**0.0024**	0.2131			
Loading (%)	32.50	**8.49**	**-5.62**	**-8.07**	**1.91**	-0.61	-0.61
p-values		**< 0.0001**	**< 0.0001**	**< 0.0001**	**0.0117**	0.3396	0.4467

4.3.1.2 Nanospheres release

Nanospheres were produced benchtop with different concentrations of PLGA (10 or 20 mg/ml in solvent solution) and retinoic acid (5 or 2.5 mg/ml in solvent solution). Their size and PDI were measured after purification (Table 5). The nanospheres sizes were in a range of 300-350 nm, with a PDI < 0.2 for 10/5 and 20/5 nanospheres, and <0.5 for 20/2.5.

Table 5: Benchtop RA-loaded nanospheres size and PDI

Nanospheres PLGA to drug ratio	**Size (nm)**	**PDI**
10/5	342.1	0.105
20/5	323.4	0.198
20/2.5	305.7	0.485

The release kinetics of the nanospheres was then tested using the NanoDis System (Figure 28). After 15 min, a high burst release was observed for all formulations, reaching 83% after one hour for 20/2.5 nanospheres and 97% for 10/5 and 20/2.5. The

burst release of the nanospheres could be slightly reduced by increasing the amount of PLGA in the formulation but remained high.

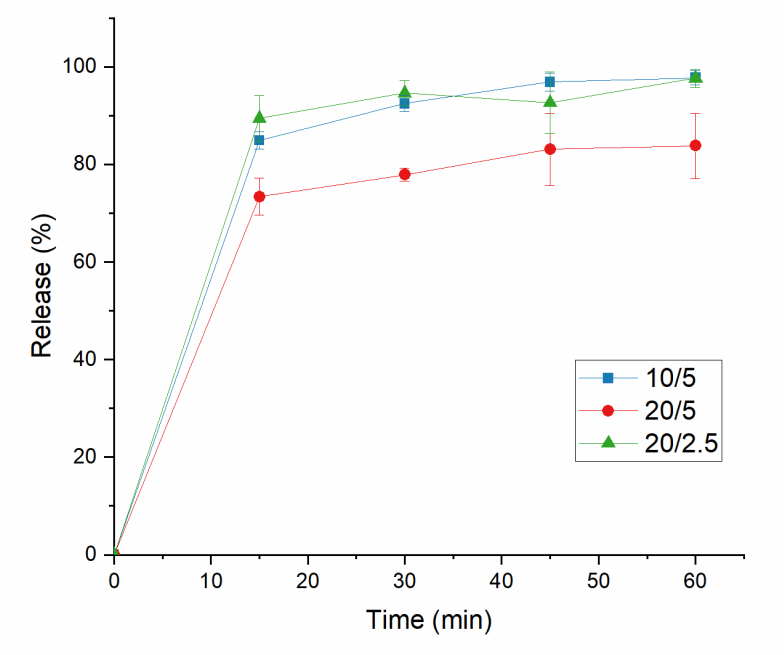

Figure 28: NanoDis release of PLGA nanospheres loaded with retinoic acid. Different formulations were produced with different concentrations of PLGA and of retinoic acid, labelled “PLGA concentration [mg/ml]/RA concentration [mg/ml]” in the solvent solution.

Furthermore, stability issues were noticed with nanospheres. The nanospheres precipitated over time, leading to a size increase of the nanoparticles. These problems of high burst release and of colloidal stability drove us to develop another type of nanoparticles, PLGA nanocapsules. Indeed, their oily core might lead to better encapsulation of RA in the core of the particles, instead of loading on their surface, thus prompting a better extended release kinetic.

4.3.2 Nanocapsules loaded with retinoic acid

4.3.2.1 Retinoic acid solubility in oils

Before starting producing nanocapsules, RA solubility in oil was assessed to select the best oil for the formulation. RA had a solubility of 10.5 mg/ml in oleic acid, 5.9 mg/ml in castor oil, 2.8 mg/ml in Miglyol and 1.5 mg/ml in soybean oil.

As a result, oleic acid seemed to be the best candidate for nanocapsules formulation.

4.3.2.2 DoE of oleic acid nanocapsules

To better understand the impact of the formulation parameters on the nanoparticles' properties, a design of experiments was performed with a Box-Behnken design. The nanoparticles were produced benchtop and characterized for size, PDI and encapsulation efficiency.

The data were fitted with various models and their fit were confirmed with an ANOVA. All the models used had significant fit with not significant lack-of-fit. Size values fitted on a reduced quadratic model, with a R^2 of 0.9548. PDI values fitted on a linear model, with a R^2 of 0.7308. Finally, encapsulation efficiency fitted on reduced quadratic model with a R^2 of 0.9794.

As can be seen from Figure 29 and Table 6, PLGA concentration and oleic acid concentrations had significant impact on size and PDI, while retinoic acid concentration had no significant effect on the responses studied. Increasing PLGA and oil concentration increased nanocapsules sizes. Increasing PLGA concentration reduced PDI, while increasing oil concentration had an opposite effect. Indeed, it seems that increasing the oily core of nanocapsules might destabilize the formulation. Concerning EE, only oleic acid has a significant impact on this response, where EE increased with oleic acid concentration.

The optimal formulation had to have a high PLGA concentration, to obtain controlled release, as well as a high RA concentration and a high EE to obtain high RA loading. As all the nanocapsules produced had small sizes under 200 nm and acceptable PDI, these responses were not taken into account in the desirability calculation. Desirability of 1 was obtained for a large variety of formulations, as visible on Figure 29.

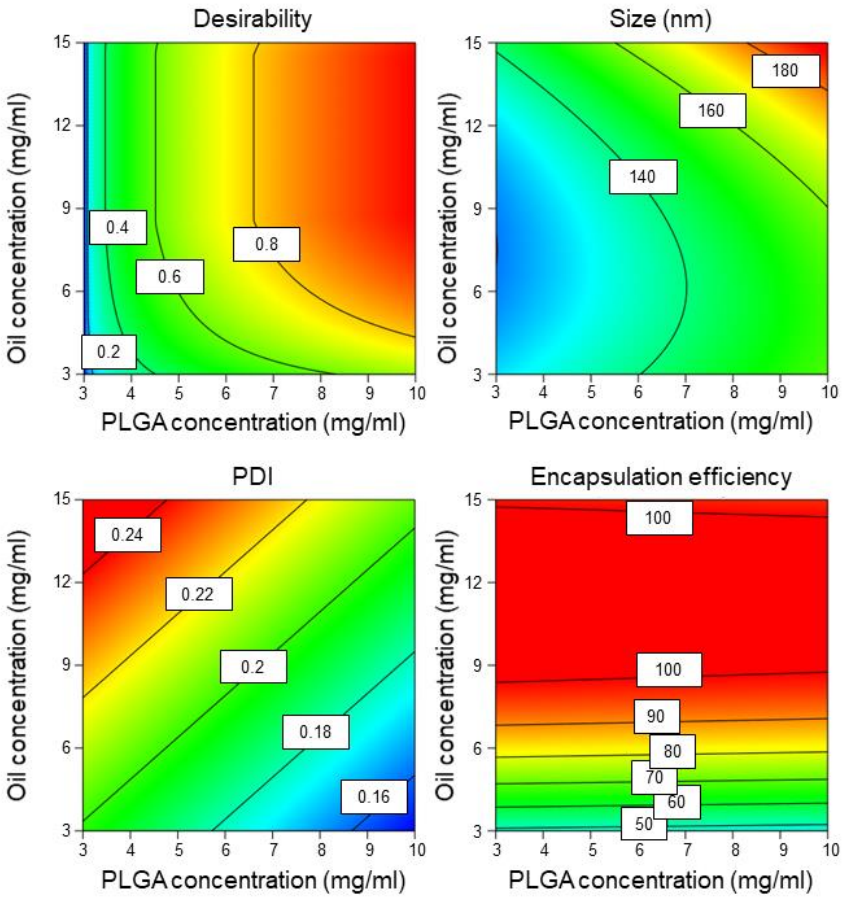

Figure 29: Summary of Box-Behnken design of benchtop production of nanocapsules loaded with retinoic acid. Rainbow graphs show the impact of oleic acid and PLGA concentration on desirability, size, PDI and encapsulation efficiency, with a RA concentration fixed at 300 µg/ml. The color scale varies from blue (smallest values) to red (highest values).

Table 6: Box-Behnken design coefficient table of benchtop production of nanocapsules loaded with retinoic acid. ***p-value*< 0.05**

	Intercept	PLGA (A)	Oleic acid (B)	Solvent:non-solvent (C)	AB	BC	B^2
Size (nm)	136.63	**19.55**	**12.66**	3,67	**5.64**		**14.14**
p-values		**< 0.0001**	**< 0.0001**	0,0818	**0.0461**		**0.0002**
PDI	0.1982	**-0.0237**	**0.0268**	0,0033			
p-values		**0.0018**	**0.0006**	0,5852			
EE (%)	99.14	-0.90	**29.55**	2,84		-4.60	**-29.24**
p-values		0.5786	**< 0.0001**	0,0941		0.0591	**< 0.0001**

To confirm the models, nanocapsules were prepared benchtop by mixing 5 ml of a solvent solution of 6.8 µg/ml PLGA, 8.7 µg/ml oleic acid and 300 µg/ml RA in acetone, with 10 ml of 1% (w/v) PS80 in water. The nanocapsules had a size (148 nm), PDI (0.19) and EE (>99.9%) in the predicted range (predicted values 142 nm, PDI 0.20 and EE >99.9%), confirming the models.

4.3.2.3 MJR production of nanocapsules

First, nanocapsules were produced using different flow rates to find the optimal process parameters for their production, while keeping their composition constant (Figure 30).

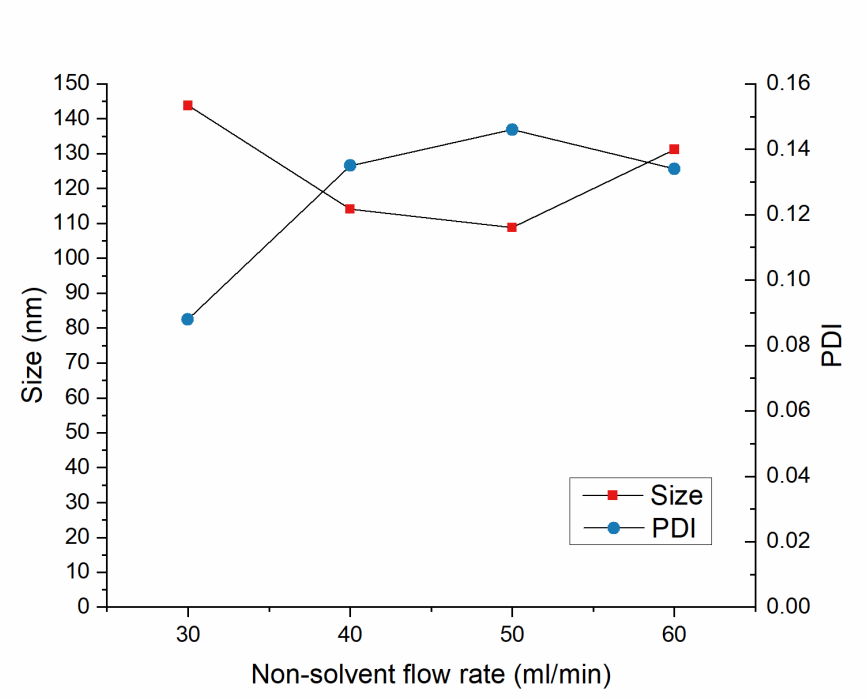

Figure 30: Nanocapsules size and PDI produced using the MicroJet reactor technology, at different non-solvent flow rates, keeping the solvent:non-solvent flow rates ratio at 1:2 (n=1). The nanocapsules were produced with a solvent solution containing 1% (w/v) PLGA, 1.5% (w/v) oleic acid and 0.03% (w/v) retinoic acid, and a non-solvent solution of 1% (w/v) PS80.

The nanocapsules size varied from 148 nm to a minimum of 108 nm, obtained with a non-solvent flow rate of 50 ml/min and a corresponding solvent flow rate of 25 ml/min. All the nanocapsules produced had an acceptable PDI below 0.2. Thus, the 25/50 ml/min configuration was kept for the production of the RA-loaded nanocapsules.

4.3.2.4 Nanocapsules with P188 and Span 80

To increase the stability of the oily core and to help reducing burst release, Span 80 (sorbitan monooleate) was added to the formulation in the solvent solution. The nanocapsules were produced with P188 or with PS80 in the non-solvent solution. The formulations were produced benchtop with different amount of Span 80 (Figure 31). The nanocapsules produced with P188 were larger than the PS80 nanocapsules by

around 100 nm. The PDI of the formulations were all under 0.20 for the P188 and under 0.25 for the PS80 nanocapsules. Span 80 concentration increased slightly the size of the P188 nanocapsules, from 202 to 236 nm, and had a larger impact on PS80 nanocapsules size, which increased from 88 to 144 nm. Despite the size increase, the formulations prepared with 5 mg/ml of Span 80 were selected for release testing, hoping that Span 80 would improve the nanocapsules release properties.

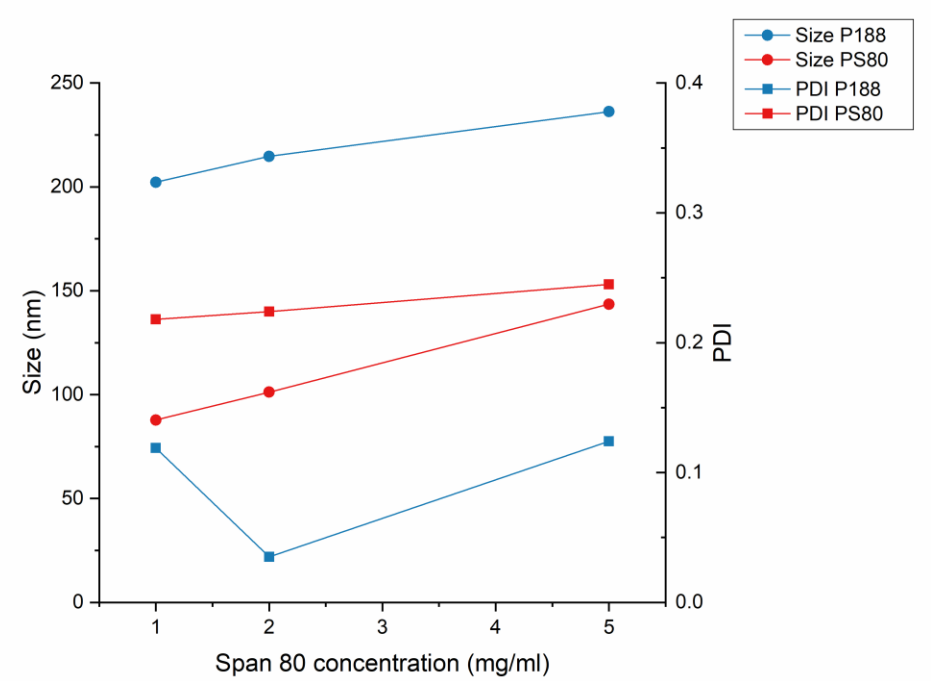

Figure 31: Nanocapsules size and PDI depending on Span 80 concentration, (n=1). The nanocapsules were produced benchtop with a solvent solution containing 0.3% (w/v) PLGA, 0.9% (w/v) oleic acid, 0.03% (w/v) retinoic acid and varying concentration of Span 80, and a non-solvent solution of 1% (w/v) of either PS80 or P188.

4.3.2.5 Chitosan-coated nanocapsules

To try to improve the release properties of the nanocapsules in another way, the particles were coated with an extra layer of chitosan. Indeed, coating particle with chitosan has been shown to reduce the particles burst release [86,136]. Chitosan was added in the non-solvent solution and the nanocapsules were prepared by benchtop

nanoprecipitation. Acetic acid also had to be added to dissolve chitosan in water. The chitosan-coated nanocapsules were first prepared benchtop with different amounts of chitosan. To act as control, the nanocapsules were also prepared without chitosan, with and without acetic acid in the solvent solution. The nanocapsules sizes, PDI and zeta potentials were measured by DLS (Figure 32). Adding acetic acid in the formulation alone doubled the nanocapsules size (from 98 to 197 nm). Chitosan coating increased the nanocapsules size even more, to 227, 235 and 266 nm for 0.5, 1 and 2 mg/ml of chitosan respectively. Increasing the amount of chitosan in the formulation increased the size of the particles. The nanocapsules had acceptable PDI under 0.3. When coating the capsules with chitosan, the zeta potentials of the nanocapsules became positive (~30 mV). Indeed, chitosan is a positively charged polymer at acidic pH. When adding acetic acid to the formulation without chitosan, the zeta potential of the PLGA nanocapsules increased from -35 mV to close to neutral at -8 mV. Indeed, as the pH of the solution was close to PLGA pKa, the polymer lost its negative charges due to its carboxyl groups. The lower surface charge fostered agglomeration, explaining the size increase of the nanocapsules in acetic acid. As small particle sizes are more favorable for BBB crossing, the nanocapsules coating with 0.5 mg/ml of chitosan were chosen as the best formulation.

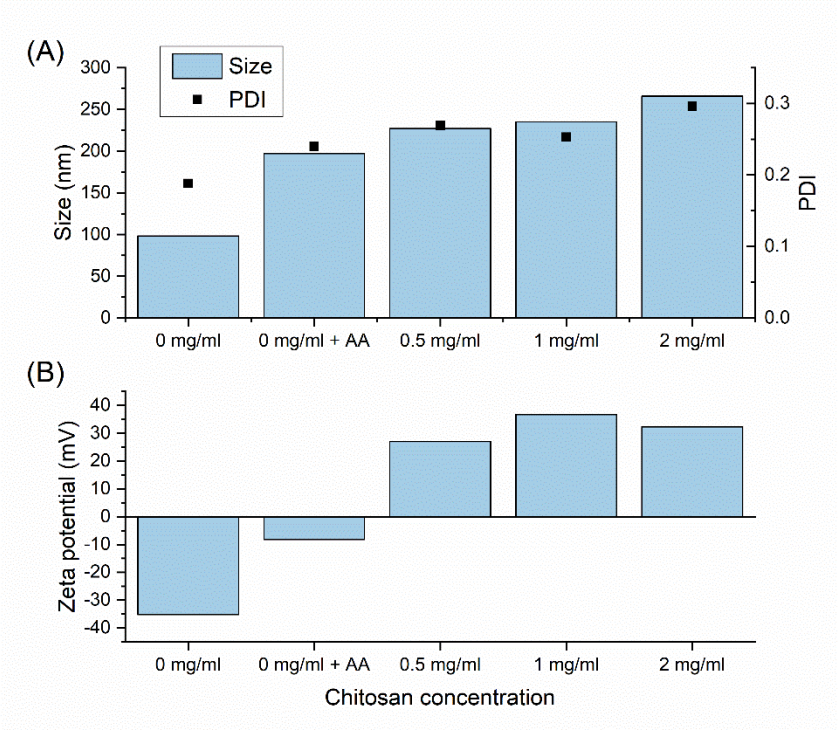

Figure 32: Nanocapsules sizes and PDI (**A**) and zeta potentials (**B**) after coating with chitosan (n=1). The nanocapsules were prepared with acetic acid (AA) in their non-solvent solution to dissolve chitosan, except for 0 mg/ml where no AA was used.

4.3.3 Release testing of nanocapsules loaded with retinoic acid

Nanocapsules prepared benchtop or with the MicroJet reactor, coated with either PS80 or P188, and with and without chitosan coating were prepared and their release was measured. First, a classical dialysis method and the NanoDis System were compared to select the best method for the release testing of our particles. Finally, the NanoDis System was used to measure the burst release of the different formulations.

4.3.3.1 Nanocapsules characterization

The PLGA nanocapsules were produced with the MJR technology or benchtop. Depending on the formulations, nanocapsules of different sizes were produced. Particles with size from 120 to 422 nm were produced, with a polydispersity index (PDI) from 0.09 to 0.32 (Table 7). The nanocapsules prepared benchtop had larger sizes

than the ones prepared with the MJR technology despite having the same composition, due to differences in mixing properties. When comparing P188 and PS80 nanocapsules, PS80 nanocapsules had the smallest size (120.7 nm against 185.7 nm). As coating the particles with chitosan increased their size PLGA and oleic acid concentrations were reduced from 1 and 1.5% (w/v) to produce the chitosan-coated nanocapsules with a concentration of 0.3 and 0.9% (w/v) respectively, labelled PS80-C and P188-C. This was done to keep nanoparticles' size in a comparable range to non-coated particles. Reducing PLGA and oil concentrations allowed the production of 254.4 nm for P188-C nanocapsules and 137.2 nm for PS80-C nanocapsules, respectively. When keeping the PLGA and oleic acid concentrations at 1 and 1.5% (w/v) (PS80-C high), the chitosan-coated particles had a large size of over 400 nm. The nanocapsules had negative zeta potentials around -40 mV, except when coated with chitosan, where their zeta potentials turned positive to values between 25 and 30 mV.

Table 7: Sizes, PDI and zeta potentials of PLGA nanocapsules

Nanocapsules	Size (nm)	PDI	Zeta potential (mV)
P188	185.7	0.18	-42.1
P188 benchtop	251.7	0.10	-52.4
PS80	120.7	0.23	-38.5
PS80 benchtop	189.0	0.25	-49.1
P188-C	254.4	0.09	25.5
PS80-C	137.2	0.32	30.4
PS80-C high	422.8	0.17	28.4

The encapsulation efficiency for all formulations was higher than 99%. This high encapsulation efficiency was possible due to the oleic acid core inside the nanocapsules. After several rinse cycles of the nanocapsules by TFF, the retinoic

concentration of the nanocapsules stayed stable, confirming the high encapsulation efficiency of the nanocapsules. The size, PDI, and count rate of the particles were unchanged after TFF purification.

The P188 nanocapsules were imaged by cryo-TEM (Figure 33). The particles were spherical and seemed to be smaller and have a larger polydispersity than what was measured by DLS, with diameters ranging from 20 to 130 nm. This size difference is to be expected as the hydrodynamic shell is not measured here by TEM.

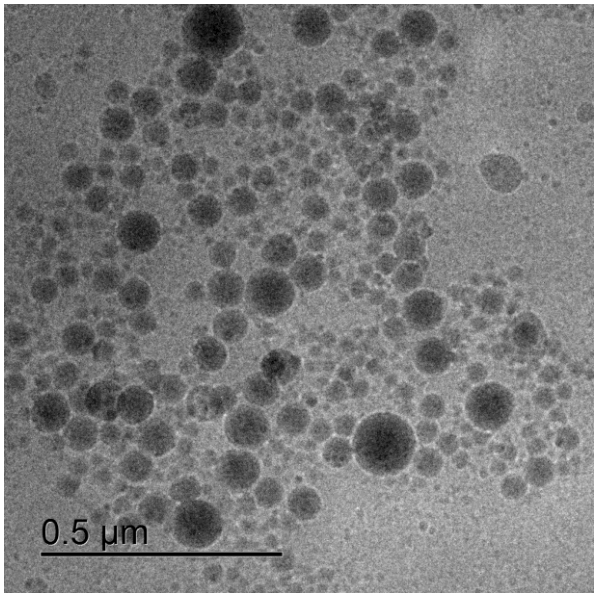

Figure 33: Cryo-TEM micrograph of P188 nanocapsules

4.3.3.2 Solubility in release media

Retinoic acid is a very hydrophobic molecule. Due to its poor solubility in water (<1 µg/ml), sink conditions for the tested concentrations could not be reached in PBS (Phosphate Buffered Saline). Surfactants had to be added to increase RA solubility in PBS pH 7.4. To do so, polysorbate 80 or SDS were added to PBS at 0.5% (w/v). The surfactants increased RA solubility after 3h of stirring, in PBS-PS80 and PBS-SDS to

92.3 ± 3.6 µg/ml and 84.6 ± 0.4 µg/ml respectively. RA solubility stayed constant after 24h of stirring and was measured to be 92.5 ± 2.1 µg/ml and 85.8 ± 2.9 µg/ml in PBS-PS80 and PBS-SDS respectively.

4.3.3.3 Dialysis release

The release from the nanocapsules was tested by dialysis. Free RA dissolved in release medium was used as control to assess the permeation kinetic of RA through the dialysis membrane. Two release media were compared: PBS pH 7.4 supplemented with either polysorbate 80 or SDS. The permeation kinetic of RA through the membrane was slow, despite testing membranes with different MW cut-offs. A high MWCO dialysis membrane of 300 kDa was used, as when a lower MWCO (14 kD) dialysis membrane was used, dissolved RA was not able to not cross the membrane even after 48h of stirring. It is very likely that the added surfactants formed micelles loading RA which prevented permeation of RA across the membrane despite the MWCO being, at least theoretically, sufficient for the permeation of this small molecule (Mw_{RA} = 300.44 g/mol).

In PBS-SDS and when using RA by itself, release took place over a time span of 30 hours (Figure 34). In PBS-PS80 media, only 85% of the full RA amount passed the membrane towards the acceptor compartment after 48h. The longer release time in PS80 might again be due to the formation of PS80-micelles around RA, which inhibited the permeation of the RA molecule through the membrane. There was no significant difference between the release profiles of RA encapsulated in PLGA and RA dissolved alone in the donor compartment, showing that the kinetic is controlled solely by the membrane permeation rather than the carriers. The release profile measured was

therefore not representative of the actual release happening inside the dialysis tube. These results could have easily been misinterpreted if not for the control of the permeation kinetics of the free drug.

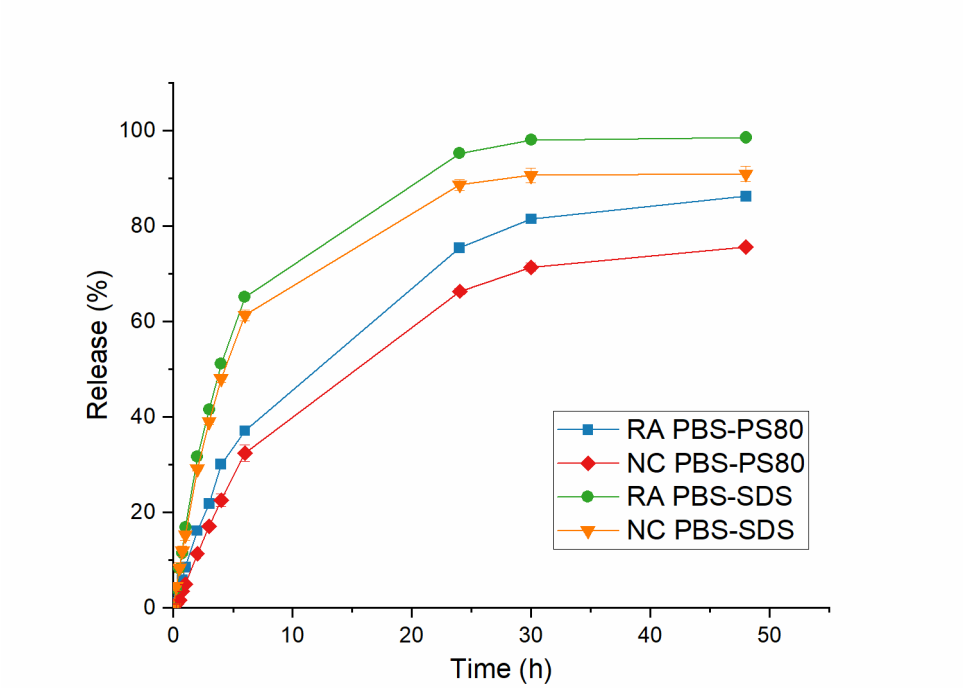

Figure 34: Release profile of P188 nanocapsules (NC) and dissolved retinoic acid (RA) in PBS-PS80 and PBS-SDS by dialysis. NC (n=3) and RA (n=1)

4.3.3.4 NanoDis release

To determine the filter efficiency and the lag phase between the time the API is released and the time the API is found in the filtrate, a control sample of RA dissolved in release medium was used (Figure 35.A). When using 500 kD filters, RA dissolved in medium could cross the filters after the first time point at a rate of 87% in PBS-PS80 and 82% in PBS-SDS. In PBS-PS80, 97% of the initial RA amount was found in the filtrate after the third time point (45 min) while in PBS-SDS, the crossing percentage remained stable at 80%. RA therefore demonstrated the ability to cross the hollow fiber

filters in higher amount when dissolved in PBS-PS80 than in PBS-SDS, probably due to mild interaction between SDS and the filters.

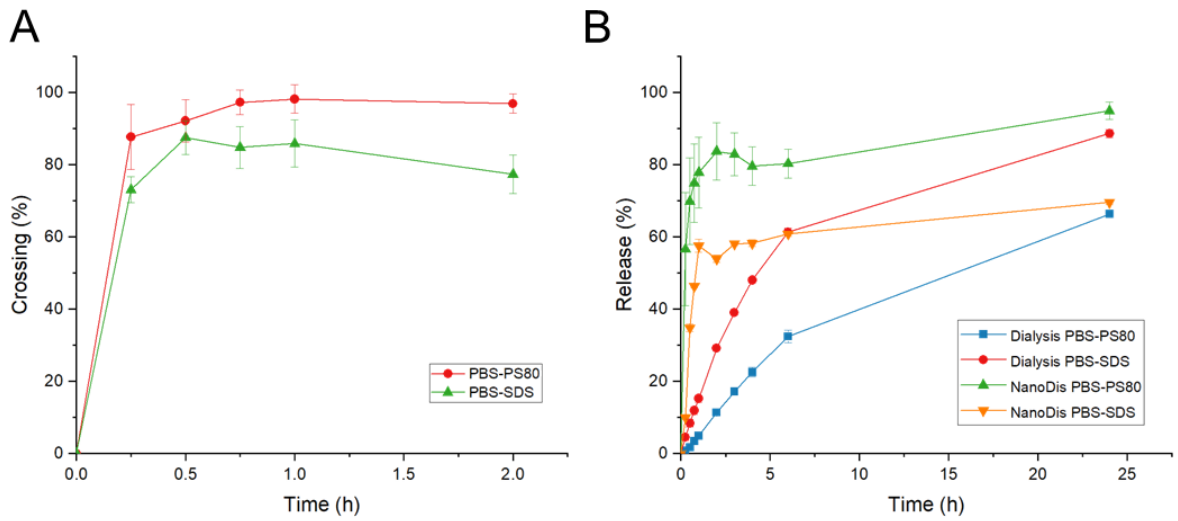

Figure 35: A. Crossing of dissolved RA in PBS-PS80 and PBS-SDS through hollow fiber filters (n=3); **B**. Comparison of release profile of P188 nanocapsules measured by dialysis or using the NanoDis System in PBS-PS80 and PBS-SDS (n=3).

Next, P188 nanocapsules were tested for drug release in the same release media at sink conditions. Release profiles using the NanoDis System were compared to the ones obtained by dialysis (Figure 35.B). A high burst release of 80% and 60% after 1h in PBS-PS80 and PBS-SDS respectively was observed with the NanoDis System, while only 5% and 15% release were measured by the dialysis method. With the NanoDis set-up, release was not limited by the permeation kinetic of the dialysis membrane, which allowed a much more accurate measurement of the burst release of the particles. The burst release of the nanocapsules was severely underestimated when using dialysis, particularly at short time points.

The measured release profile in PBS-SDS with the NanoDis System reached lower values than in PBS-PS80 at the same time, likely due to the interaction of RA micelles in SDS with the filters, as observed with the dissolved RA control. After 6 hours, the measured dialysis release in PBS-SDS became higher than the one measured with the NanoDis. Thus, the selection of the release medium and its interaction with the filters should be carefully assessed before performing release experiments with the NanoDis System, as any interactions of media also impact the measured release profile of the nanocapsules and lead to an underestimation of the burst release, although less drastic than with the dialysis method.

The release profiles of different formulations with or without chitosan were measured using PBS-PS80 (Figure 36) as media. The particles prepared with either P188 or PS80 had similar release profiles with a high burst release of 85% after 1h. When the nanocapsules were coated with chitosan, burst release was markedly reduced to 50% for both particles prepared with PS80 or P188. As chitosan is positively charged, ionic interaction with retinoic acid — whose carboxylic group is negatively charged at neutral pH (pKa 4.76) — facilitates the control of the burst release. Increasing the amount of PLGA and oil in the chitosan-coated nanocapsule formulations decreased the burst release to 40% (PS80-C high). Increasing the polymer and oil contents resulted in a longer diffusion path for RA, due to the increase in size of the particles, and thereby decreased the burst release. Furthermore, increasing the PLGA and oil amount in the formulation increased the nanocapsules size, thus decreasing the surface/volume ratio. With a lower amount of RA exposed at the surface of the particles, a lower amount of RA could immediately dissolve in the medium, leading to a lower burst release. This reduction of burst release was also observed with the benchtop nanocapsules. Indeed, the formulations prepared benchtop, with similar compositions

but with larger size than their continuous-prepared counterparts, had a slightly lower burst release of 71% and 64% after 1h, reaching 79% and 72% after 24h, for P188 and PS80 benchtop nanocapsules respectively. Thus, diffusion seemed to have a slight impact in reducing the burst release. However, simply increasing the particles size, to even larger size than the nanocapsules coated with chitosan for PS80 nanocapsules, did not allow a reduction of the burst release to the same range as the nanocapsules coated with chitosan. Thus, the coating with chitosan seemed to be the driving force of the burst release reduction, rather than pure increase of the diffusion path.

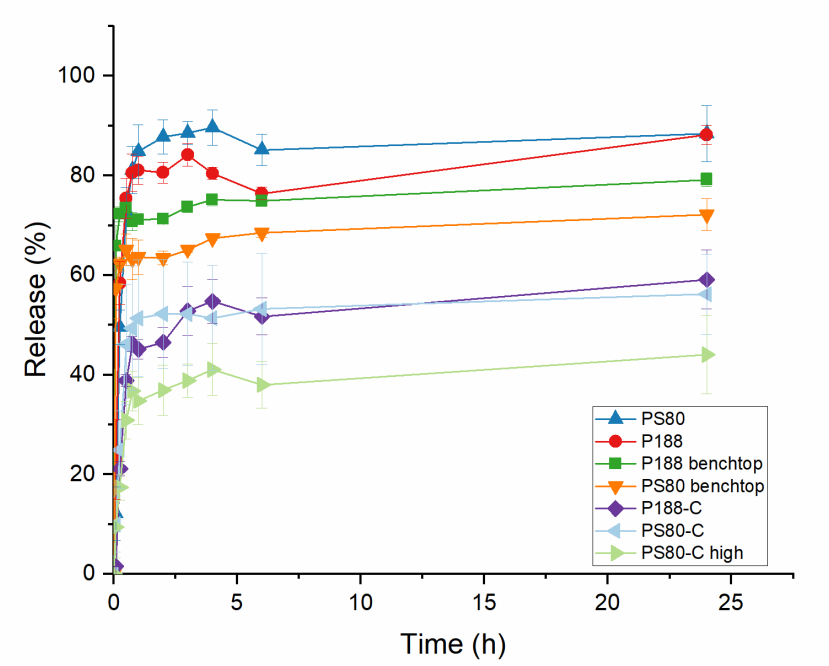

Figure 36: Release profile of PLGA nanocapsules in PBS-PS80 using the NanoDis System (n=3).

Reduction of the burst release from nanocapsules was therefore possible by coating them with chitosan. However, this change in surface charges might cause change in the protein corona forming around the particles, as the protein corona composition has

been reported to be sensitive to size and charges [129]. The particles developed here were coated with surfactants to cross the BBB by receptor-mediated transcytosis, thanks to their protein corona composition enriched in apolipoproteins. Once coated with chitosan, the nanocapsules become positively charge and might then cross the BBB by adsorption-mediated transcytosis rather than by receptor-mediated transcytosis as initially planned. Furthermore, it was possible to further reduce the burst release of chitosan-coated nanocapsules by increasing their size. Larger particles might have more difficulty crossing the BBB by endocytosis. In conclusion, a compromise should be found between the parameters of the formulation to reduce burst release to a minimum while still conserving the ability of the nanocapsules to cross the BBB to deliver their cargo to the brain.

4.4 Conclusion

In conclusion, PLGA nanospheres and nanocapsules loaded with retinoic acid were produced with the MJR technology. The formulations could be optimized to have high EE. However, the nanospheres precipitated over time and had large sizes which could hinder BBB crossing. Nanocapsules had smaller size and better colloidal stability. The release kinetics of the particles were assessed with the NanoDis System, which allowed a better characterization of the burst release of the particles than the classical dialysis method. The nanospheres and nanocapsules had high burst release, which could be reduced by coating the nanocapsules with chitosan. However, this coating might have an impact on the BBB crossing abilities of the nanoparticles, which should be assessed in further studies. If these particles then prove able to cross the BBB by adsorptive-mediated transcytosis, they could be interesting formulation for the delivery of retinoic acid to NSCs.

5. Summary and outlook

Treatments of central nervous system (CNS) diseases remains a real challenge for modern medicine due to the difficulty to cross the blood-brain barrier (BBB). Regenerative treatments based on increasing the proliferation of neural stem cells (NSCs) and their differentiation in new neuronal cells could prove interesting for improving the recovery of stroke patients, if these treatments were able to reach the deep brain structures where these cells are situated. All-trans retinoic acid (RA) is a promising molecule, which has been shown able to increase the differentiation of NSCs [105]. This molecule is physiologically present in the adult human CNS, but in a lower amount than needed to exercise its regenerative action. Its low solubility in water impedes its simple intravenous administration. Thus, loading this drug in nanoparticles able to cross the BBB seemed a good solution. Inside the large variety of nanoparticles developed to cross the BBB, PLGA nanoparticles coated with surfactants, polysorbate 80 (PS80) or poloxamer 188 (P188), are interesting, due to their ease of production, good biocompatibility and the FDA acceptance of their materials.

Hence, in this thesis, valuable information on the development of PLGA nanoparticles loaded with RA and coated with surfactants for delivery to the NSCs through the BBB were obtained.

PLGA nanoparticles were developed using the MicroJet reactor® (MJR) technology. These nanoparticles were coated with surfactants, PS80 and P188, and first loaded with a fluorescent dye, to characterize their *in vitro* interactions with a BBB model. Small nanoparticles under 100 nm could be produced in a reproducible manner, easy to number-up. *In vitro* experiments showed that the nanoparticles could be endocytosed by the brain-like endothelial cells by receptor-mediated endocytosis, probably partly through the LDLR. The nanoparticles were also found in the abluminal compartment of the model, showing their ability to be transcytosed by the endothelial

cells. PS80 and P188 nanoparticles had slightly different uptake profiles, suggesting that their interaction with the cells were conditioned by their surfactant coating, and probably the different protein coronas forming around them. However, this hypothesis could not be confirmed by performing protein corona characterization in cell medium containing human serum, or in human serum alone. Indeed, the techniques used were not specific enough to differentiate between the coronas forming on the formulations without coating or coated with P188 or PS80. Initially, deeper studies to characterize the protein corona using fluorescent and circular dichroism spectroscopy and LC/MS-MS had been planned with an external partner in Zagreb (Croatia) at the Institute for Medical Research and Occupational Health, but could not be performed due to COVID-19 interferences. A better understanding of the qualitative composition of the protein corona forming around the nanoparticles might have helped better understand their differences in uptake profile *in vitro.*

In a second part, the nanoparticles were loaded with RA. First, nanospheres were produced with the MJR technology but their sizes were too big for efficient BBB crossing and their release kinetics showed a high burst release. To solve this issue, nanocapsules were produced with an oily core of oleic acid. The produced nanocapsules had lower size and high encapsulation efficiency. However, the addition of oleic acid alone did not reduce the burst release of the particles. The nanocapsules were coated with chitosan, which helped reduced the burst release of the nanocapsules. Indeed, as chitosan is positively charged, RA which is negatively charged at neutral pH might interact more with the chitosan coating of the particles, thus preventing its fast release. However, coating the nanocapsules with chitosan modifies the surface properties of the particles, giving them a positive zeta potential. This surface modification implies that a different protein corona might form around the

particles once in the blood, which might not be as enriched in apolipoproteins than the particles simply coated with surfactants. Nevertheless, the positive charges of the particles might allow them to cross the BBB by adsorptive-mediated transcytosis instead of receptor-mediated transcytosis, as first planned. This hypothesis would need to be tested by additional protein corona studies as well as *in vitro* studies. If these particles are shown able to cross the BBB, they could then be very interesting for the delivery of retinoic acid to the brain, thanks to their high loading and their ease of production. Next, these nanoparticles would need to be tested on NSCs to check their ability to induce their differentiation in new neuronal cells and their toxicity. Following these experiments, the RA content in the formulation will need to be optimized to insure correct release properties with low burst release, low cell toxicity (on the BBB endothelial cells as well as on NSCs) and efficient NSCs differentiation.

6. Annexes

6.1 References

1. World Health Organization The Top 10 Causes of Death Available online: https://www.who.int/news-room/fact-sheets/detail/the-top-10-causes-of-death (accessed on 22 February 2019).
2. Jaffer, H.; Morris, V.B.; Stewart, D.; Labhasetwar, V. Advances in Stroke Therapy. *Drug Deliv. Transl. Res.* **2011**, *1*, 409–419, doi:10.1007/s13346-011-0046-y.
3. Prabhakaran, S.; Ruff, I.; Bernstein, R.A. Acute Stroke Intervention: A Systematic Review. *JAMA* **2015**, *313*, 1451–1462, doi:10.1001/jama.2015.3058.
4. Sarvari, S.; Moakedi, F.; Hone, E.; Simpkins, J.W.; Ren, X. Mechanisms in Blood-Brain Barrier Opening and Metabolism-Challenged Cerebrovascular Ischemia with Emphasis on Ischemic Stroke. *Metab. Brain Dis.* **2020**, *35*, 851–868, doi:10.1007/s11011-020-00573-8.
5. Bhaskar, S.; Stanwell, P.; Cordato, D.; Attia, J.; Levi, C. Reperfusion Therapy in Acute Ischemic Stroke: Dawn of a New Era? *BMC Neurol.* **2018**, *18*, 8, doi:10.1186/s12883-017-1007-y.
6. Bernardo-Castro, S.; Sousa, J.A.; Brás, A.; Cecília, C.; Rodrigues, B.; Almendra, L.; Machado, C.; Santo, G.; Silva, F.; Ferreira, L.; et al. Pathophysiology of Blood–Brain Barrier Permeability Throughout the Different Stages of Ischemic Stroke and Its Implication on Hemorrhagic Transformation and Recovery. *Front. Neurol.* **2020**, *11*, doi:10.3389/fneur.2020.594672.
7. Zhang, J.; Yang, Y.; Sun, H.; Xing, Y. Hemorrhagic Transformation after Cerebral Infarction: Current Concepts and Challenges. *Ann. Transl. Med.* **2014**, *2*, doi:10.3978/j.issn.2305-5839.2014.08.08.
8. Teasell, R.; Rice, D.; Richardson, M.; Campbell, N.; Madady, M.; Hussein, N.; Murie-Fernandez, M.; Page, S. The next Revolution in Stroke Care. *Expert Rev. Neurother.* **2014**, *14*, 1307–1314, doi:10.1586/14737175.2014.968130.
9. Dobkin, B.H. Rehabilitation after Stroke. *N. Engl. J. Med.* **2005**, *352*, 1677–1684, doi:10.1056/NEJMcp043511.
10. Obernier, K.; Alvarez-Buylla, A. Neural Stem Cells: Origin, Heterogeneity and Regulation in the Adult Mammalian Brain. *Development* **2019**, *146*, doi:10.1242/dev.156059.
11. Zhao, X.; Moore, D. Neural Stem Cells: Developmental Mechanisms and Disease Modeling. *Cell Tissue Res.* **2018**, *371*, 1–6, doi:10.1007/s00441-017-2738-1.
12. Pino, A.; Fumagalli, G.; Bifari, F.; Decimo, I. New Neurons in Adult Brain: Distribution, Molecular Mechanisms and Therapies. *Biochem. Pharmacol.* **2017**, *141*, 4–22, doi:10.1016/j.bcp.2017.07.003.
13. Malatesta, P.; Appolloni, I.; Calzolari, F. Radial Glia and Neural Stem Cells. *Cell Tissue Res.* **2008**, *331*, 165–178, doi:10.1007/s00441-007-0481-8.
14. Galli, R.; Gritti, A.; Bonfanti, L.; Vescovi, A.L. Neural Stem Cells. *Circ. Res.* **2003**, *92*, 598–608, doi:10.1161/01.RES.0000065580.02404.F4.
15. Swayne, L.A.; Sanchez-Arias, J.C.; Agbay, A.; Willerth, S.M. What Are Neural Stem Cells, and Why Are They Important? Available online: https://kids.frontiersin.org/article/10.3389/frym.2016.00020 (accessed on 5 January 2021).

16. Abbott, N.J.; Rönnbäck, L.; Hansson, E. Astrocyte–Endothelial Interactions at the Blood–Brain Barrier. *Nat. Rev. Neurosci.* **2006**, *7*, 41–53, doi:10.1038/nrn1824.
17. Sweeney, M.D.; Sagare, A.P.; Zlokovic, B.V. Blood–Brain Barrier Breakdown in Alzheimer Disease and Other Neurodegenerative Disorders. *Nat. Rev. Neurol.* **2018**, *14*, 133–150, doi:10.1038/nrneurol.2017.188.
18. Abbott, N.J.; Patabendige, A.A.K.; Dolman, D.E.M.; Yusof, S.R.; Begley, D.J. Structure and Function of the Blood–Brain Barrier. *Neurobiol. Dis.* **2010**, *37*, 13–25, doi:10.1016/j.nbd.2009.07.030.
19. Hawkins, B.T.; Davis, T.P. The Blood-Brain Barrier/Neurovascular Unit in Health and Disease. *Pharmacol. Rev.* **2005**, *57*, 173–185, doi:10.1124/pr.57.2.4.
20. Saraiva, C.; Praça, C.; Ferreira, R.; Santos, T.; Ferreira, L.; Bernardino, L. Nanoparticle-Mediated Brain Drug Delivery: Overcoming Blood–Brain Barrier to Treat Neurodegenerative Diseases. *J. Controlled Release* **2016**, *235*, 34–47, doi:10.1016/j.jconrel.2016.05.044.
21. Ballabh, P.; Braun, A.; Nedergaard, M. The Blood–Brain Barrier: An Overview: Structure, Regulation, and Clinical Implications. *Neurobiol. Dis.* **2004**, *16*, 1–13, doi:10.1016/j.nbd.2003.12.016.
22. Lombardo, S.M.; Schneider, M.; Türeli, A.E.; Türeli, N.G. Key for Crossing the BBB with Nanoparticles: The Rational Design. *Beilstein J. Nanotechnol.* **2020**, *11*, 866–883, doi:10.3762/bjnano.11.72.
23. Sanchez-Covarrubias, L.; Slosky, L.M.; Thompson, B.J.; Davis, T.P.; Ronaldson, P.T. Transporters at CNS Barrier Sites: Obstacles or Opportunities for Drug Delivery? *Curr. Pharm. Des.* **2014**, *20*, 1422–1449.
24. Banks, W.A.; Owen, J.B.; Erickson, M.A. Insulin in the Brain: There and Back Again. *Pharmacol. Ther.* **2012**, *136*, 82–93, doi:10.1016/j.pharmthera.2012.07.006.
25. Boado, R.J.; Li, J.Y.; Nagaya, M.; Zhang, C.; Pardridge, W.M. Selective Expression of the Large Neutral Amino Acid Transporter at the Blood–Brain Barrier. *Proc. Natl. Acad. Sci. U. S. A.* **1999**, *96*, 12079–12084.
26. Zhang, Z.; Zhan, C. 5 - Receptor-Mediated Transportation through BBB. In *Brain Targeted Drug Delivery System*; Gao, H., Gao, X., Eds.; Academic Press, 2019; pp. 105–128 ISBN 978-0-12-814001-7.
27. Schinkel, A.H.; Wagenaar, E.; Mol, C.A.; Deemter, L. van P-Glycoprotein in the Blood-Brain Barrier of Mice Influences the Brain Penetration and Pharmacological Activity of Many Drugs. *J. Clin. Invest.* **1996**, *97*, 2517–2524, doi:10.1172/JCI118699.
28. Kim, R.B. Drugs as P-Glycoprotein Substrates, Inhibitors, and Inducers. *Drug Metab. Rev.* **2002**, *34*, 47–54, doi:10.1081/dmr-120001389.
29. Jones, A.R.; Shusta, E.V. Blood-Brain Barrier Transport of Therapeutics via Receptor-Mediation. *Pharm. Res.* **2007**, *24*, 1759–1771, doi:10.1007/s11095-007-9379-0.
30. Lajoie, J.M.; Shusta, E.V. Targeting Receptor-Mediated Transport for Delivery of Biologics Across the Blood-Brain Barrier. *Annu. Rev. Pharmacol. Toxicol.* **2015**, *55*, 613–631, doi:10.1146/annurev-pharmtox-010814-124852.
31. Hervé, F.; Ghinea, N.; Scherrmann, J.-M. CNS Delivery Via Adsorptive Transcytosis. *AAPS J.* **2008**, *10*, 455–472, doi:10.1208/s12248-008-9055-2.
32. Lu, W. Adsorptive-Mediated Brain Delivery Systems. *Curr. Pharm. Biotechnol.* **2012**, *13*, 2340–2348, doi:10.2174/138920112803341851.

33. Zhu, X.; Jin, K.; Huang, Y.; Pang, Z. 7 - Brain Drug Delivery by Adsorption-Mediated Transcytosis. In *Brain Targeted Drug Delivery System*; Gao, H., Gao, X., Eds.; Academic Press, 2019; pp. 159–183 ISBN 978-0-12-814001-7.
34. Bickel, U.; Yoshikawa, T.; Pardridge, W.M. Delivery of Peptides and Proteins through the Blood–Brain Barrier. *Adv. Drug Deliv. Rev.* **2001**, *46*, 247–279, doi:10.1016/S0169-409X(00)00139-3.
35. Kreuter, J.; Alyautdin, R.N.; Kharkevich, D.A.; Ivanov, A.A. Passage of Peptides through the Blood-Brain Barrier with Colloidal Polymer Particles (Nanoparticles). *Brain Res.* **1995**, *674*, 171–174, doi:10.1016/0006-8993(95)00023-J.
36. Kreuter, J.; Petrov, V.E.; Kharkevich, D.A.; Alyautdin, R.N. Influence of the Type of Surfactant on the Analgesic Effects Induced by the Peptide Dalargin after Its Delivery across the Blood–Brain Barrier Using Surfactant-Coated Nanoparticles. *J. Controlled Release* **1997**, *49*, 81–87, doi:10.1016/S0168-3659(97)00061-8.
37. Kreuter, J.; Ramge, P.; Petrov, V.; Hamm, S.; Gelperina, S.E.; Engelhardt, B.; Alyautdin, R.; von Briesen, H.; Begley, D.J. Direct Evidence That Polysorbate-80-Coated Poly(Butylcyanoacrylate) Nanoparticles Deliver Drugs to the CNS via Specific Mechanisms Requiring Prior Binding of Drug to the Nanoparticles. *Pharm. Res.* **2003**, *20*, 409–416, doi:10.1023/a:1022604120952.
38. Lück, M. Plasmaproteinadsorption Als Möglicher Schlüsselfaktor Für Eine Kontrollierte Arzneistoffapplikation Mit Partikulären Trägern. PhD thesis, Freie Universität: Berlin, 1997.
39. Kreuter, J.; Shamenkov, D.; Petrov, V.; Ramge, P.; Cychutek, K.; Koch-Brandt, C.; Alyautdin, R. Apolipoprotein-Mediated Transport of Nanoparticle-Bound Drugs Across the Blood-Brain Barrier. *J. Drug Target.* **2002**, *10*, 317–325, doi:10.1080/10611860290031877.
40. Ambruosi, A.; Gelperina, S.; Khalansky, A.; Tanski, S.; Theisen, A.; Kreuter, J. Influence of Surfactants, Polymer and Doxorubicin Loading on the Anti-Tumour Effect of Poly(Butyl Cyanoacrylate) Nanoparticles in a Rat Glioma Model. *J. Microencapsul.* **2006**, *23*, 582–592, doi:10.1080/02652040600788080.
41. Kreuter, J. Influence of the Surface Properties on Nanoparticle-Mediated Transport of Drugs to the Brain. *J. Nanosci. Nanotechnol.* **2004**, *4*, 484–488, doi:10.1166/jnn.2003.077.
42. Petri, B.; Bootz, A.; Khalansky, A.; Hekmatara, T.; Müller, R.; Uhl, R.; Kreuter, J.; Gelperina, S. Chemotherapy of Brain Tumour Using Doxorubicin Bound to Surfactant-Coated Poly(Butyl Cyanoacrylate) Nanoparticles: Revisiting the Role of Surfactants. *J. Controlled Release* **2007**, *117*, 51–58, doi:10.1016/j.jconrel.2006.10.015.
43. Gelperina, S.; Maksimenko, O.; Khalansky, A.; Vanchugova, L.; Shipulo, E.; Abbasova, K.; Berdiev, R.; Wohlfart, S.; Chepurnova, N.; Kreuter, J. Drug Delivery to the Brain Using Surfactant-Coated Poly(Lactide-Co-Glycolide) Nanoparticles: Influence of the Formulation Parameters. *Eur. J. Pharm. Biopharm.* **2010**, *74*, 157–163, doi:10.1016/j.ejpb.2009.09.003.
44. Tahara, K.; Miyazaki, Y.; Kawashima, Y.; Kreuter, J.; Yamamoto, H. Brain Targeting with Surface-Modified Poly(d,l-Lactic-Co-Glycolic Acid) Nanoparticles Delivered via Carotid Artery Administration. *Eur. J. Pharm. Biopharm.* **2011**, *77*, 84–88, doi:10.1016/j.ejpb.2010.11.002.
45. Ren, T.; Xu, N.; Cao, C.; Yuan, W.; Yu, X.; Chen, J.; Ren, J. Preparation and Therapeutic Efficacy of Polysorbate-80-Coated Amphotericin B/PLA-b-PEG

Nanoparticles. *J. Biomater. Sci. Polym. Ed.* **2009**, *20*, 1369–1380, doi:10.1163/092050609X12457418779185.
46. Raudszus, B.; Partikel, K.; Mulac, D.; Langer, K. Characterisation and Cellular Uptake of Polysorbate 80-Coated PLA Nanoparticles. *Mater. Today Proc.* **2017**, *4*, S193–S199, doi:10.1016/j.matpr.2017.09.186.
47. Chen, Y.-C.; Hsieh, W.-Y.; Lee, W.-F.; Zeng, D.-T. Effects of Surface Modification of PLGA-PEG-PLGA Nanoparticles on Loperamide Delivery Efficiency across the Blood–Brain Barrier. *J. Biomater. Appl.* **2013**, *27*, 909–922, doi:10.1177/0885328211429495.
48. Gao, K.; Jiang, X. Influence of Particle Size on Transport of Methotrexate across Blood Brain Barrier by Polysorbate 80-Coated Polybutylcyanoacrylate Nanoparticles. *Int. J. Pharm.* **2006**, *310*, 213–219, doi:10.1016/j.ijpharm.2005.11.040.
49. Oh, N.; Park, J.-H. Endocytosis and Exocytosis of Nanoparticles in Mammalian Cells. *Int. J. Nanomedicine* **2014**, *9*, 51–63, doi:10.2147/IJN.S26592.
50. Zhang, S.; Li, J.; Lykotrafitis, G.; Bao, G.; Suresh, S. Size-Dependent Endocytosis of Nanoparticles. *Adv. Mater.* **2009**, *21*, 419–424, doi:10.1002/adma.200801393.
51. Jo, D.H.; Kim, J.H.; Lee, T.G.; Kim, J.H. Size, Surface Charge, and Shape Determine Therapeutic Effects of Nanoparticles on Brain and Retinal Diseases. *Nanomedicine Nanotechnol. Biol. Med.* **2015**, *11*, 1603–1611, doi:10.1016/j.nano.2015.04.015.
52. De Jong, W.H.; Hagens, W.I.; Krystek, P.; Burger, M.C.; Sips, A.J.A.M.; Geertsma, R.E. Particle Size-Dependent Organ Distribution of Gold Nanoparticles after Intravenous Administration. *Biomaterials* **2008**, *29*, 1912–1919, doi:10.1016/j.biomaterials.2007.12.037.
53. Sonavane, G.; Tomoda, K.; Makino, K. Biodistribution of Colloidal Gold Nanoparticles after Intravenous Administration: Effect of Particle Size. *Colloids Surf. B Biointerfaces* **2008**, *66*, 274–280, doi:10.1016/j.colsurfb.2008.07.004.
54. Khlebtsov, N.; Dykman, L. Biodistribution and Toxicity of Engineered Gold Nanoparticles: A Review of in Vitro and in Vivo Studies. *Chem. Soc. Rev.* **2011**, *40*, 1647–1671, doi:10.1039/c0cs00018c.
55. Nicholson, C.; Hrabětová, S. Brain Extracellular Space: The Final Frontier of Neuroscience. *Biophys. J.* **2017**, *113*, 2133–2142, doi:10.1016/j.bpj.2017.06.052.
56. Syková, E.; Nicholson, C. Diffusion in Brain Extracellular Space. *Physiol. Rev.* **2008**, *88*, 1277–1340, doi:10.1152/physrev.00027.2007.
57. Godin, A.G.; Varela, J.A.; Gao, Z.; Danné, N.; Dupuis, J.P.; Lounis, B.; Groc, L.; Cognet, L. Single-Nanotube Tracking Reveals the Nanoscale Organization of the Extracellular Space in the Live Brain. *Nat. Nanotechnol.* **2017**, *12*, 238–243, doi:10.1038/nnano.2016.248.
58. Lin, J.; Zhang, H.; Chen, Z.; Zheng, Y. Penetration of Lipid Membranes by Gold Nanoparticles: Insights into Cellular Uptake, Cytotoxicity, and Their Relationship. *ACS Nano* **2010**, *4*, 5421–5429, doi:10.1021/nn1010792.
59. Goodman, C.M.; McCusker, C.D.; Yilmaz, T.; Rotello, V.M. Toxicity of Gold Nanoparticles Functionalized with Cationic and Anionic Side Chains. *Bioconjug. Chem.* **2004**, *15*, 897–900, doi:10.1021/bc049951i.

60. Lin, J.-Q.; Zheng, Y.-G.; Zhang, H.-W.; Chen, Z. A Simulation Study on Nanoscale Holes Generated by Gold Nanoparticles on Negative Lipid Bilayers. *Langmuir* **2011**, *27*, 8323–8332, doi:10.1021/la201086u.
61. Suk, J.S.; Xu, Q.; Kim, N.; Hanes, J.; Ensign, L.M. PEGylation as a Strategy for Improving Nanoparticle-Based Drug and Gene Delivery. *Adv. Drug Deliv. Rev.* **2016**, *99*, 28–51, doi:10.1016/j.addr.2015.09.012.
62. Hu, K.; Shi, Y.; Jiang, W.; Han, J.; Huang, S.; Jiang, X. Lactoferrin Conjugated PEG-PLGA Nanoparticles for Brain Delivery: Preparation, Characterization and Efficacy in Parkinson's Disease. *Int. J. Pharm.* **2011**, *415*, 273–283, doi:10.1016/j.ijpharm.2011.05.062.
63. Li, J.; Feng, L.; Fan, L.; Zha, Y.; Guo, L.; Zhang, Q.; Chen, J.; Pang, Z.; Wang, Y.; Jiang, X.; et al. Targeting the Brain with PEG–PLGA Nanoparticles Modified with Phage-Displayed Peptides. *Biomaterials* **2011**, *32*, 4943–4950, doi:10.1016/j.biomaterials.2011.03.031.
64. Liu, Z.; Gao, X.; Kang, T.; Jiang, M.; Miao, D.; Gu, G.; Hu, Q.; Song, Q.; Yao, L.; Tu, Y.; et al. B6 Peptide-Modified PEG-PLA Nanoparticles for Enhanced Brain Delivery of Neuroprotective Peptide. *Bioconjug. Chem.* **2013**, *24*, 997–1007, doi:10.1021/bc400055h.
65. Guo, J.; Gao, X.; Su, L.; Xia, H.; Gu, G.; Pang, Z.; Jiang, X.; Yao, L.; Chen, J.; Chen, H. Aptamer-Functionalized PEG–PLGA Nanoparticles for Enhanced Anti-Glioma Drug Delivery. *Biomaterials* **2011**, *32*, 8010–8020, doi:10.1016/j.biomaterials.2011.07.004.
66. Nance, E.A.; Woodworth, G.F.; Sailor, K.A.; Shih, T.-Y.; Xu, Q.; Swaminathan, G.; Xiang, D.; Eberhart, C.; Hanes, J. A Dense Poly(Ethylene Glycol) Coating Improves Penetration of Large Polymeric Nanoparticles within Brain Tissue. *Sci. Transl. Med.* **2012**, *4*, 149ra119, doi:10.1126/scitranslmed.3003594.
67. Tosi, G.; Vilella, A.; Veratti, P.; Belletti, D.; Pederzoli, F.; Ruozi, B.; Vandelli, M.A.; Zoli, M.; Forni, F. Exploiting Bacterial Pathways for BBB Crossing with PLGA Nanoparticles Modified with a Mutated Form of Diphtheria Toxin (CRM197): In Vivo Experiments. *Mol. Pharm.* **2015**, *12*, 3672–3684, doi:10.1021/acs.molpharmaceut.5b00446.
68. Sulheim, E.; Baghirov, H.; von Haartman, E.; Bøe, A.; Åslund, A.K.O.; Mørch, Y.; Davies, C. de L. Cellular Uptake and Intracellular Degradation of Poly(Alkyl Cyanoacrylate) Nanoparticles. *J. Nanobiotechnology* **2016**, *14*, doi:10.1186/s12951-015-0156-7.
69. Makadia, H.K.; Siegel, S.J.; Makadia, H.K.; Siegel, S.J. Poly Lactic-Co-Glycolic Acid (PLGA) as Biodegradable Controlled Drug Delivery Carrier. *Polymers* **2011**, *3*, 1377–1397, doi:10.3390/polym3031377.
70. Xin, H.; Jiang, X.; Gu, J.; Sha, X.; Chen, L.; Law, K.; Chen, Y.; Wang, X.; Jiang, Y.; Fang, X. Angiopep-Conjugated Poly(Ethylene Glycol)-Co-Poly(ε-Caprolactone) Nanoparticles as Dual-Targeting Drug Delivery System for Brain Glioma. *Biomaterials* **2011**, *32*, 4293–4305, doi:10.1016/j.biomaterials.2011.02.044.
71. Aktaş, Y.; Yemisci, M.; Andrieux, K.; Gürsoy, R.N.; Alonso, M.J.; Fernandez-Megia, E.; Novoa-Carballal, R.; Quiñoá, E.; Riguera, R.; Sargon, M.F.; et al. Development and Brain Delivery of Chitosan−PEG Nanoparticles Functionalized with the Monoclonal Antibody OX26. *Bioconjug. Chem.* **2005**, *16*, 1503–1511, doi:10.1021/bc050217o.

72. Gu, J.; Al-Bayati, K.; Ho, E.A. Development of Antibody-Modified Chitosan Nanoparticles for the Targeted Delivery of SiRNA across the Blood-Brain Barrier as a Strategy for Inhibiting HIV Replication in Astrocytes. *Drug Deliv. Transl. Res.* **2017**, *7*, 497–506, doi:10.1007/s13346-017-0368-5.
73. Lepeltier, E.; Bourgaux, C.; Couvreur, P. Nanoprecipitation and the “Ouzo Effect”: Application to Drug Delivery Devices. *Adv. Drug Deliv. Rev.* **2014**, *71*, 86–97, doi:10.1016/j.addr.2013.12.009.
74. Crucho, C.I.C.; Barros, M.T. Polymeric Nanoparticles: A Study on the Preparation Variables and Characterization Methods. *Mater. Sci. Eng. C* **2017**, *80*, 771–784, doi:10.1016/j.msec.2017.06.004.
75. Botet, R. The “Ouzo Effect”, Recent Developments and Application to Therapeutic Drug Carrying. *J. Phys. Conf. Ser.* **2012**, *352*, 012047, doi:10.1088/1742-6596/352/1/012047.
76. Huang, W.; Zhang, C. Tuning the Size of Poly(Lactic-Co-Glycolic Acid) (PLGA) Nanoparticles Fabricated by Nanoprecipitation. *Biotechnol. J.* **2018**, *13*, doi:10.1002/biot.201700203.
77. Galindo-Rodriguez, S.; Allémann, E.; Fessi, H.; Doelker, E. Physicochemical Parameters Associated with Nanoparticle Formation in the Salting-Out, Emulsification-Diffusion, and Nanoprecipitation Methods. *Pharm. Res.* **2004**, *21*, 1428–1439, doi:10.1023/B:PHAM.0000036917.75634.be.
78. Scholes, P.D.; Coombes, A.G.A.; Illum, L.; Daviz, S.S.; Vert, M.; Davies, M.C. The Preparation of Sub-200 Nm Poly(Lactide-Co-Glycolide) Microspheres for Site-Specific Drug Delivery. *J. Controlled Release* **1993**, *25*, 145–153, doi:10.1016/0168-3659(93)90103-C.
79. Rong, X.; Xie, Y.; Hao, X.; Chen, T.; Wang, Y.; Liu, Y. Applications of Polymeric Nanocapsules in Field of Drug Delivery Systems. *Curr. Drug Discov. Technol.* **2011**, *8*, 173–187, doi:10.2174/157016311796799008.
80. Vauthier, C.; Bouchemal, K. Processing and Scale-up of Polymeric Nanoparticles. In *Intracellular Delivery: Fundamentals and Applications*; Prokop, A., Ed.; Fundamental Biomedical Technologies; Springer Netherlands: Dordrecht, 2011; pp. 433–456 ISBN 978-94-007-1248-5.
81. Günday Türeli, N.; Türeli, A.E.; Schneider, M. Optimization of Ciprofloxacin Complex Loaded PLGA Nanoparticles for Pulmonary Treatment of Cystic Fibrosis Infections: Design of Experiments Approach. *Int. J. Pharm.* **2016**, *515*, 343–351, doi:10.1016/j.ijpharm.2016.10.025.
82. Liu, Y.; Cheng, C.; Liu, Y.; Prud’homme, R.K.; Fox, R.O. Mixing in a Multi-Inlet Vortex Mixer (MIVM) for Flash Nano-Precipitation. *Chem. Eng. Sci.* **2008**, *63*, 2829–2842, doi:10.1016/j.ces.2007.10.020.
83. Saarinen-Savolainen, P.; Järvinen, T.; Taipale, H.; Urtti, A. Method for Evaluating Drug Release from Liposomes in Sink Conditions. *Int. J. Pharm.* **1997**, *159*, 27–33, doi:10.1016/S0378-5173(97)00264-0.
84. Govender, T.; Stolnik, S.; Garnett, M.C.; Illum, L.; Davis, S.S. PLGA Nanoparticles Prepared by Nanoprecipitation: Drug Loading and Release Studies of a Water Soluble Drug. *J. Controlled Release* **1999**, *57*, 171–185, doi:10.1016/S0168-3659(98)00116-3.
85. Rodrigues de Azevedo, C.; von Stosch, M.; Costa, M.S.; Ramos, A.M.; Cardoso, M.M.; Danhier, F.; Préat, V.; Oliveira, R. Modeling of the Burst Release from PLGA Micro- and Nanoparticles as Function of Physicochemical Parameters and

Formulation Characteristics. *Int. J. Pharm.* **2017**, *532*, 229–240, doi:10.1016/j.ijpharm.2017.08.118.
86. Budhian, A.; Siegel, S.J.; Winey, K.I. Controlling the in Vitro Release Profiles for a System of Haloperidol-Loaded PLGA Nanoparticles. *Int. J. Pharm.* **2008**, *346*, 151–159, doi:10.1016/j.ijpharm.2007.06.011.
87. Singh, R.; Lillard, J.W. Nanoparticle-Based Targeted Drug Delivery. *Exp. Mol. Pathol.* **2009**, *86*, 215–223, doi:10.1016/j.yexmp.2008.12.004.
88. D'Souza, S. A Review of In Vitro Drug Release Test Methods for Nano-Sized Dosage Forms Available online: https://www.hindawi.com/journals/ap/2014/304757/ (accessed on 8 July 2020).
89. Yang, X.; Trinh, H.M.; Agrahari, V.; Sheng, Y.; Pal, D.; Mitra, A.K. Nanoparticle-Based Topical Ophthalmic Gel Formulation for Sustained Release of Hydrocortisone Butyrate. *AAPS PharmSciTech* **2015**, *17*, 294–306, doi:10.1208/s12249-015-0354-5.
90. Dinesh Kumar, V.; Verma, P.R.P.; Singh, S.K. Development and Evaluation of Biodegradable Polymeric Nanoparticles for the Effective Delivery of Quercetin Using a Quality by Design Approach. *LWT - Food Sci. Technol.* **2015**, *61*, 330–338, doi:10.1016/j.lwt.2014.12.020.
91. Sant, S.; Nadeau, V.; Hildgen, P. Effect of Porosity on the Release Kinetics of Propafenone-Loaded PEG-g-PLA Nanoparticles. *J. Controlled Release* **2005**, *107*, 203–214, doi:10.1016/j.jconrel.2005.02.017.
92. Wang, Y.; Yang, X.; Yang, J.; Wang, Y.; Chen, R.; Wu, J.; Liu, Y.; Zhang, N. Self-Assembled Nanoparticles of Methotrexate Conjugated O-Carboxymethyl Chitosan: Preparation, Characterization and Drug Release Behavior in Vitro. *Carbohydr. Polym.* **2011**, *86*, 1665–1670, doi:10.1016/j.carbpol.2011.06.080.
93. Modi, S.; Anderson, B.D. Determination of Drug Release Kinetics from Nanoparticles: Overcoming Pitfalls of the Dynamic Dialysis Method. *Mol. Pharm.* **2013**, *10*, 3076–3089, doi:10.1021/mp400154a.
94. Zambito, Y.; Pedreschi, E.; Di Colo, G. Is Dialysis a Reliable Method for Studying Drug Release from Nanoparticulate Systems?—A Case Study. *Int. J. Pharm.* **2012**, *434*, 28–34, doi:10.1016/j.ijpharm.2012.05.020.
95. D'Souza, S. A Review of In Vitro Drug Release Test Methods for Nano-Sized Dosage Forms Available online: https://www.hindawi.com/journals/ap/2014/304757/ (accessed on 12 January 2021).
96. Nothnagel, L.; Wacker, M.G. How to Measure Release from Nanosized Carriers? *Eur. J. Pharm. Sci.* **2018**, *120*, 199–211, doi:10.1016/j.ejps.2018.05.004.
97. Siepmann, J.; Siepmann, F. Sink Conditions Do Not Guarantee the Absence of Saturation Effects. *Int. J. Pharm.* **2020**, *577*, 119009, doi:10.1016/j.ijpharm.2019.119009.
98. Weng, J.; Tong, H.H.Y.; Chow, S.F. In Vitro Release Study of the Polymeric Drug Nanoparticles: Development and Validation of a Novel Method. *Pharmaceutics* **2020**, *12*, doi:10.3390/pharmaceutics12080732.
99. Hasan, A.S.; Socha, M.; Lamprecht, A.; Ghazouani, F.E.; Sapin, A.; Hoffman, M.; Maincent, P.; Ubrich, N. Effect of the Microencapsulation of Nanoparticles on the Reduction of Burst Release. *Int. J. Pharm.* **2007**, *344*, 53–61, doi:10.1016/j.ijpharm.2007.05.066.
100. Nimesh, S.; Manchanda, R.; Kumar, R.; Saxena, A.; Chaudhary, P.; Yadav, V.; Mozumdar, S.; Chandra, R. Preparation, Characterization and in Vitro Drug

Release Studies of Novel Polymeric Nanoparticles. *Int. J. Pharm.* **2006**, *323*, 146–152, doi:10.1016/j.ijpharm.2006.05.065.
101. Dalwadi, G.; Benson, H.A.E.; Chen, Y. Comparison of Diafiltration and Tangential Flow Filtration for Purification of Nanoparticle Suspensions. *Pharm. Res.* **2005**, *22*, 2152–2162, doi:10.1007/s11095-005-7781-z.
102. Li, Q.; Reeve, C.; Martinez, L.; Wright, S. 2.62 - Scale-up in Biotechnology. In *Comprehensive Biotechnology (Third Edition)*; Moo-Young, M., Ed.; Pergamon: Oxford, 2019; pp. 919–932 ISBN 978-0-444-64047-5.
103. Maia, J.; Santos, T.; Aday, S.; Agasse, F.; Cortes, L.; Malva, J.O.; Bernardino, L.; Ferreira, L. Controlling the Neuronal Differentiation of Stem Cells by the Intracellular Delivery of Retinoic Acid-Loaded Nanoparticles. *ACS Nano* **2011**, *5*, 97–106, doi:10.1021/nn101724r.
104. Santos, T.; Ferreira, R.; Maia, J.; Agasse, F.; Xapelli, S.; Cortes, L.; Bragança, J.; Malva, J.O.; Ferreira, L.; Bernardino, L. Polymeric Nanoparticles to Control the Differentiation of Neural Stem Cells in the Subventricular Zone of the Brain. *ACS Nano* **2012**, *6*, 10463–10474, doi:10.1021/nn304541h.
105. Maden, M. Retinoic Acid in the Development, Regeneration and Maintenance of the Nervous System. *Nat. Rev. Neurosci.* **2007**, *8*, 755–765, doi:10.1038/nrn2212.
106. Szuts, E.Z.; Harosi, F.I. Solubility of Retinoids in Water. *Arch. Biochem. Biophys.* **1991**, *287*, 297–304, doi:10.1016/0003-9861(91)90482-X.
107. Tan, B.-T.; Wang, L.; Li, S.; Long, Z.-Y.; Wu, Y.-M.; Liu, Y. Retinoic Acid Induced the Differentiation of Neural Stem Cells from Embryonic Spinal Cord into Functional Neurons in Vitro. *Int. J. Clin. Exp. Pathol.* **2015**, *8*, 8129–8135.
108. Christie, V.B.; Maltman, D.J.; Henderson, A.P.; Whiting, A.; Marder, T.B.; Lako, M.; Przyborski, S.A. Retinoid Supplementation of Differentiating Human Neural Progenitors and Embryonic Stem Cells Leads to Enhanced Neurogenesis in Vitro. *J. Neurosci. Methods* **2010**, *193*, 239–245, doi:10.1016/j.jneumeth.2010.08.022.
109. Wohl, C.A.; Weiss, S. Retinoic Acid Enhances Neuronal Proliferation and Astroglial Differentiation in Cultures of CNS Stem Cell–Derived Precursors. *J. Neurobiol.* **1998**, *37*, 281–290, doi:10.1002/(SICI)1097-4695(19981105)37:2<281::AID-NEU7>3.0.CO;2-J.
110. Capjak, I.; Goreta, S.Š.; Jurašin, D.D.; Vrček, I.V. How Protein Coronas Determine the Fate of Engineered Nanoparticles in Biological Environment. *Arh. Hig. Rada Toksikol.* **2017**, *68*, 245–253, doi:10.1515/aiht-2017-68-3054.
111. Pederzoli, F.; Tosi, G.; Vandelli, M.A.; Belletti, D.; Forni, F.; Ruozi, B. Protein Corona and Nanoparticles: How Can We Investigate on?: Protein Corona and Nanoparticles. *Wiley Interdiscip. Rev. Nanomed. Nanobiotechnol.* **2017**, *9*, e1467, doi:10.1002/wnan.1467.
112. Monopoli, M.P.; Pitek, A.S.; Lynch, I.; Dawson, K.A. Formation and Characterization of the Nanoparticle–Protein Corona. In *Nanomaterial Interfaces in Biology: Methods and Protocols*; Bergese, P., Hamad-Schifferli, K., Eds.; Methods in Molecular Biology; Humana Press: Totowa, NJ, 2013; pp. 137–155 ISBN 978-1-62703-462-3.
113. Brun, E.; Sicard – Roselli, C. Could Nanoparticle Corona Characterization Help for Biological Consequence Prediction? *Cancer Nanotechnol.* **2014**, *5*, 7, doi:10.1186/s12645-014-0007-5.

114. Francia, V.; Yang, K.; Deville, S.; Reker-Smit, C.; Nelissen, I.; Salvati, A. Corona Composition Can Affect the Mechanisms Cells Use to Internalize Nanoparticles. *ACS Nano* **2019**, *13*, 11107–11121, doi:10.1021/acsnano.9b03824.
115. Docter, D.; Distler, U.; Storck, W.; Kuharev, J.; Wünsch, D.; Hahlbrock, A.; Knauer, S.K.; Tenzer, S.; Stauber, R.H. Quantitative Profiling of the Protein Coronas That Form around Nanoparticles. *Nat. Protoc.* **2014**, *9*, 2030–2044, doi:10.1038/nprot.2014.139.
116. Pedroso, D.C.S.; Tellechea, A.; Moura, L.; Fidalgo-Carvalho, I.; Duarte, J.; Carvalho, E.; Ferreira, L. Improved Survival, Vascular Differentiation and Wound Healing Potential of Stem Cells Co-Cultured with Endothelial Cells. *PLOS ONE* **2011**, *6*, e16114, doi:10.1371/journal.pone.0016114.
117. Vandenhaute, E.; Dehouck, L.; Boucau, M.-C.; Sevin, E.; Uzbekov, R.; Tardivel, M.; Gosselet, F.; Fenart, L.; Cecchelli, R.; Dehouck, M.-P. Modelling the Neurovascular Unit and the Blood-Brain Barrier with the Unique Function of Pericytes. *Curr. Neurovasc. Res.* **2011**, *8*, 258–269, doi:10.2174/156720211798121016.
118. Shimizu, F.; Sano, Y.; Abe, M.; Maeda, T.; Ohtsuki, S.; Terasaki, T.; Kanda, T. Peripheral Nerve Pericytes Modify the Blood–Nerve Barrier Function and Tight Junctional Molecules through the Secretion of Various Soluble Factors. *J. Cell. Physiol.* **2011**, *226*, 255–266, doi:10.1002/jcp.22337.
119. Moya, E.L.J.; Vandenhaute, E.; Rizzi, E.; Boucau, M.-C.; Hachani, J.; Maubon, N.; Gosselet, F.; Dehouck, M.-P. Miniaturization and Automation of a Human In Vitro Blood–Brain Barrier Model for the High-Throughput Screening of Compounds in the Early Stage of Drug Discovery. *Pharmaceutics* **2021**, *13*, 892.
120. Cecchelli, R.; Aday, S.; Sevin, E.; Almeida, C.; Culot, M.; Dehouck, L.; Coisne, C.; Engelhardt, B.; Dehouck, M.-P.; Ferreira, L. A Stable and Reproducible Human Blood-Brain Barrier Model Derived from Hematopoietic Stem Cells. *PLoS ONE* **2014**, *9*, doi:10.1371/journal.pone.0099733.
121. Vandenhaute, E.; Drolez, A.; Sevin, E.; Gosselet, F.; Mysiorek, C.; Dehouck, M.-P. Adapting Coculture in Vitro Models of the Blood-Brain Barrier for Use in Cancer Research: Maintaining an Appropriate Endothelial Monolayer for the Assessment of Transendothelial Migration. *Lab. Investig. J. Tech. Methods Pathol.* **2016**, *96*, 588–598, doi:10.1038/labinvest.2016.35.
122. Ravenstijn, P.G.M.; Merlini, M.; Hameetman, M.; Murray, T.K.; Ward, M.A.; Lewis, H.; Ball, G.; Mottart, C.; de Ville de Goyet, C.; Lemarchand, T.; et al. The Exploration of Rotenone as a Toxin for Inducing Parkinson's Disease in Rats, for Application in BBB Transport and PK-PD Experiments. *J. Pharmacol. Toxicol. Methods* **2008**, *57*, 114–130, doi:10.1016/j.vascn.2007.10.003.
123. Dehouck, B.; Fenart, L.; Dehouck, M.-P.; Pierce, A.; Torpier, G.; Cecchelli, R. A New Function for the LDL Receptor: Transcytosis of LDL across the Blood–Brain Barrier. *J. Cell Biol.* **1997**, *138*, 877–889, doi:10.1083/jcb.138.4.877.
124. Candela, P.; Gosselet, F.; Saint-Pol, J.; Sevin, E.; Boucau, M.-C.; Boulanger, E.; Cecchelli, R.; Fenart, L. Apical-to-Basolateral Transport of Amyloid-β Peptides through Blood-Brain Barrier Cells Is Mediated by the Receptor for Advanced Glycation End-Products and Is Restricted by P-Glycoprotein. *J. Alzheimers Dis.* **2010**, *22*, 849–859, doi:10.3233/JAD-2010-100462.
125. Saint-Pol, J.; Candela, P.; Boucau, M.-C.; Fenart, L.; Gosselet, F. Oxysterols Decrease Apical-to-Basolateral Transport of Aß Peptides via an ABCB1-Mediated Process in an in Vitro Blood-Brain Barrier Model Constituted of Bovine

Brain Capillary Endothelial Cells. *Brain Res.* **2013**, *1517*, 1–15, doi:10.1016/j.brainres.2013.04.008.
126. Okura, T.; Hattori, A.; Takano, Y.; Sato, T.; Hammarlund-Udenaes, M.; Terasaki, T.; Deguchi, Y. Involvement of the Pyrilamine Transporter, a Putative Organic Cation Transporter, in Blood-Brain Barrier Transport of Oxycodone. *Drug Metab. Dispos. Biol. Fate Chem.* **2008**, *36*, 2005–2013, doi:10.1124/dmd.108.022087.
127. Georgieva, J.V.; Kalicharan, D.; Couraud, P.-O.; Romero, I.A.; Weksler, B.; Hoekstra, D.; Zuhorn, I.S. Surface Characteristics of Nanoparticles Determine Their Intracellular Fate in and Processing by Human Blood–Brain Barrier Endothelial Cells In Vitro. *Mol. Ther.* **2011**, *19*, 318–325, doi:10.1038/mt.2010.236.
128. Morad, G.; Carman, C.V.; Hagedorn, E.J.; Perlin, J.R.; Zon, L.I.; Mustafaoglu, N.; Park, T.-E.; Ingber, D.E.; Daisy, C.C.; Moses, M.A. Tumor-Derived Extracellular Vesicles Breach the Intact Blood-Brain Barrier via Transcytosis. *ACS Nano* **2019**, *13*, 13853–13865, doi:10.1021/acsnano.9b04397.
129. del Pino, P.; Pelaz, B.; Zhang, Q.; Maffre, P.; Ulrich Nienhaus, G.; J. Parak, W. Protein Corona Formation around Nanoparticles – from the Past to the Future. *Mater. Horiz.* **2014**, *1*, 301–313, doi:10.1039/C3MH00106G.
130. Monopoli, M.P.; Åberg, C.; Salvati, A.; Dawson, K.A. Biomolecular Coronas Provide the Biological Identity of Nanosized Materials. *Nat. Nanotechnol.* **2012**, *7*, 779–786, doi:10.1038/nnano.2012.207.
131. Zhu, X.-D.; Zhuang, Y.; Ben, J.-J.; Qian, L.-L.; Huang, H.-P.; Bai, H.; Sha, J.-H.; He, Z.-G.; Chen, Q. Caveolae-Dependent Endocytosis Is Required for Class A Macrophage Scavenger Receptor-Mediated Apoptosis in Macrophages *. *J. Biol. Chem.* **2011**, *286*, 8231–8239, doi:10.1074/jbc.M110.145888.
132. Kanai, Y.; Wang, D.; Hirokawa, N. KIF13B Enhances the Endocytosis of LRP1 by Recruiting LRP1 to Caveolae. *J. Cell Biol.* **2014**, *204*, 395–408, doi:10.1083/jcb.201309066.
133. Fukasawa, M.; Adachi, H.; Hirota, K.; Tsujimoto, M.; Arai, H.; Inoue, K. SRB1, a Class B Scavenger Receptor, Recognizes Both Negatively Charged Liposomes and Apoptotic Cells. *Exp. Cell Res.* **1996**, *222*, 246–250, doi:10.1006/excr.1996.0030.
134. Tosi, G.; Fano, R.A.; Bondioli, L.; Badiali, L.; Benassi, R.; Rivasi, F.; Ruozi, B.; Forni, F.; Vandelli, M.A. Investigation on Mechanisms of Glycopeptide Nanoparticles for Drug Delivery across the Blood–Brain Barrier. *Nanomed.* **2011**, *6*, 423–436, doi:10.2217/nnm.11.11.
135. Yoo, J.; Won, Y.-Y. Phenomenology of the Initial Burst Release of Drugs from PLGA Microparticles. *ACS Biomater. Sci. Eng.* **2020**, *6*, 6053–6062, doi:10.1021/acsbiomaterials.0c01228.
136. Jain, G.K.; Pathan, S.A.; Akhter, S.; Ahmad, N.; Jain, N.; Talegaonkar, S.; Khar, R.K.; Ahmad, F.J. Mechanistic Study of Hydrolytic Erosion and Drug Release Behaviour of PLGA Nanoparticles: Influence of Chitosan. *Polym. Degrad. Stab.* **2010**, *95*, 2360–2366, doi:10.1016/j.polymdegradstab.2010.08.015.

6.2 Scientific Output

Articles

- Lombardo, S. M.; Schneider, M.; Türeli, A. E.; Günday Türeli, N. Beilstein J. Nanotechnol. 2020, 11, 866–883. doi:10.3762/bjnano.11.72
- Lombardo, S. M.; Günday Türeli, N.; Koch, M.; Schneider, M.; Türeli, A. E. International Journal of Pharmaceutics 2021, 609, 121215, doi:10.1016/j.ijpharm.2021.121215.

Oral presentations

- NANOSTEM 1st scientific meeting, July 2019, talk, “PLGA nanoparticles for delivery through the BBB”
- CRS 2020 Germany, flash talk, “Tackling Surface Stabilized PLGA Nanoparticles Ability to Pass the BBB”
- NANOSTEM 2nd scientific meeting, July 2020, talk, “PLGA nanoparticles for delivery through the BBB”
- CRS 2021 Germany, flash talk, “Release study of PLGA nanocapsules loaded with retinoic acid using an innovative “sample and separate” method: the NanoDis technology”
- NANOSTEM 3rd scientific meeting, July 2021, talk, “PLGA nanoparticles for delivery through the BBB”
- ESB 2021, talk, “Comparison of release profile of nanocapsules measured with dialysis and an innovative sample and separate technique, the NanoDis system”

Poster presentations

- CRS 2019, poster session, “Tackling Surface Stabilized PLGA Nanoparticles Ability to Pass the BBB”
- CRS 2020 Germany, poster session, “Tackling Surface Stabilized PLGA Nanoparticles Ability to Pass the BBB”

6.3 Curriculum Vitae

Name: Sonia Lombardo

Date of birth: December 2nd, 1994, in Suresnes (France)

Email address: sonia.marie.lombardo@gmail.com

Education

2020 – University Paris Saclay – PharmD degree – “Very Good” distinction

2017-2018 – University Paris Saclay – Master 2 Pharmacotechnology and Biopharmacy

2013-2017 – University Paris Saclay – 2nd-5th year of Pharmacy studies, specialised in pharmaceutical industry

2012-2013 – University Paris VI – First year of health profession studies (PACES)

Work experiences

2018-2021 (3 years) – MyBiotech – Überherrn (Germany) – Marie Curie ITN H2020 Thesis – NANOSTEM project

2018 (6 months) – E.A. 6295 Nanomedicines and Nanoprobes – Tours (France) – Internship in galenic research

2017 (5 months) – Roche – Basel (Switzerland) – Internship in Late Stage Pharmaceutical Development

2016-2017 (6 months) – AGEPS – Nanterre (France) – Internship in pharmaceutical production, subcontracting department

2016 (2 months) – Institut Galien Paris Sud CNRS 8612 – Chatenay-Malabry (France) – Internship in galenic research

6.4 Acknowledgments

This thesis is the accomplishment of three years of work and collaboration with many people, which I would like to sincerely thank here.

First, I would like to express all my gratitude to my supervisors at MyBiotech, Dr. Nazende Günday-Türeli and Dr. Emre Türeli, which provided me with essential scientific guidance during these three years. You were always available for any concerns I had and having you as mentors to look up to definitely made me grow as a scientist.

I would also like to thank Prof. Marc Schneider for all his help during this time. Your supervision during the lab seminars provided me with crucial advices and support during these three years and definitely made the writing of this manuscript easier. Thank you for including me in your team, even from afar.

I would like to thank the European Union H2020 Marie Skłodowska-Curie Actions for my funding and the whole NANOSTEM consortium for all their support.

More especially, to Elisa Jimenez-Moya, Prof. Marie-Pierre Dehouck, Dr. Caroline Mysiorek and Prof. Fabien Gosselet, thank you for all your support concerning the in vitro test of our nanoparticles as well as our article writing.

To Elisa especially, thank you for your great help and support during these three years. I thought we made a great team and I will miss our little skype meetings.

To Johannes, Elena, Agnes, Marijas, Marcel and Aljoscha, thank you for all your help with my microscope measurements during these 3 years.

To Enes Gök, thank you for your great help during your time here.

To Birgit Rosenkränzer and Dominik Kolling, thank you for your help with all my SDS-PAGE experiments.

To Simon Herber, thank you for helping me translate my abstract in German.

To all my colleagues at MyBiotech, Cemre, Lara, Esra, Selin, Li Bin, Ailing, Linda, Simon, Nicolas, Carlos, Melina, Melanie and everyone else, thank you for your support and the great atmosphere you set in the office and the lab. Thank you for your

companionship during these three years, which would have been quite lonely without you.

To all my fellow scientists at Saarland University, Agnes, Johannes, Elena, Karola, Thorben, Alexandra, Aljoscha, Nesma, Salma, Enkeleda, Tom, Marcel, Marijas, Sabrina and everyone else, thank you for making me part of the team and the good times we had during my three months with you.

To all the NANOSTEM ESRs, Federico, Alena, Roberta, Ines, Francesca, Angela, Eleonora, Elisa, Georges, Sara, Matteo, Patrick and Eirini, you were the greatest team of PhD students one could have hoped for. I really regret that COVID-19 prevented us from spending more time together face to face but we will all meet again, for sure.

À ma mère, merci pour ton soutien indéfectible durant toutes mes années d'études, et elles furent longues. Merci d'avoir cru en moi et de n'avoir jamais douté que j'y viendrais à bout.

À mes plus chers amis, Céline, Julien, Vincent, Alexandra, Pauline, Baptiste, Marie, Charlotte, merci pour tout votre soutien pendant ces trois années loin de Rueil, d'être venu me voir jusque dans mon petit village allemand et pour toutes nos soirées Discord qui m'ont fait rire durant des moments difficiles.

To all, thank you for everything.

Sonia Lombardo